Extreme infrared variables from UKIDSS – II. An end-of-survey catalogue of eruptive YSOs and unusual stars

P. W. Lucas,[1]★ L. C. Smith,[1] C. Contreras Peña,[2] D. Froebrich,[3] J. E. Drew,[1]
M. S. N. Kumar,[1] J. Borissova,[4,5] D. Minniti,[6,5,7] R. Kurtev[4,5] and M. Monguió[1]

[1]*Centre for Astrophysics, University of Hertfordshire, College Lane, Hatfield AL10 9AB, UK*
[2]*School of Physics, University of Exeter, Stocker Road, Exeter EX4 4QL, UK*
[3]*Centre for Astrophysics and Planetary Science, University of Kent, Canterbury CT2 7NH, UK*
[4]*Instituto de Física y Astronomía, Universidad de Valparaíso, ave. Gran Bretaña, 1111, Casilla 5030, Valparaíso, Chile*
[5]*Millennium Institute of Astrophysics, Av. Vicuna Mackenna 4860, 782-0436 Macul, Santiago, Chile*
[6]*Departamento de Ciencias Fisicas, Universidad Andres Bello, Republica 220, Santiago, Chile*
[7]*Vatican Observatory, V-00120 Vatican City State, Italy*

ABSTRACT

We present a catalogue of 618 high-amplitude infrared variable stars ($1 < \Delta K < 5\,\mathrm{mag}$) detected by the two widely separated epochs of 2.2 µm data in the UKIDSS Galactic plane survey, from searches covering $\sim$1470 deg^2. Most were discovered by a search of all fields at $30 < l < 230°$. Sources include new dusty Mira variables, three new cataclysmic variable candidates, a blazar and a peculiar source that may be an interacting binary system. However, $\sim$60 per cent are young stellar obbjects (YSOs), based on spatial association with star-forming regions at distances ranging from 300 pc to over 10 kpc. This confirms our initial result in Contreras Peña et al. (Paper I) that YSOs dominate the high-amplitude infrared variable sky in the Galactic disc. It is also supported by recently published VISTA Variables in the Via Lactea (VVV) results at $295 < l < 350°$. The spectral energy distributions of the YSOs indicate class I or flat-spectrum systems in most cases, as in the VVV sample. A large number of variable YSOs are associated with the Cygnus X complex and other groups are associated with the North America/Pelican nebula, the Gemini OB1 molecular cloud, the Rosette complex, the Cone nebula, the W51 star-forming region and the S86 and S236 H II regions. Most of the YSO variability is likely due to variable/episodic accretion on time-scales of years, albeit usually less extreme than classical FUors and EXors. Luminosities at the 2010 Wide-field Infrared Survey Explorer epoch range from $\sim$0.1 to $10^3\,\mathrm{L}_\odot$ but only rarely exceed $10^{2.5}\,\mathrm{L}_\odot$.

Key words: stars: AGB and post-AGB – novae, cataclysmic variables – stars: protostars – stars: variables: T Tauri, Herbig Ae/Be – galaxies: active.

1 INTRODUCTION

The advent of the wide-field infrared (IR) telescopes in recent years has enabled the first panoramic explorations of the variable sky in the near-IR waveband. The UKIDSS Galactic Plane Survey (UGPS, Lawrence et al. 2007; Lucas et al. 2008) surveyed the northern and equatorial Galactic plane at two epochs, while in the Southern hemisphere, the VVV survey (VISTA Variables in the Via Lactea, Minniti et al. 2010) surveyed 560 deg^2 of the Galactic bulge and disc at several dozen epochs from 2010 to 2015. An important subject for such surveys is the phenomenon of eruptive variability in young stellar obbjects (YSOs) in which the variability is driven by episodic accretion. Given that YSOs suffer increasingly high extinction at earlier stages of pre-main sequence (pre-MS) evolution, IR observation is needed to place the study of variable accretion on a firm observational footing. Equally important is the possibility of making significant unexpected discoveries in other areas of astronomy.

Episodic accretion is a serious unresolved matter in star formation (reviewed by Audard et al. 2014), owing to the effect that it may have on masses and ages inferred from Hertzsprung–Russell (HR) diagrams for pre-MS clusters. This may help to resolve the luminosity problem (Kenyon et al. 1990; Enoch et al. 2009; Caratti o Garatti et al. 2012) which is that typical luminosities of class I YSOs in nearby clusters are lower than expected for stars that should lie on Hayashi tracks above the MS. Variable accretion may also explain the scatter of pre-MS stars about any given isochrone in

★ E-mail: p.w.lucas@herts.ac.uk

HR diagrams, e.g. Mayne & Naylor (2008), Weights et al. (2009). Some theoretical work has suggested that episodic accretion has a lingering effect on the location of pre-MS stars on the HR diagram (Baraffe, Chabrier & Gallardo 2009, Baraffe, Vorobyov & Chabrier 2012), while another study indicates that there is little effect on low-mass stars (Hosokawa, Offner & Krumholz 2011). Aside from the effect on stellar luminosity and radius, the effect of variable accretion on planet formation is worthy of investigation (Cieza et al. 2016).

While low level accretion variations are thought to be understood in terms of the role of the stellar magnetosphere in generating multiple, often unstable accretion flows (e.g. Romanova, Kulkarni & Lovelace 2008), theories of episodic accretion are quite diverse. E.g. Zhu, Hartmann & Gammie (2009) proposed an imbalance between mass transport rates determined by gravitational instability in the outer disc and magnetorotational instability in the inner disc. Bonnell & Bastien (1992) proposed that outbursts are triggered by a binary companion passing through the perioastron of an eccentric orbit, a model that may apply to the short-period eruptive variable LRLL 54361 (Muzerolle et al. 2013). Vorobyov & Basu (2015) proposed that outer disc fragmentation due to gravitational instability can cause fragments to spiral inward to the protostar via exchange of angular momentum with spiral arms and other fragments in the disc, the resulting outbursts being most common in the class I stage of evolution.

The UGPS surveyed 1868 deg^2 of the northern and equatorial Galactic plane in the *J*, *H* and *K* passbands from 2005 to 2013. The survey used the Wide Field Camera (WFCAM, Casali et al. 2007) mounted on the 3.8-m United Kingdom Infrared Telescope. With the aims of detecting rarely seen high-amplitude IR variable stars and measuring proper motions, a second epoch of *K* photometry was obtained for most of the UGPS area with a time baseline of 1.8–8 yr. New high proper motion discoveries were presented by Smith et al. (2014). Initial discoveries from the variable star search were presented in Paper I of this series (Contreras Peña et al. 2014) which described 45 stars from the fifth and seventh UGPS data releases with variations above 1 mag in *K*. These near-IR surveys have been complemented by two-epoch mid-IR searches of data from the *Spitzer Space Telescope* (Werner et al. 2004) and the Wide-field Infrared Survey Explorer (WISE, Wright et al. 2010), see Scholz, Froebrich & Wood (2013) and Antoniucci et al. (2014).

In Paper I, we found that most of the 45 high-amplitude IR variable stars detected in our search of 155 deg^2 of the Galactic plane were YSOs. This suggested that highly variable YSOs dominate the near-IR variable sky on Galactic disc sightlines, a result that had not been predicted. The space density of these sources also appeared to be higher than that of highly variable asymptotic giant branch stars (AGB stars). However, most of the variable YSOs were located in just two nearby star-forming complexes (the Serpens OB2 region and parts of Cygnus X) so it was possible that the results would not be replicated in a pan-Galactic search. A search for high-amplitude variables in 118 deg^2 of the VVV Galactic disc data set confirmed the dominance of YSOs on mid-plane sightlines in the inner Galaxy (longitudes $295 < l < 350°$), see Contreras Peña et al. (2017a,b), hereafter CP17a, CP17b. That study found that the variable YSOs had a variety of light-curve types but systems dominated by short-term variations generally varied by <1.5 mag in *K*, whereas higher amplitudes were more often associated with outbursts with durations of a few years, most often seen amongst class I and flat-spectrum YSOs. A similar rarity of high-amplitude short-term eruptions is seen in optical studies of T Tauri stars and

Herbig Ae/Be stars, see Herbst et al. (1994), Herbst & Shevchenko (1999), Findeisen et al. (2013), Cody et al. (2014) and Stauffer et al. (2014). Cody et al. (2017) found a few examples of short-duration bursts (hours to days) with optical amplitudes slightly over 1 mag and one case of a 2 mag burst, providing the exception that proves the rule. High-amplitude short-term optical changes are more often reductions in flux below the usual level: the UXor phenomenon, usually but not always attributed to extinction (Calvet et al. 2004; Herbst & Shevchenko 1999; Findeisen et al. 2013; Cody et al. 2014). Such extinction-driven variability will of course have a much lower amplitude in the IR than the optical, though the YSOVAR survey data indicate that variable reddening can dominate the low-amplitude variability observed on short time-scales even at mid-IR wavelengths, e.g. Wolk et al. (2015).

The VVV study of CP17a greatly increased the available sample of candidate eruptive variable YSOs. The mean amplitude of $\sim$1.7 mag in K_s was lower than is traditionally associated with eruptive variables in the FUor and EXor subclasses but the continuous distribution of amplitudes seemed to argue against setting an arbitrary threshold. We adopted a 1 mag threshold in Paper I and CP17a on the grounds that this is the level above which short-term variations become rather rare, such that variability is more often long term, i.e. time-scales of years rather than days. A limitation of the VVV sample is that it is dominated by sources at distances, $d > 2$ kpc, often suffering high extinction. This inhibits spatially resolved follow-up and optical investigation and selects against less luminous sources.

In this work, we present the results of a search for high-amplitude variable stars in all UGPS fields with two epochs of *K* photometry at longitudes $l > 30°$. This allows us to confirm the prevalence of high-amplitude YSOs across a much broader range of Galactic sightlines and detect low-luminosity variables in nearby, well-studied star-forming regions (SFRs). The non-YSOs in the catalogue are likely to be of interest in a variety of subfields of astronomy. We also include the results of our previous UGPS searches in our catalogue for ease of reference. In Section 2, we describe our search methods and present the catalogue, which includes information gleaned from public multiwaveband data sets and the literature. A third epoch of near-IR photometry from 2MASS (Skrutskie et al. 2006) is provided where available. In Section 3, we provide an overview of the properties of catalogue members. We summarize the few previously known variable stars, describe the identification of likely YSOs and give a breakdown of non-YSOs into various categories. In Section 4, we discuss the properties of likely YSOs in detail, including a description of the groups of highly variable YSOs found in several well-studied SFRs. In Section 5 we briefly discuss a few of the highest amplitude variables, the nearest pre-MS variables and a single object with unique properties. A summary of our main findings is presented in Section 6.

2 VARIABLE SEARCH

The variable stars in our catalogue were found in several searches of the UGPS data as the survey progressed, all of which were minor variations on the same strategy. A minimum variation $\Delta K = 1$ mag was adopted, as in Paper I. Below this level short-term variability becomes much more common in YSOs, see e.g. Carpenter, Hillenbrand & Skrutskie (2001), Paper I and Section 4.1.3. Detection at both epochs was required, with a brightness threshold $K < 16$ in at least one epoch. Very high amplitude variables detected at only one epoch will therefore be missed, such as the eruptive YSO detected in UKIDSS by Nikoghosyan, Azatyan and Khachatryan (2017). All of

the many candidates identified by catalogue-based selections were inspected visually to identify genuine variable stars, using the FITS images publicly available at the WFCAM Science Archive (WSA). We summarize the searches here and give full details in Appendix A in order to not encumber the main text with excessive detail.

First, the 45 variables discovered in Paper I were found by searching the fifth and seventh UGPS data releases (DR5 and DR7) available in the WSA, these containing data for 156 deg² of two-epoch sky. An additional search of the DR8 is described in the PhD thesis of Contreras Peña (2015). It used the same method, adding 26 variables in a further 104 deg² of two-epoch sky. These searches used SQL queries of the public data releases and they were inefficient : only 2 per cent of candidates passed visual inspection because most of the available two-epoch sky was in fairly crowded parts of the first Galactic quadrant, where blends increase the number of false positives despite the quality cuts. Many false positive candidates were also created by bad pixels.

Later searches were undertaken using the publicly available FITS catalogues for each field. All of these are now available for the full survey area, though not all the second epoch data are included in the most recent SQL data release (DR10). Using this approach, we initially performed a very efficient search of the less crowded star fields at $l > 60°$, using a method that minimized the number of candidates caused by bad pixels. After completion of the survey, we extended the search to include both previously unobserved fields at $l > 60°$ and more crowded fields at $30 < l < 60°$. This final search also included some candidates flagged as having possible bad pixels in the aperture and some candidates arising from the third epoch of data available for a small proportion of fields due to doubts about data quality at an earlier epoch. Only a small number of bona fide variables were found amongst using third epoch data or sources with possible bad pixels (the latter are flagged in the catalogue but are thought to have reliable photometry). Unlike our early searches of the SQL data releases, the searches of the FITS catalogues include sources bright enough to have a 'possible saturation' warning in the SQL releases. Stars with $K > 11$ generally appear to have reliable photometry (see Appendix A). The catalogue does not include any sources with $K < 11$ at both epochs and we flag all photometry that might be influenced by saturation.
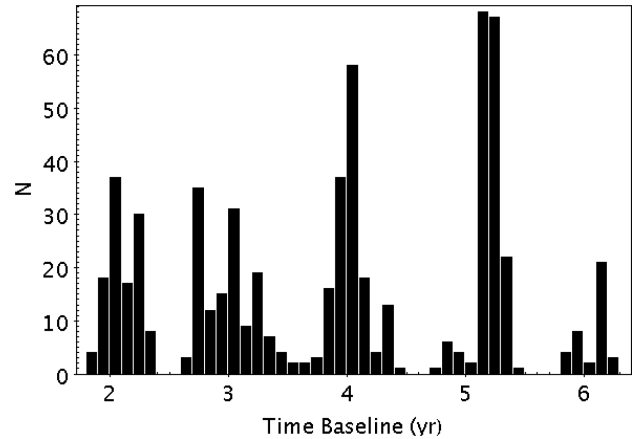

Figure 2. Distribution of time baselines for the 618 variable stars in the catalogue.

We decided to not to investigate FITS catalogue-based candidates at $l < 30°$ because ∼2500 candidates were found, of which under 5 per cent would be real (and limited time remained for this project). We note that UGPS fields at $l < 20°$ are included in the new extension of the multi-epoch VVV survey, VVVX, so these fields may be more readily searched at a later date. An area of ∼75 deg² at $15 < l < 30°$ located off the mid-plane was included in the early SQL searches of DR5 and DR7, see Paper I.

In summary, we have searched all of the UGPS area that may be readily searched for high-amplitude variables, finding a total of 618 variables in ∼1470 deg² of sky, see Fig. 1. The FITS catalogue searches yielded 547 of these, all at $l > 30°$, and the remaining 71 were found by the earlier SQL-based searches. The time baseline of the two UGPS epochs for these sources ranges from 1.8 to 6.3 yr, as illustrated in Fig. 2. These variables may be termed extreme because only 1 star in ∼105 000 was observed to vary in this manner, based on a count of 591 variables at $l > 30°$ from 62 million stars that passed all our algorithmic selections save variability. Additional variables could be found by relaxing our quality cuts (see Appendix A) or by matching primary and secondary detections of
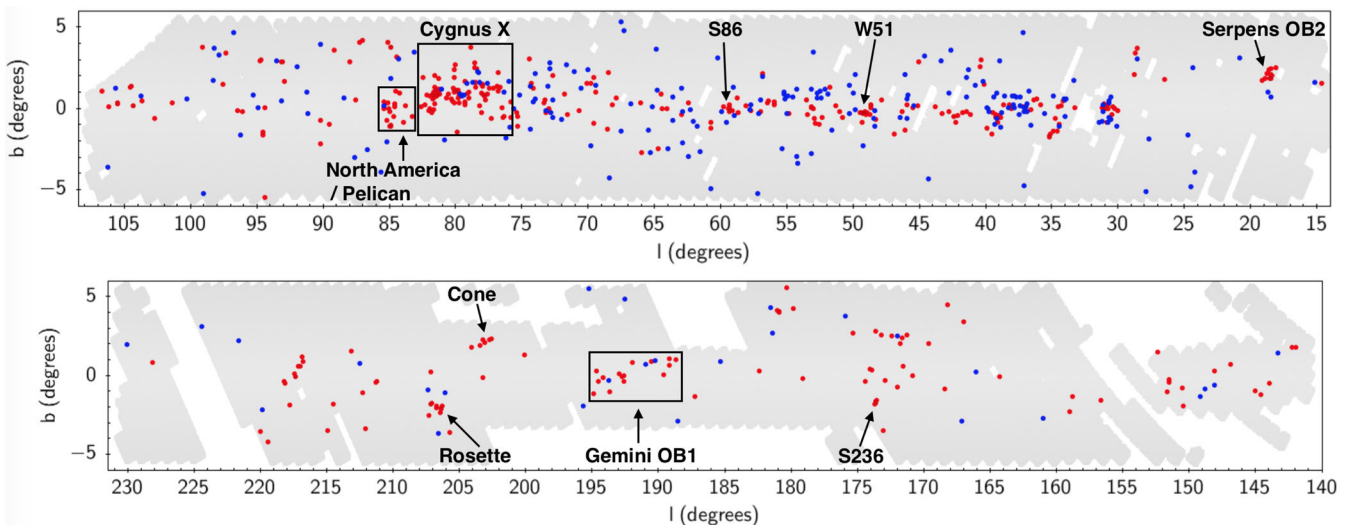
Figure 1. Locations of the 618 variable stars in Galactic coordinates. Likely YSOs (red dots) are identified by spatial association with SFRs, see Section 3.3. Other sources are shown in blue and the UGPS two-epoch coverage is shown as a grey background. Groups of likely YSOs in well-studied SFRs are indicated (see Section 4.2) though some are unresolved in this large-scale view. At $l < 30°$, only part of the surveyed area has been searched, see Paper I. The vertical scale is slightly exaggerated for clarity.

the same source in the small overlap regions in adjacent fields via the SQL tables in the forthcoming final UKIDSS data release (which will include all the two-epoch data). However, such searches would yield a very small proportion of discoveries from a lot of candidates.

The completeness and depth of our search declines unavoidably with decreasing longitude, as increasing source confusion causes a growing proportion of sources to fail our quality cuts or escape detection entirely. Our quality cuts would be expected to remove ~50 per cent of normal stars but we note that nearby class I YSOs are often seen as spatially resolved nebulae that would typically not satisfy our requirements for a stellar image profile and low ellipticity (necessary to reduce candidates caused by blends). A recent UKIRT-based study of H_2 jet-driving YSOs in the Cygnus X region (Makin & Froebrich 2017) has found a number of highly variable YSOs missed by our search, principally sources that failed the image profile or ellipticity cuts at one of the two K epochs. Consequently, our quality cuts appear to lead to completeness of only ~30 per cent for jet-driving sources in the Cygnus X region at $d = 1.4$ kpc, though the issue would be less significant for more distant YSOs or more evolved systems, given that YSOs with 2.12 μm jets are generally class I systems (Davis et al. 2009). As noted in Paper I, simulated searches of the VVV light curves for the 816 variables in CP17a showed that UKIDSS two epoch searches would be expected to recover only 25 per cent of those variables as high-amplitude systems. The VVV sampling is itself quite sparse, detecting ~80 per cent of highly variable YSOs with stellar image profiles (see CP17a). The overwhelming majority of highly variable YSOs and other highly variable stars therefore remain to be discovered in the northern and equatorial Galactic plane.

2.1 The catalogue

In Table 1, we present the catalogue of 618 high-amplitude IR variables, including photometry from optical to far- IR public surveys. The first 10 rows are shown in the printed version of the paper and a description of all the columns is given in Appendix B. There we also

describe our quality control on the list-driven photometry from the WISE All-Sky data base (following a similar procedure to Koenig & Leisawitz 2014) and details of our multiwaveband cross-matching procedure. The contents of most columns are obvious from the column label but here we note that 'K_c' is a UGPS K magnitude that is always contemporaneous with the UGPS J and H photometry and 'K_o' is the other UGPS K measurement. Also, ΔK is the amplitude of variation based on the two UGPS fluxes and ΔK_{all} is the amplitude after taking account of 2MASS K_s photometry, where available (neglecting the slight difference in the bandpass).

3 OVERVIEW OF CATALOGUE MEMBERS

3.1 Amplitude distribution

Histograms of the variability amplitude are shown in Fig. 3. The distribution of ΔK falls steeply from 1 to 2.5 mag but a low level tail extends up to 5 mag. The distribution of ΔK_{all}, which includes the third epoch of K_s photometry from 2MASS available for 43 per cent of the catalogue, has a slight shift to higher amplitudes as one would expect. The tail with $\Delta K_{all} > 2.5$ includes 43 sources. The proportion of sources with $\Delta K > 1.5$ is 34 per cent, falling to 13 per cent with $\Delta K > 2$. For the subset with a third epoch from 2MASS, 43 per cent have $\Delta K_{all} > 1.5$ and 21 per cent have $\Delta K_{all} > 2$. The likely YSOs (shaded in red) have a very similar distribution of ΔK to the full sample.

While it might be tempting to ascribe the drop above 2.5 mag to a physical difference, we note that the VVV sample of 816 high-amplitude variables (with much better sampled light curves) does not show this feature but rather a fairly smooth decline with increasing amplitude. Inspection of the distribution for UGPS (using different binning choices and trying a vertical log scale) suggests that the edge at 2.5 mag is due to a chance underdensity at 2.4–2.5 mag. The more significant feature appears to be a change from a linear decline in log (N) with increasing amplitude to an approximately flat distribution at higher amplitudes, as distinct from a

Table 1. Catalogue of 618 high-amplitude IR variable stars from UGPS.

Number	UGPS designation	Other name	RA (deg)	Dec. (deg)	l (deg)	b (deg)	J	J_{err}	H	H_{err}	K_c	$K_{c,err}$	K_o	$K_{o,err}$
1	UGPS J032726.66+584508.5	[GMM2009] AFGL490 25	51.8611	58.7524	141.9958	1.7798			17.95	0.05	14.25	0.02	12.98	0.02
2	UGPS J032904.43+583617.6	[GMM2009] AFGL490 337	52.2685	58.6049	142.2539	1.7771	16.90	0.02	15.63	0.02	14.67	0.02	15.88	0.03
3	UGPS J032946.55+554538.1		52.4440	55.7606	143.9428	−0.5137	19.03	0.09	16.48	0.02	14.01	0.02	12.12	0.02
4	UGPS J033048.77+544852.8		52.7032	54.8147	144.6023	−1.2077	18.55	0.05	16.86	0.02	15.88	0.03	14.86	0.02
5	UGPS J033352.60+574259.2		53.4692	57.7165	143.2822	1.4112	18.41	0.05	16.84	0.02	15.50	0.02	16.82	0.07
6	UGPS J033410.59+544603.0		53.5442	54.7675	145.0261	−0.9674	15.65	0.02	14.85	0.02	14.49	0.02	13.36	0.02
7	UGPS J035121.92+545646.8		57.8413	54.9463	146.8871	0.6713	17.93	0.03	15.94	0.02	14.31	0.02	15.61	0.02
8	UGPS J035220.42+531052.9		58.0851	53.1814	148.1109	−0.6085	19.23	0.07	18.19	0.05	17.44	0.08	15.37	0.02
9	UGPS J035442.91+515708.3		58.6788	51.9523	149.1704	−1.3286	16.68	0.02	16.00	0.02	15.31	0.02	13.97	0.02
10	UGPS J035454.09+523007.8		58.7254	52.5022	148.8411	−0.8873	17.72	0.03	16.64	0.02	15.91	0.03	17.41	0.09
...														

K_c epoch	MJD a (days)	MJD b (days)	Saturation flag	Bad pixel flag	ΔK	ΔK_{all}	Source type	d (kpc)	Ref. for d	Association	Ref. for Association
a	53673.52904	54742.63889	0000		1.27	2.28	YSO	0.9	1	AFGL490 SFR	2,3
b	53673.40762	54757.62116	0000		1.21	1.21	YSO	0.9	1	AFGL490 SFR	2,3
a	55483.56806	56293.37766	0000		1.89	1.89	YSO			New pre-MS cluster, no .1, centred on IRAS 03262+5536	
a	55490.4603	56293.40218	0000		1.02	1.02	YSO			New pre-MS cluster, no. 2, matching IRAS 03270+5438	
a	55482.54308	56291.23234	0000		1.32	1.32					
a	55490.51391	56293.40543	0000		1.13	1.29	YSO				
a	55490.55902	56293.42058	0000		1.30	1.30	YSO				
a	55508.56666	56584.51157	0000		2.07	2.07					
a	55476.64744	56601.43958	0000		1.34	1.34					
a	55476.64744	56601.43958	0000		1.51	1.51					
...											

Table 1 – *continued*

Spatial group	α	SED class	r	i	Hα	Optical MJD	J	H (2MASS)	K_s	W1	W2	W3	W4	[24]	I1	I2	I3	I4	PACS [70] (mJy)
	0.94	I							15.26	11.52	9.32	6.37	3.75		10.72	9.35			
							17.00	15.53	14.76	13.90	13.08				13.79	13.15			
	0.37	I							15.40	13.48	11.84	10.09	7.10	4.98	11.20	10.05			
															14.51	13.66			
	0.19	Flat	19.32	17.85	18.81	53655.0	15.25	14.12	13.22	13.96	13.55	9.99	6.54						
	0.04	Flat					17.17	15.94	14.88	13.22	11.97	9.43	7.40		12.42	11.60			
										14.64	14.24	11.55			14.56	14.23			
			19.71	18.0	19.06	54066.0	16.32	15.94	15.24	13.84	12.94	11.15							
...																			

Note. Only the first 10 rows of the table are shown here, split into three sections. The full table is available in the online supplementary information.

References: (1) Testi, Palla & Natta (1998); (2) Gutermuth et al. (2009); (3) Masiunas et al. (2012); (4) Wouterloot, Brand & Fiegle (1993); (5) Froebrich, Scholz & Raftery (2007); (6) Camargo, Bonatto & Bica (2015); (7) Lumsden et al. (2013); (8) Campbell, Persson & Matthews (1989); (9) Walmsley et al. (1975); (10) Di Francesco et al. (2008); (11) Lundquist et al. (2014); (12) Balanutsa et al. (2014); (13) Solin, Ukkonen & Haikala (2012); (14) Buckner & Froebrich (2013); (15) Dobashi (2011); (16) Prisinzano et al. (2011); (17) Wang et al. (2009); (18) Casoli et al. (1986); (19) Kronberger et al. (2006); (20) Lim et al. (2015); (21) Liu et al. (2014); (22) Evans & Blair (1981); (23) Gyulbudaghian (2011); (24) Lada & Lada (2003); (25) Carpenter, Snell & Schloerb (1995b); (26) Moffat, Jackson & Fitzgerald (1979); (27) Reich, Reich & Furst (1997); (28) Magnier et al. (1999); (29) Kawamura et al. (1998); (30) Dunham et al. (2010); (31) Bica, Dutra & Barbuy (2003a); (32) Chavarría et al. (2008); (33) Leistra, Cotera & Liebert (2006); (34) Bica et al. (2003b); (35) Reid et al. (2009); (36) Dutra & Bica (2001); (37) Shimoikura et al. (2013); (38) Ackermann et al. (2015); (39) Perez, The & Westerlund (1987); (40) Román-Zúñiga et al. (2008); (41) Wang et al. (2008); (42) Phelps & Lada (1997); (43) Cambrésy et al. (2013); (44) Poulton et al. (2008); (45) Kato & Uemura (2001); (46) Kamezaki et al. (2014); (47) Reipurth et al. (2004); (48) Venuti et al. (2014); (49) Dahm & Simon (2005); (50) Lee, Snell & Dickman (1996); (51) Lennon et al. (1990); (52) Puga et al. (2009); (53) Horner, Lada & Lada (1997); (54) Lee, Snell & Dickman (1991); (55) Elia et al. (2013); (56) Di Francesco et al. (2008); (57) May, Alvarez & Bronfman (1997); (58) Contreras Peña (2015); (59) Kamiński, Miller & Tylenda (2007); (60) Høg et al. (2000); (61) Contreras Peña et al. (2014); (62) Cohen (1980); (63) Forbes (2000); (64) Jiménez-Esteban et al. (2006); (65) Radhakrishnan et al. (1972); (66) Mallick et al. (2013); (67) Georgelin & Georgelin (1970); (68) Ageorges et al. (1997); (69) Hashimoto (1994); (70) Robitaille et al. (2008); (71) Engels et al. (1983); (72) Eden et al. (2012); (73) Anderson & Bania (2009); (74) Veneziani et al. (2013); (75) Teyssier, Hennebelle & Pérault (2002); (76) Kuchar & Bania (1994); (77) Morales et al. (2013); (78) Billot et al. (2011); (79) Nakano et al. (2003); (80) Peretto & Fuller (2009); (81) Anderson et al. (2012); (82) Simpson et al. (2012); (83) Watson et al. (2003); (84) Chengalur et al. (1993); (85) Avalos et al. (2009); (86) Fontani, Cesaroni & Furuya (2010); (87) Schlingman et al. (2011); (88) Ramírez Alegría, Marín-Franch & Herrero (2014); (89) Alexander & Kobulnicky (2012); (90) Wink, Altenhoff & Mezger (1982); (91) Rathborne et al. (2010); (92) Ragan, Bergin & Gutermuth (2009); (93) Solomon et al. (1987); (94) Faustini et al. (2009); (95) Lockman, Pisano & Howard (1996); (96) Anderson et al. (2009); (97) Bronfman, Nyman & May (1996); (98) Zhang et al. (2009); (99) Rygl et al. (2014); (100) Mauerhan, Van Dyk & Morris (2011); (101) Wood & Churchwell (1989); (102) Alexander et al. (2013); (103) Ellsworth-Bowers et al. (2013); (104) Eden et al. (2013); (105) Wienen et al. (2012); (106) Dirienzo et al. (2012); (107) Rosolowsky et al. (2010); (108) Codella et al. (1995); (109) Williams, Fuller & Sridharan (2004); (110) Simon et al. (2006); (111) Churchwell et al. (2006); (112) Simon et al. (2001); (113) Lewis & Grinspoon (1990); (114) Kolpak et al. (2003); (115) Herbig & Jones (1983); (116) Mercer et al. (2005); (117) Nagayama et al. (2011); (118) Parsons (2011); (119) Kang et al. (2009); (120) Cyganowski et al. (2008); (121) Kwok, Volk & Bidelman (1997); (122) Lundquist et al. (2015); (123) Bania, Anderson & Balser (2012); (124) Viironen et al. (2009); (125) Stephenson (1989); (126) Billot et al. (2010); (127) Bica, Bonatto & Dutra (2008); (128) Riaz et al. (2012); (129) Chapin et al. (2008); (130) Xu et al. (2009); (131) Corradi et al. (2011); (132) Wu et al. (2012); (133) Belczyński et al. (2000); (134) Raj et al. (2015); (135) Kharchenko et al. (2013); (136) Yun & Clemens (1995); (137) Balog & Kenyon (2002); (138) Eder, Lewis & Terzian (1988); (139) Günther et al. (2012); (140) Lin, Webb & Barret (2012); (141) Rygl et al. (2010); (142) Kurtz, Churchwell & Wood (1994); (143) Urquhart et al. (2011); (144) Tadross (2009); (145) Hennemann et al. (2008); (146) Tej et al. (2007); (147) Delgado, Alfaro & Cabrera-Cano (1997); (148) Massey, Johnson & Degioia-Eastwood (1995); (149) Straižys et al. (2014); (150) Dickel, Wendker & Bieritz (1969); (151) Kryukova et al. (2014); (152) Le Duigou & Knödlseder (2002); (153) Downes & Rinehart (1966); (154) Schneider et al. (2007); (155) Rygl et al. (2012); (156) Maíz Apellániz et al. (2015); (157) Maia, Moraux & Joncour (2016); (158) Schneider et al. (2006); (159) Dobashi et al. (1994); (160) Beerer et al. (2010); (161) Rivilla et al. (2014); (162) Marston et al. (2004); (163) Laugalys & Straižys (2002); (164) Laugalys et al. (2006); (165) Guieu et al. (2009); (166) Rebull et al. (2011); (167) Scholz et al. (2013); (168) Cambrésy et al. (2002); (169) Yung, Nakashima & Henkel (2014); (170) Dickinson & Turner (1991); (172) Arvidsson, Kerton & Foster (2009); (173) Dame & Thaddeus (1985); (174) Bernes (1977); (175) Samus et al. (2010); (176) Getman et al. (2012); (177) Contreras et al. (2002); (178) Kuchar & Clark (1997); (179) Harvey et al. (2008); (180) Jilinski et al. (2003); (181) Liu et al. (2012); (182) Kerton (2002); (183) Patriarchi et al. (2001); (184) Kerton & Brunt (2003); (185) Kumar, Keto & Clerkin (2006); (186) Bruch, Fischer & Wilmsen (1987); (187) Saral et al. (2017); (188) Marton et al. (2017).

decline to $N = 0$. Since a variety of light-curve types are seen in high-amplitude YSOs (CP17a), the UGPS amplitude distribution cannot be simply interpreted.

3.2 Known variable stars and other identifications

To identify known variable sources, we performed searches of the SIMBAD data base, supplemented by checks of the General Catalogue of Variable Stars (Samus et al. 2010), the GAIA Photometric Science Alerts data base, the OGLE-III catalogue of variable stars, the K2 archive of the *Kepler* satellite and the *CoRoT* catalogues available at the VizieR data base. In addition, we searched the Witham et al. (2008) catalogue of IPHAS Hα emitters, the Viironen et al. (2009) catalogue of IPHAS PN candidates and the full list of individual source catalogues used by Acero et al. (2015) for

automatic source association with the *FERMI* catalogue of high energy sources.

Only 22 of the 618 variable stars were previously known as variable stars before our UGPS searches. Most of these, 15/22, are long-period variables on the AGB, these typically appearing as isolated bright red stars in the WISE three colour images. A smaller group, 5/22, are cataclysmic variables (CVs, either dwarf novae or novae). Nova Cyg 2008 (source 391) has the second highest amplitude in our catalogue, with $\Delta K = 4.40$. Most of the variable AGB stars and AGB star candidates (11/15) are OH/IR stars or OH/IR candidates but two are classified as carbon stars (source 335 = IRAS 19304+2529 and source 591 = RAFGL 5625) and one (source 389 = IRAS 19558+3333) is an 8.4 GHz radio source likely to be a D-type symbiotic star (Belczyński et al. 2000; Seaquist & Ivison 1994), a system containing a Mira variable and a compact
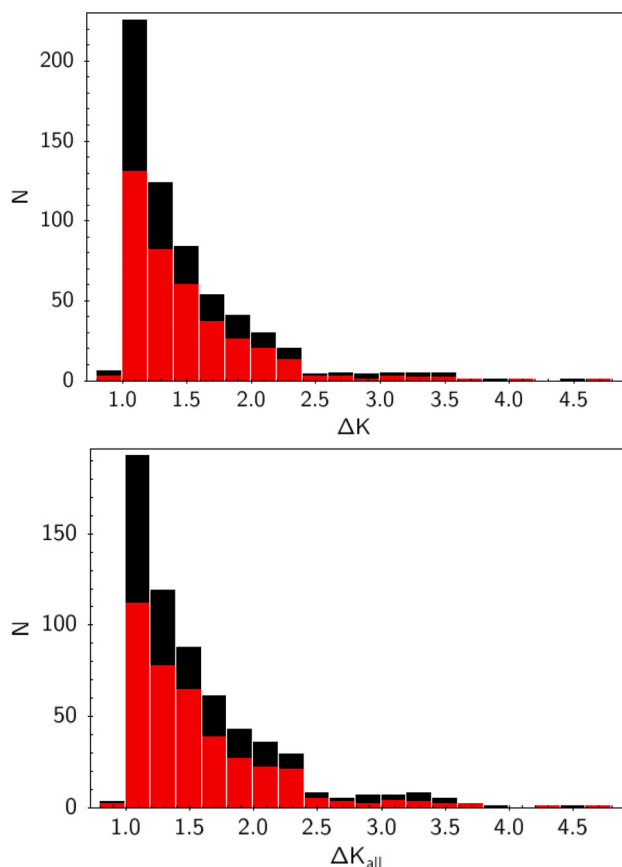
Figure 3. Distribution of amplitudes for the 618 variable stars in the catalogue. Upper panel: two-epoch amplitude ΔK from UGPS. Lower panel: amplitude ΔK_{all}, which includes a third epoch of photometry in K_s from 2MASS, where available. The subset classified as likely YSOs is shown in red. A few sources have $\Delta K = 0.98$–1.00 due to small calibration adjustments between the FITS catalogue photometry and DR10, see Appendix B.

object with a circumstellar disc. Source 301 (IRAS 19210+1448) is classified as a likely O-rich AGB star (Kwok et al. 1997); this seems probable because it is a very bright IR source (W4 = −2.4 in the WISE 22 µm passband) that satisfies our AGB star selection (see Section 3.4.1), even though it is on the outskirts of the W51 star formation region in a field containing several YSOs from the catalogue of Kang et al. (2009). For some of the AGB stars, it is unclear from the literature whether variability had been verified in past studies but typically the 'probability of variability' column in the *IRAS* catalogue of point sources (Beichman 1988) has a value above 90 per cent.

The two remaining known variables are source 366, the binary central star of planetary nebula IPHASX J194359.5+170901 (=the Necklace nebula, see Corradi et al. (2011) and source 551 (=2MASS J20500940+4426522), a candidate eruptive variable YSO in the North America/Pelican nebula from the two epoch mid-IR search of Scholz et al. (2013). The latter has received little attention since its discovery. We discuss it further in Section 4.2.2.

Apart from known variable stars, 81 sources were listed in SIMBAD as known YSOs or YSO candidates. The number of YSOs in the catalogue is actually much higher, see below. Five sources in the Cygnus X region are identified in Makin & Froebrich (2017) as YSOs driving molecular outflows, see Section 4.2.1. In addition, four catalogue members (sources 41, 103, 326 and 555) are emission-line stars included in a list of candidate PNe from the IPHAS survey (Viironen et al. 2009). However, it is uncertain

whether any of these actually are PNe. Sources 103 and 555 are located in SFRs, have low PN scores (0.38 and 0.36 respectively, as defined in Viironen et al. 2009) and have red spectral energy distributions (SEDs) consistent with our YSO interpretation. Sources 41 and 326 have PN scores of 2.02 and 1.01, respectively, which are more promising indications of PN status. However, source 41 is one of several red or green sources visible in the WISE three colour image and its near-IR colours are consistent with either a classical T Tauri star or a PN. The YSO interpretation seems more likely, given the presence of adjacent YSO candidates and because such objects are more common than PNe. Source 326 is in a field with less evidence for star-forming activity and the near-IR colours would be unusual for a YSO ($J - H = 0.27$ and $H - K = 0.61$). However, it has a very high-amplitude ($\Delta K_{all} = 2.96$), having faded monotonically from $K_s = 13.19$ in 2000 June (2MASS data) to $K = 14.79$ in 2005 September and $K = 16.15$ in 2010 July. Such a high IR amplitude would be extreme for the usual PN mechanism of a binary central star in which a hot white dwarf component irradiates one hemisphere of the companion star (as in the Necklace nebula). The nature of this Hα-emitting source is therefore unclear. [We note that sources 41 and 326 lack WISE W3 detections so it is not possible to distinguish them from YSOs in the W1–W2 versus W2–W3 plane in the manner indicated by Koenig & Leisawitz (2014), in fig. 10 of that work.]

One other catalogue member, source 83, was identified as a blazar of type II by Ackermann et al. (2015). This variable is the gamma-ray source 3FGL J0631.2+2019 from the *Fermi* Large Area Telescope Third Source Catalog (Acero et al. 2015).

3.3 Proportion of YSOs

We classify the majority of the individual variable stars (390/618 or 63 per cent) as likely YSOs. This was initially based on 395 sources (64 per cent) identified as YSOs in the literature or having spatial associations with SFRs, determined with the SIMBAD data base and simple inspection of the WISE mid-IR three colour images available at the Infrared Processing and Analysis Centre (IPAC). Subsequently, we re-classified four sources as likely AGB stars projected against SFRs and one source as an evolved star of uncertain nature (see Section 3.4.1). We searched for indications of star formation within a 5 arcmin radius of each variable. This radius was found in Paper I to be large enough to include most sources associated with pre-MS clusters but small enough to avoid including a high proportion of chance associations. The SIMBAD search was then expanded to a 10 arcmin radius to aid YSO identification and distance estimates but matches at 5–10 arcmin were treated with caution and associated distances are given in the catalogue only if it seems likely that there is a genuine association with a spatially extended SFR.

In SIMBAD, we searched for objects generally accepted as star formation indicators such as H II regions, YSOs and YSO candidates, molecular clouds, infrared dark cloud (IRDCs), Herbig–Haro objects, class II methanol masers, millimetre (mm) and submillimetre (submm) sources and clusters with ages ≤10 Myr. We required a minimum of five SIMBAD indicators within a 5 arcmin radius to classify a variable star as a YSO, unless the variable itself was listed as a YSO or YSO candidate or it was located within 5 arcmin of a pre-MS cluster. In the WISE three colour images (blue, green and red corresponding to the W1 (3.3 µm), W2 (4.6 µm and W3 (12 µm) filters, respectively) we required either a bright red or pink nebula to be present (indicating a likely H II region) or at least five red, yellow or green stars within 5 arcmin (normal stars generally appearing blue in WISE). Examples are given in Fig. 4. In the great majority of cases the designation as a likely YSO was clear from
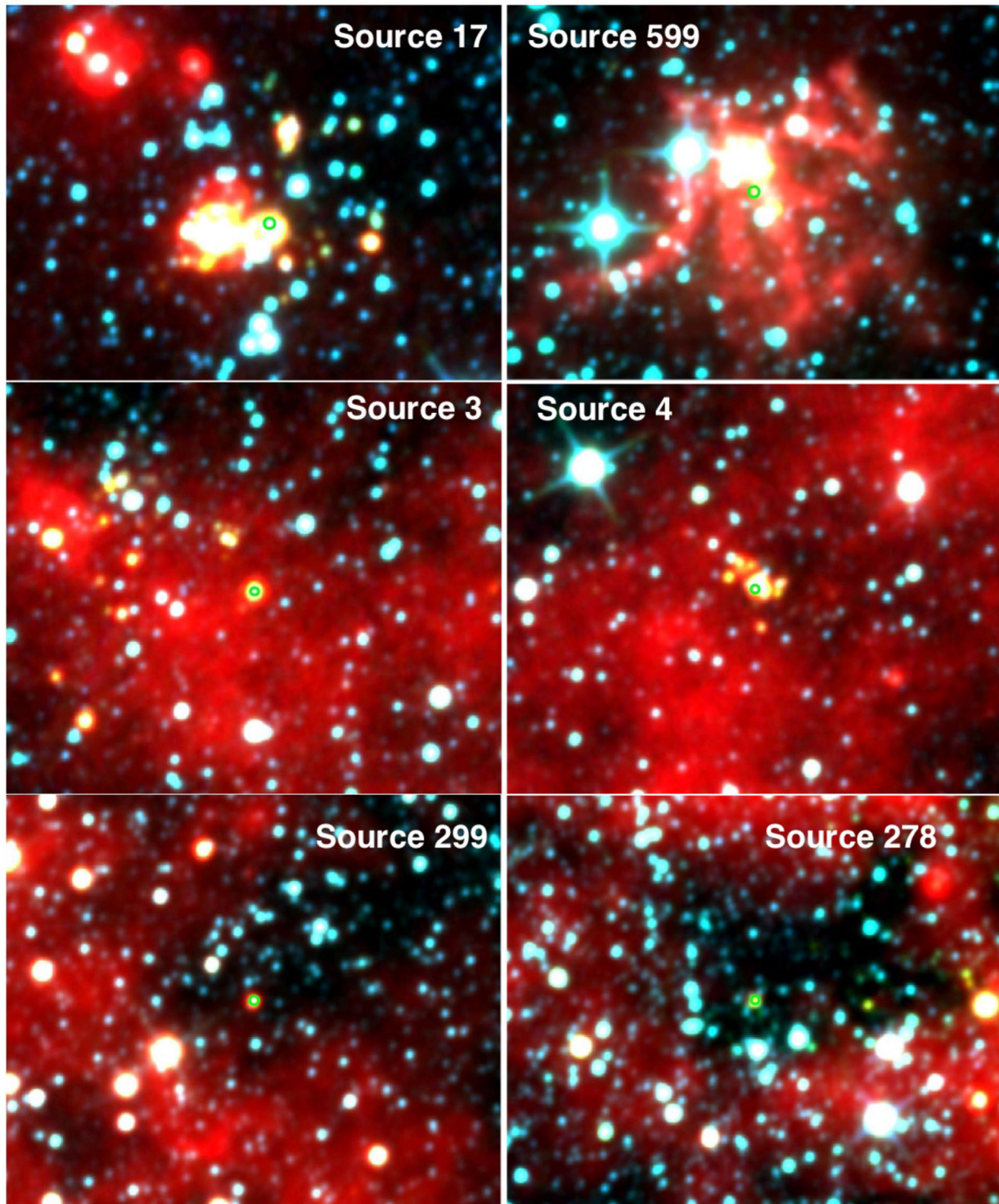
Figure 4. Examples of YSO/non-YSO classification using WISE three colour images: W1 (3.3 μm, blue), W2 (4.6 μm, green) and W3 (12 μm, red). Normal stars usually appear blue, whereas YSOs often appear red, yellow or green. Each image is 10 arcmin across with north at the top and east at left. The variable stars are marked with a green circle at the centre of each panel, though not all are clearly seen in WISE. The variables in the top and middle panels are classified as likely YSOs, but those in the lower panels are not. Source 17 is in the clearly apparent pre-MS cluster [FSR2007] 0671 (Froebrich et al. 2007), so the WISE image was not required. Source 599 is in a previously uncatalogued SFR and likely H II region associated with IRAS 21401+5228, see Section 4.3. Source 3 is at the edge of a small uncatalogued group or cluster of pre-MS stars centred on IRAS 03262+5536. Source 4 is in a marginally resolved uncatalogued group of YSOs. Sources 299 and 278 are in inner Galaxy mid-plane fields where YSO identification is more difficult. The field around source 299 contains several bright stars that have red edges, but most of these are probably distant AGB stars (see the text). The source 278 field contains several rather faint green sources in the dark area at right of centre. This is likely an IRDC, but it is unclear whether the green stars are YSOs or background stars.
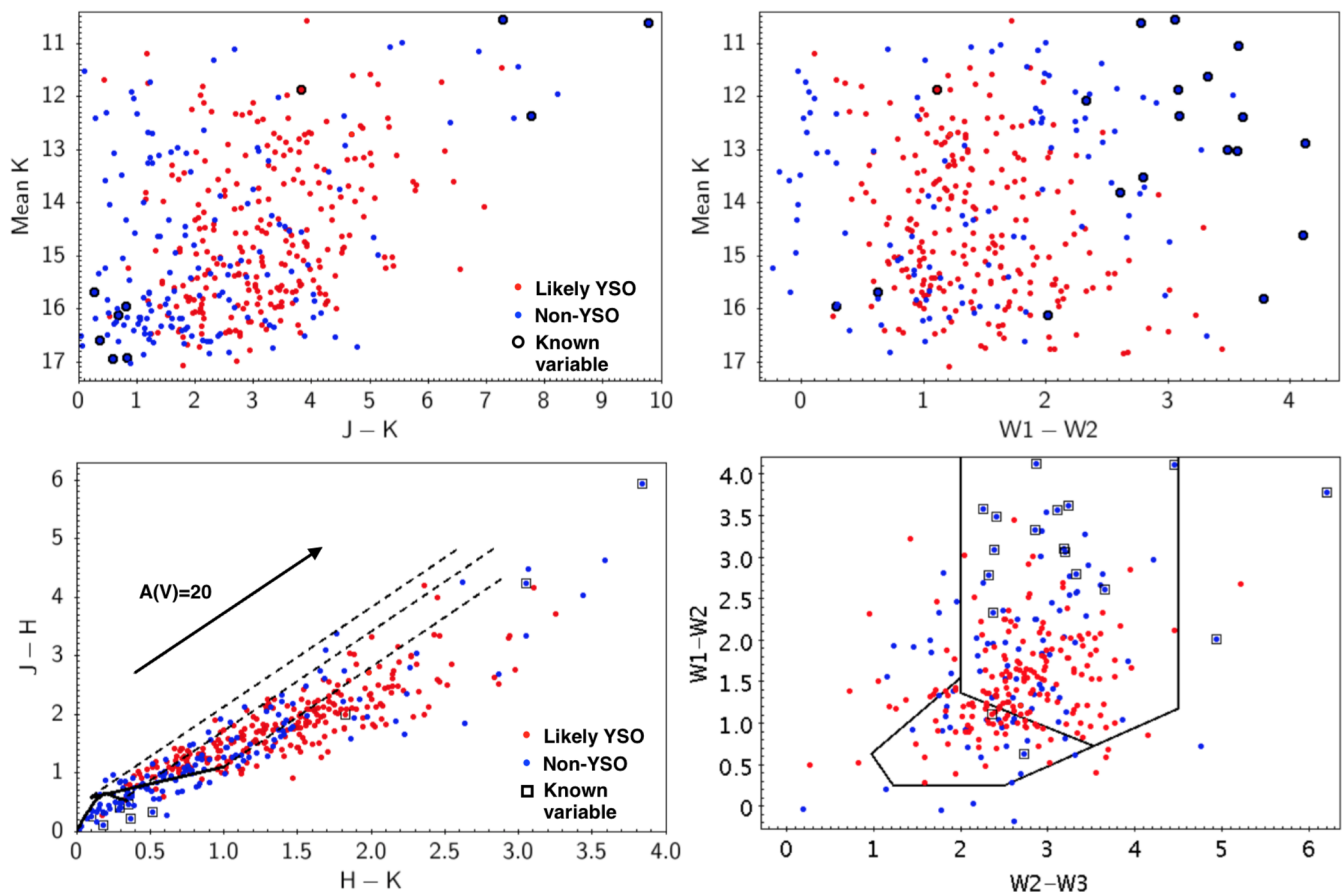
Figure 5. CMDs and two colour diagram for likely YSOs (red points) and non-YSOs (blue points). Known variables are circled in black circles in the upper panels and black squares in the lower panels. Upper left: mean UGPS K versus $J - K$. Upper right: mean UGPS K versus W1–W2. Lower left: near-IR two colour diagram, with dashed lines illustrating the reddening paths from the CTTS (solid line) and the MS (curve). Reddened MS stars should lie between the left and central dashed lines, whereas classical T Tauri stars may lie between the left and right dashed lines. Protostars and other stars with large amounts of circumstellar matter may lie to the right of all the dashed lines. Lower right: W1–W2 versus W3–W4, with solid lines enclosing the typical locations of class I YSOs (upper part) and class II YSOs (lower part), see Koenig & Leisawitz (2014). The locations of the likely YSOs in the lower panels support their position-based classification. Known variables are mostly dusty AGB stars (sources redder than most YSOs, often undetected in J) or CVs (faint blue sources, often undetected in W1 and W2).

the apparent spatial association, such sources typically appearing as red, yellow or green stars themselves if they were detected by WISE. (Sources fainter than W3 = 11 are often undetected in the W3 passband so faint YSOs with red SEDs typically appear green (due to their large W1–W2 colour) rather than red in the three colour images). Additional care with inspection of WISE images was required on inner galaxy mid-plane sightlines, defined $l < 65°$ and $|b| < 1°$, owing to (i) the presence of numerous bright AGB stars and (ii) numerous spatially extensive IRDCs. The O-rich AGB stars common in the inner Galaxy (excepting unusually red dusty types) typically have $0 < \text{W1–W3} < 1.25$, $\text{W3} < 7$ (e.g. Tu & Wang 2013). They appear slightly red around the edges of the stellar profile in WISE three colour images but they are noticeably less red than YSOs, see Fig. 4 (lower left panel). We therefore did not consider such slightly red and unusually bright stars as an indication of star formation, given the notable lack of any accompanying population of fainter red, yellow or green stars in the field. IRDCs tended to cause all faint background stars in an area of a few square arcminutes to appear green in WISE three colour images (see Fig. 4, lower right panel), similar to many bona fide YSOs. IRDCs are often but not always associated with active star formation so without more detailed analysis it was not always possible to assign YSO status to

sources in fields with extensive IRDCs using the WISE and UGPS images alone. Consequently, a small number of possible YSOs are not identified as such in the 'Source Type' column of the catalogue but we note the possibility in the 'Association' column.

The red colours of the likely YSOs support this classification, with most showing signs of $(H - K)$ colour excess in the near-IR two colour diagram (Fig. 5, lower panel)[1] or a location within the YSO selection region of Koenig & Leisawitz (2014) in the W1–W2 versus W2–W3 diagram (Fig. 5, solid lines in the lower right panel). The YSO selection region in the latter plot is divided into class I (upper part) and class II (lower part) with flat-spectrum systems spanning the division. Koenig & Leisawitz (2014) show that this selection region is not exclusive: it includes active galactic nuclei (AGN) and AGB stars (the latter marked as blue data points enclosed in black boxes in the class I YSO region) but it does at least serve

---

[1] The reddening vector displayed in Fig. 5 is based on the Rieke & Lebofsky (1985) extinction law. This is essentially indistinguishable from the very slightly curved reddening tracks derived by Stead & Hoare (2009) for UKIDSS data, after allowing for the effects of spectral type and changes in the effective wavelength of the broad-band filters with extinction.
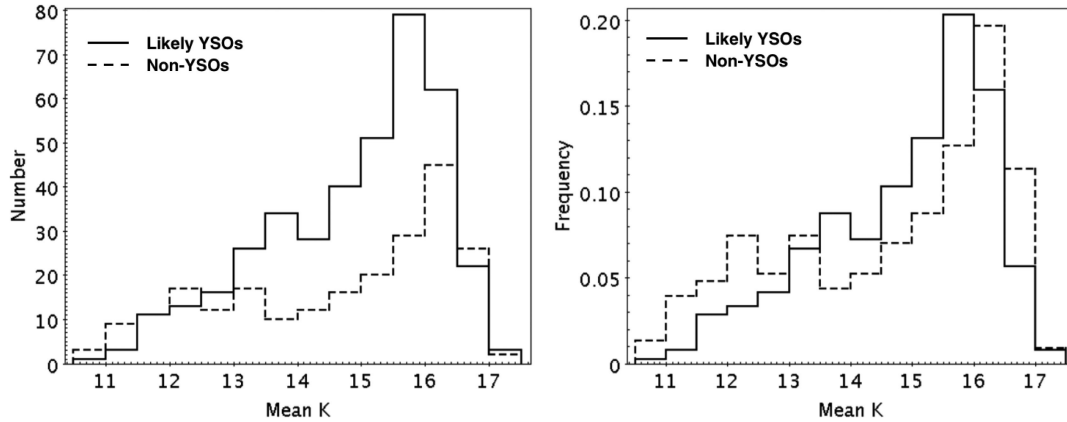
Figure 6. Mean UGPS *K* magnitude distributions for likely YSOs and non-YSOs. Left: absolute numbers. Right: normalized distributions, each with unit area.

to show consistency with our position-based classification. Sources that lie outside the YSO selection region are not excluded as YSOs since the selection was designed to include most but not all YSOs. Class III YSOs have WISE colours near zero on both axes: there appear to be very few in the catalogue.

The comparison of the W1–W2 colours with those of normal stars in the Galactic plane is stark, e.g. 233 of the 390 YSO candidates are detected in W1 and W2 and almost all (231/233) have W1–W2 > 0.25. By contrast, in a random sample of UGPS stars in the two-epoch footprint, we found that only 4 per cent have W1–W2 > 0.25 (based on a sample with W2<14, a limit that includes the bulk of the YSO candidates). The 37 per cent of stars not spatially associated with SFRs tend to have bluer near-IR colours (Fig. 5, upper left panel), except for the brighter stars that are likely to be dusty AGB stars in many cases (see Section 3.4.1).

To quantify the incidence of chance associations with SFRs, we randomly selected 200 of the 62 million stars that passed all our selections save variability from the UGPS two-epoch sky at $30 < l < 230°$. We inspected SIMBAD and the WISE three colour images for these in the same manner as the variables and found that 13 per cent were spatially associated with SFRs by chance. However, since non-YSOs account for no more than half the catalogue, this means that the 'likely YSO' proportion of 64 per cent is reduced by only about 6.5 per cent, leaving 57–58 per cent as YSOs. Five likely YSOs were subsequently re-classified as AGB stars or evolved stars, see Section 3.4.1 below, but this does not significantly affect the proportion. We should also allow for the presence of some relatively isolated YSOs with too few star formation indicators within 5 arcmin to pass our selection. This seems likely given the existence of a substantial group of faint stars with W1–W2 colours and $(H − K)$ colour excesses similar to the likely YSOs in the two colour diagrams, see Figs 5 and 7. Therefore, we round up the figure and quote the proportion of YSOs in the catalogue as 60 per cent, to 1 s.f.

We note that that catalogue includes a small number of published YSO candidates not yet listed as such in SIMBAD, typically relatively isolated objects that did not pass our position-based selection. E.g. sources 286 and 291, located about 0.5° away from the W51 complex and source 171, located about 0.4° from the W43 cluster (Saral et al. 2017). Similarly, the recent machine learning-based all-sky selection of YSO candidates by Marton et al. (2016) (based on AllWISE and 2MASS photometry) includes 28 members of the catalogue, six of which failed our YSO selection due to their relative isolation and a further two of which we classify as dusty AGB

stars in Section 3.4.1. For the sake of consistency (since we cannot identify all such omissions from SIMBAD), we do not include these candidates in our total of 390 likely YSOs but we note their candidacy in the 'Association' column of the catalogue. The nature of high-amplitude IR variability is such that it often involves sources with IR excess due to circumstellar matter, sometimes rare objects that would not be considered as likely contaminants even in the very careful colour-based YSO searches mentioned above. By retaining the 'unclassified' status of these relatively isolated YSO candidates we aim to assist follow-up searches for rare objects in the catalogue.

The 60 per cent proportion of YSOs is similar to the proportions found in VVV (c. 50 per cent, see CP17a) and our initial UGPS study (66 per cent, see Paper I). This confirms our earlier conclusion that they dominate the high-amplitude near-IR variable sky on Galactic disc sightlines and extends the previous result to a much wider range of longitudes. The observed mean surface density of variable YSOs (0.25 deg^{-2}) is very similar to that seen in Paper I and the magnitude distribution rises towards our sensitivity limit even in nearby SFRs. In Paper I, we argued that the mean space density of high-amplitude YSOs is higher than that of Mira variables in the Galactic disc (Miras being the commonest type of high-amplitude variable seen in the optical waveband, see e.g. the General Catalogue of Variable Stars, Samus et al. 2010). Our new results support this, particularly given that high-amplitude YSO variability extends down to low-mass systems (see Section 4.1.3) and the rising magnitude distribution. We refer to Paper I for the details of the argument.

3.4 Non-YSO variables

The distributions of mean UGPS *K* magnitudes are a little different for the 'likely YSO' and 'non-YSO' subsets, see Fig. 6. (We use 'non-YSO' to refer to the subset that did not pass our YSO selection even though there will be some YSOs in that group, see Section 3.4.3.) The proportion of non-YSOs is relatively high at *K* < 13.5 and at *K* > 16.

To aid our discussion of non-YSOs, in Fig. 7, we plot mean UGPS *K* versus W1–W2 and mean UGPS *K* versus I1–I2 colour–magnitude diagrams (CMDs) for the non-YSOs only, with stars in our dusty AGB star selection region (see Fig. 8 indicated with green squares. The various IRAC I1 and I2 data sets are generally slightly deeper than the WISE All-Sky catalogue W1 and W2 data but cover only part of the area. The I1–I2 ([3.6]–[4.5]) and W1–W2 ([3.4]–[4.6]) colours are based on similar passbands but while the two colours correlate closely and agree for blue stars,
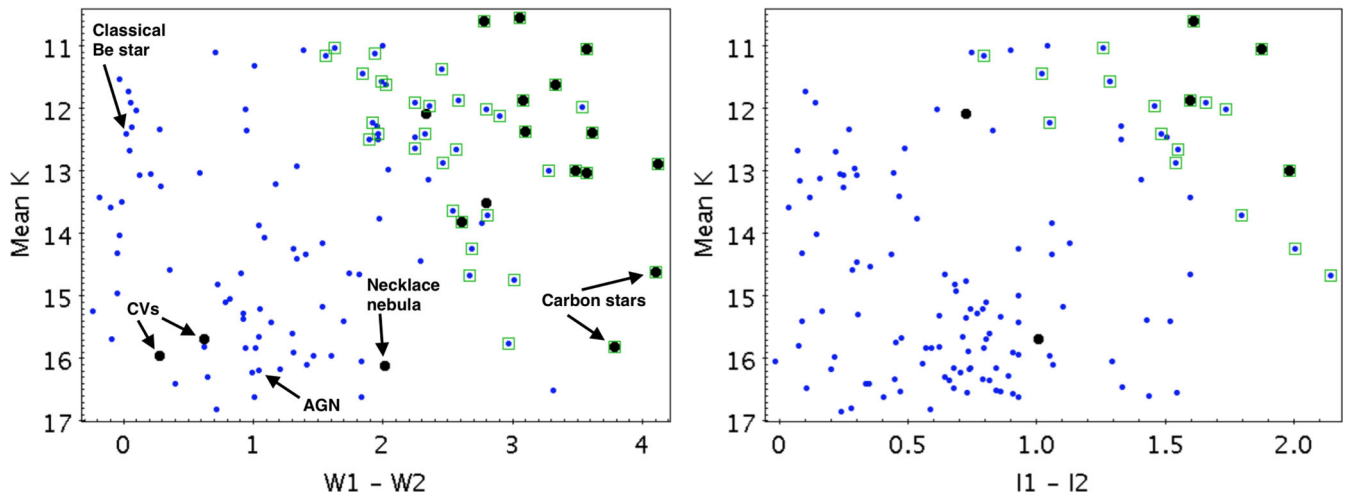
Figure 7. CMDs for non-YSOs. Left: mean UGPS *K* versus WISE W1–W2. Right: mean UGPS *K* versus *Spitzer*/IRAC I1–I2. The IRAC I1 and I2 data are a little deeper than WISE W1 and W2, but they do not cover the full area of the UGPS catalogue. Known variables are marked in black and variables in our dusty AGB star selection region in Fig. 8 are enclosed in green squares. Dusty AGB stars mostly found at the upper right. The nature of the small group of bright blue variable stars in the left-hand panel is unclear, see the text. The larger group of faint variables includes both faint red stars (some of which will be relatively isolated YSOs) and faint blue variables such as CVs, EBs and AGN, seen in greater numbers in the upper left panel of Fig. 5.

W1–W2 has progressively larger values than I1–I2 for redder stars in our catalogue. (This is true for both non-YSOs and likely YSOs). Cutri et al. (2012) noted that W1–I1 becomes progressively larger with increasing I1–I2 for red sources at high Galactic latitude, with considerable scatter about the mean trend, but they did not discuss the cause. They found W2–I2 to be colour-independent: we see the same trend for these two pairs of filters in our sample of highly variable sources. The W1:I1 differences for sources with red SEDs may in part be due to the slightly shorter effective wavelength of W1 than I1 but we note that it could be a signpost of strong 3.1 μm absorption by molecules such as water ice in the W1 passband, which is centred at 3.4 μm but has significant response down to 2.8 μm.

Circumstellar water ice would only be present in systems with cold circumstellar matter such as YSOs and very red O-rich AGB stars (OH/IR stars) with high mass-loss rates (e.g. Meyer et al. 1998; Sylvester et al. 1999). However, two other strong 3.0–3.1 μm absorbers, hydrogen cyanide (HCN) and acetylene (C_2H_2), are commonly observed in dusty AGB stars, arising either from the circumstellar shell (in O-rich AGB systems) or in the photospheres of carbon stars, see Groenewegen, de Jong & Geballe (1994). These molecular features should often play the same role in reddening W1–W2 more than I1–I2, with acetylene becoming more important in low-metallicity stars (Yang, Chen & He 2004; Matsuura et al. 2005; van Loon et al. 2008). We note that Antoniucci et al. (2014) provide IRAC to WISE photometric transformations for YSOs (using a mostly low-amplitude sample). While they did not discuss molecular absorption, their transformations indicate a similar trend for W1–W2 to be substantially redder than I1–I2, mainly due to differences between W1 and I1.

3.4.1 Bright red variables: AGB stars

The relatively high proportion of non-YSOs at $K < 13.5$ very likely reflects the presence of many dusty AGB stars, as indicated by the extremely red colours of many bright non-YSOs in the CMDs (Figs 5 and 7) and supported by the locations of several known OH/IR stars found at the upper right of the mean *K* versus W1–

W2 plot in Fig. 7). One known AGB variable star system with similar mean *K* and W1–W2 colour to the OH/IR stars is source 389, which is thought to be a D-type symbiotic system, as noted in Section 3.2. The mean magnitude histogram of the sample of 816 VVV variables in CP17a was bimodal, due to the large number of AGB variables found at bright magnitudes. That is not the case here because most AGB stars, especially normal AGB stars, are too bright to appear in our search, owing to shorter distances to the edge of the Galactic disc and lower extinction on most sightlines in the two epoch UGPS area, compared to the VVV disc region. [Mira variables typically have absolute $M_K = -6$ to -8, e.g. Knapp et al. (2003), so $d > 25$ kpc would be required for $K > 11$, in the absence of extinction].

However, the two known carbon stars in the sample are somewhat fainter than the other known AGB stars in the sample (mean $K = 14.6$ and 15.8) indicating that these typically less luminous AGB stars can contribute to the faint end of the distribution (see e.g. Ishihara et al. 2011).

In Fig. 8, we show that the W3–W4 versus W1–W2 two colour diagram can be used to identify many of the AGB stars. The known AGB stars are mostly found at the lower right of this diagram and there is a substantial group of non-YSOs (i.e. sources not satisfying our YSO selection) that extends to the left and down from the group of known AGB stars (black circles) and candidate AGB stars (green squares) clearly separated from the majority of YSOs. [The five candidate AGB stars were identified by Lewis & Grinspoon (1990), Chengalur et al. (1993), Kwok et al. (1997) and Yung et al. (2014)]. Sources in this region of the plot, as far to the left as W1–W2 = 1.5, are in every case amongst the brightest mid-IR sources in the catalogue, as shown in the middle and lower panels of Fig. 8. All of these satisfy the criterion W2 < 7.8 that was used by Robitaille et al. (2008) to statistically distinguish 'extreme' dusty AGB stars with high mass-loss rates from YSOs and normal AGB stars (that study actually used IRAC I2, which gives almost identical magnitudes to W2 due to the similar bandpass.

Only six sources initially classified as likely YSOs are found in this 'dusty AGB star' region of the W3–W4 versus W1–W2 diagram, all of which have W2<7.8. These can readily be explained
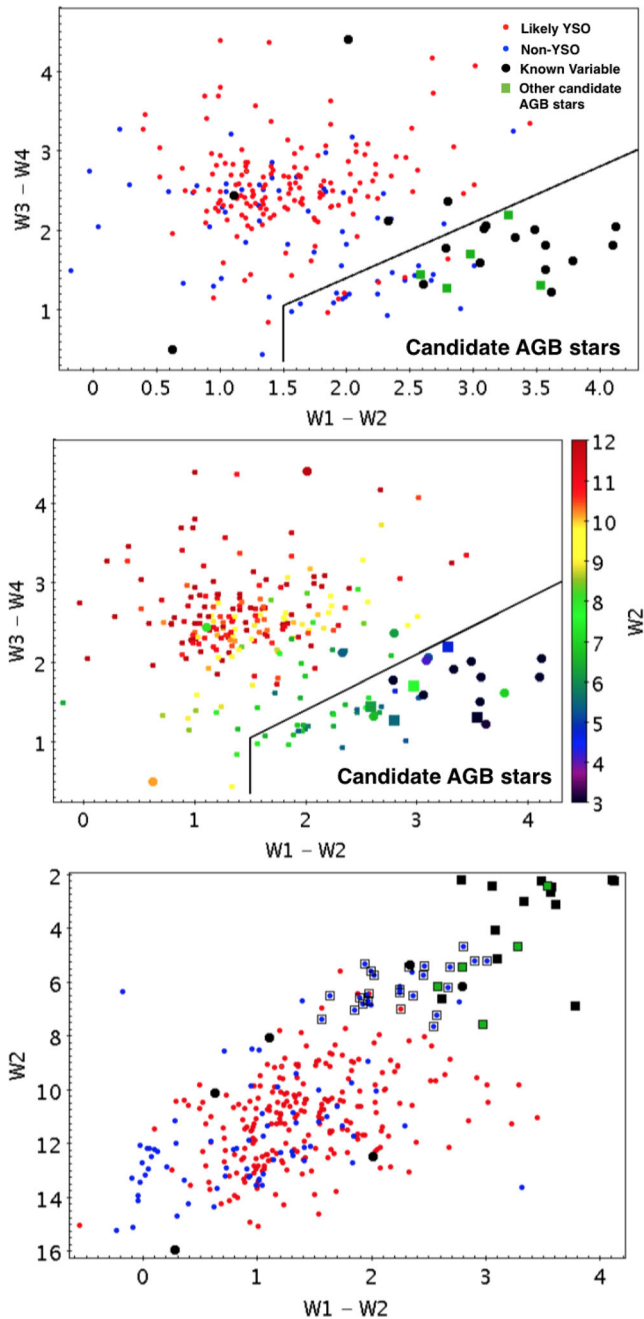
Figure 8. Selection of candidate AGB stars. Top: WISE two colour diagram with likely YSOs in red, non-YSOs in blue, known variables as large black points and other candidate AGB stars from the literature as large green squares. The known variables are mainly dusty AGB stars located at lower right, save for a CV at lower left, a PN central star at top and a candidate eruptive YSO at centre left. The dividing line encompasses most of the known AGB stars, while including only five sources projected against SFRs. Middle: as upper panel but with W2 mag colour-coded to illustrate how the simple colour selection picks out the brightest mid-IR stars. Bottom: W2 versus W1–W2 CMD with the same colour coding as the upper panel. The 42 sources in the AGB selection region are enclosed in squares.

as chance projections of AGB stars against SFRs (see Section 3.3) with the exception of sources 143(=GPSV3) and 239(=GPSV15). Source 143 was classified as an eruptive variable YSO in Paper I on the basis of an emission-line spectrum, location in the Serpens OB2 association and luminosity-based problems

with an AGB star classification. A similar classification was given for source 239 in Paper I for similar reasons, though this object is isolated rather than located in an SFR. For the present, we classify it as a likely YSO rather than an AGB star but we note that its nature is uncertain. With these two exceptions, we classify 40 sources as likely AGB variable stars that satisfy:

$$W3 - W4 < 0.7(W1 - W2)$$

$$W1 - W2 > 1.5$$

as indicated by the solid lines in Fig. 8. Of the 40 stars, 22 were previously known as AGB stars or candidate AGB stars, though four of the candidates were identified only by the selection of Robitaille et al. (2008), which we do not plot as candidates because there is much more scatter in colour and magnitude when their 'standard AGB stars' are included and these were not identified as variable. The sources in our selection region generally follow the K-[12] versus $H - K$ colour–colour locus defined by van Loon et al. (1998) for O-rich AGB stars, though source 301 is closer to the carbon star locus shown in that work. (The two known carbon stars in the sample are among 15/40 stars in the region that were undetected in H).

The cut at W1–W2 = 1.5 was imposed because the two stars just to the left of this boundary are less luminous in the mid-IR (W2 > 7.8), though one of these, source 203, has W2 = 7.87, I2 = 7.77 and therefore might be an AGB star despite being classified as a likely YSO due to its location in an IRDC that appears to host several YSOs. Two known AGB stars, source 351(=GLMP 939 = IRAS 19374+1626) and source 216(=IRAS 18569+0553), lie a little way outside our AGB region in Fig. 8, closer to the main group of YSOs. Several other stars located close to the AGB region are bright mid-IR stars that may well be AGB stars but our selection appears to capture the majority of the dusty variable AGB population with sufficient colour separation to suggest that it might be useful in other studies. We note that several authors have previously published colour selections for AGB stars or OH/IR stars (e.g. van der Veen & Habing 1990; Lewis & Grinspoon 1990; van Loon et al. 1998; Ishihara et al. 2011), but our selection differs in that it is defined for the high-amplitude variable sky. In particular, Koenig & Leisawitz (2014) proposed a very similar scheme to separate AGB stars from YSOs in the W3–W4 versus W1–W2 two colour diagram. However, their template sample of dusty AGB stars did not include any sources with W1–W2 > 3, with the result that their proposed selection would misclassify some of the reddest known variable AGB stars in our catalogue as YSOs (these having W3-W4 > 2 by a small margin). Our selection therefore appears to be better for the reddest AGB stars, which lie in a region of colour space where there are no YSO candidates. The selection of Koenig & Leisawitz (2014) would be better for bluer, more typical AGB stars with less circumstellar matter but these are generally saturated in UGPS, as noted above.

An additional evolved star, of uncertain nature, is source 507(=GPSV34, see Paper I and Contreras Peña 2015). This bright and fairly red source (mean UGPS $K = 12.35$, W1–W2 = 0.95, $J - H = 2.74$, $H - K = 1.82$) is projected in the Cygnus X star-forming complex near the DR17 H II region. It lies outside our AGB star selection region (since it is not red enough in W1–W2) and Contreras Peña (2015) showed that a mass-losing AGB star that followed the typical colour–luminosity relation of Ishihara et al. (2011) would be at a distance of ∼35 kpc, far outside the Galactic disc. The spectrum presented in Contreras Peña (2015) shows strong $\Delta v = 2$ ^{13}CO absorption lines, indicating an evolved star

that has been through at least the first dredge up to increase the $^{13}C/^{12}C$ ratio. Some remaining possibilities may be a mass-losing AGB star in the Galactic halo or a relatively low-luminosity AGB star such as a J-type carbon star (Morgan et al. 2003). We note that there are also a variety of the rare R Cor Bor stars, thought to be formed from binary white dwarf mergers, and related cooler objects (DY Per stars), in which large optical variations are caused by dust formation events and semiregular pulsations (e.g. Tisserand et al. 2009; Otero et al. 2014). While these extinction events do not typically have high amplitude in the IR, we should not discount the possibility.

3.4.2 Bright blue variables

Amongst the bright, non-YSO population there is a fairly distinct blue group of seven stars in the left-hand panel of Fig. 7 with $0 < W1 - W2 < 0.1$, $11 < K < 13$. These sources all have relatively blue near-IR colours ($J - K_c < 1.25$), relatively low amplitudes ($1 < \Delta K < 1.5$, and $1 < \Delta K_{all} < 1.5$). One of this group, source 234 (=GPSV13), is an Hα emitter previously discussed in Paper I as a likely classical Be star with extreme variability for such objects. However, none of the other six members of this bright blue group appear to be Hα emitters (based on IPHAS photometry, see Appendix B and Section 4.1.4). Balmer line emission is variable in classical Be stars so absence of Hα excess means little in individual cases but it would be somewhat surprising if all members of this group are classical Be stars. The locations of these stars in the IPHAS $r - H\alpha$ versus $r - i$ two colour diagram are consistent with moderately reddened B-type MS stars or lightly reddened G to early K-type dwarfs. Their locations in the UGPS $J - H$ versus $H - K$ diagram favour the B-type option, with extinction values $A_V \approx 2$–9, consistent with the IPHAS data for each star.

The nature of this small group is presently unclear but the simplest explanation is that most of them are eclipsing binaries (EBs) in which a smaller but more luminous early-type star is eclipsed by a less luminous giant star. In CP17a, we examined the results of Armstrong et al. (2014) for the Kepler EB sample and found that EBs with amplitudes in K_s above 1 mag should be dominated by systems with F- and G-type primaries because early-type primaries emit less of their flux in the IR. However, the one previously known EB in the CP17a sample is the detached (Algol-type) system PT Cen, an A2V+G6IV system (Budding et al. 2004) with $\Delta K_s = 1.2$. This suggests that EB configurations involving early-type primaries and subgiants, for example are a possible explanation for the small group of bright blue variables.

3.4.3 Faint red variables

The higher proportion of sources classified as non-YSOs at $K > 16$ (see Section 6) appears to be due to a combination of one or more faint, relatively blue populations adding to a redder population that has the same UGPS, WISE and IRAC colours as the YSO population, see Fig. 5. It is likely that many of the faint red sources are indeed YSOs that were not selected in our search for sources spatially associated with SFRs, as indicated by the fact that a few of them are found within the areas occupied by the spatially extensive Cygnus X and Gemini OB1 groups of variable YSOs (see Section 4.2). However, other types of faint high-amplitude variable star can be red sources. The left-hand panel of Fig. 7 shows a few faint, very red AGB stars and new candidate AGB stars. We have also mentioned source 366, the binary central star of a PN. Source 366 is located in the region at $W2 - W3 > 4$ that includes many

PNe, as shown in the W1–W2 versus W2–W3 plot in Koenig & Leisawitz (2014) (fig. 10 of that work). However, in our catalogue, it is the only non-YSO in this sparsely populated colour space (see Fig. 5) that is also an Hα emitter (see Section 4.1.4). Other PNe may however be present that are too faint for a detection in W3 (see Section 3.2) or in IPHAS or VPHAS+ Hα images.

Source 83, identified in Section 3.2 as a likely blazar is also a faint red source (mean GPS $K = 16.19$, $W1 - W2 = 1.04$, $J - H = 0.84$ and $H - K = 0.91$). It is well established that blazars, including both radio loud optically violent variable quasars and radio-quiet BL Lac objects are highly variable sources in the IR and across the electromagnetic spectrum, e.g. Takalo et al. (1992) and Webb et al. (1988). In these rare types of AGN, the consensus model involves inverse synchrotron emission by a highly beamed relativistic jet oriented very close to the line of sight, enabling variability of several magnitudes on a range of time-scales from days to years, ultimately attributable to accretion variations in the black hole disc, (Blandford & Rees 1978; Ghisellini et al. 1993). Blazars have near-IR colours in the range $1 < J - K < 2$, in the absence of Galactic extinction (Raiteri et al. 2014). While this is bluer than most YSOs in the catalogue, near-IR colours can of course be reddened by extinction and the WISE colours strongly overlap with those of YSOs (Raiteri et al. 2014).

Some low-luminosity symbiotic stars and some CVs are also red sources (e.g. Phillips 2007; Rodríguez-Flores et al. 2014; Hoard et al. 2002). It would therefore be unsafe to classify faint red variables as likely YSOs without spectroscopic data. We note that our SIMBAD- and WISE-based selections of YSOs may reasonably be expected to be a little less complete at faint magnitudes, given that UGPS contains many distant low-mass star formation regions that are unstudied (Lucas et al., in preparation) and may not be identifiable by simple inspection of WISE or UGPS images.

3.4.4 Faint blue variables

The faint blue non-YSO variables with mean UGPS $K > 14.5$ typically have $J - K < 1.5$ (see Fig. 5) and these have $J - H < 1$, $H - K < 0.72$. A total of 45 objects satisfy this colour selection, though there is no clear colour separation from the redder population. This faint blue component might plausibly be composed of CVs, EBs and AGN. Of the known variables with blue $J - K$ colours and mean UGPS $K > 15.5$, 5/6 are CVs. The sixth, source 335, is the PN binary central star mentioned above, a source distinguished by its red mid-IR colour (W1–W2 = 2.0). It is plausible that previously undetected CVs are numerous amongst the faint blue population.

In Paper I, we noted that a small proportion of AGN can vary by >1 mag in K, see Kouzuma & Yamaoka (2012). The only known AGN in our sample is a fairly red object, a member of the rare blazar subclass often characterized by variability of a few magnitudes, see Section 3.4.3. However, the broader sample of variable AGN studied by Kouzuma & Yamaoka (2012) have relatively blue near-IR colours and the very few with $\Delta K > 1$ would have relatively low amplitudes within our catalogue ($1 < \Delta K < 1.5$), similar to most of the faint blue variables. Most of the faint blue sources are located on sightlines with relatively low near-IR extinction ($|b| > 2°$) so the colours are also consistent. In the mid-IR, AGN typically display redder colours fairly similar to those of YSOs (Koenig & Leisawitz 2014), but unfortunately the sensitivity of WISE is insufficient to detect most of the faint blue variables and aid classification. Scaling up the calculation in Paper I to the area of this study, we might expect ~30 variable AGNs to be included in the sample, in

the absence of extinction. The five known CVs all displayed higher amplitudes so the data suggest it is indeed possible that AGN are contributing significantly to the faint blue membership of the catalogue.

In CP17a, we found that EBs may have a space density comparable to that of YSOs amongst the variable population with $1 < \Delta K_s < 1.6$, though not at higher amplitudes. The VVV sample of CP17a contained only 72 EBs and EB candidates (9 per cent of that sample). By randomly sampling 10 000 pairs of data points separated by at least 1.8 yr from the light curves of each of the 72 VVV sources available in CP17a (with 45–50 data points each), we estimate that only 7 per cent of all EBs would be recovered in a two epoch search, which compares with 25 per cent of YSOs (Paper I). EBs and YSOs made up 9 per cent and about 50 per cent of the VVV sample, respectively. If we assume they would be present in the same relative proportions in the area surveyed here and correct for the lower EB proportion recovered by two epoch sampling, we estimate EBs should make up ∼3 per cent of the catalogue, or ∼18 objects. Alternatively, if we simply scale the 72 EBs found amongst 12 million VVV stars to the 62 million UGPS stars selected for the present search and then correct for the 7 per cent recovery fraction then we expect ∼24 EBs in the present data set. Both estimates are crude, owing to differences in Galactic populations on different sightlines and the fact that the search of CP17a was incomplete due to being based on typically only 17 early data points. (This is rather low for detection of eclipses covering perhaps ∼10 per cent of orbital phase, a typical fraction for deep eclipses in the Kepler Eclipsing Binary Catalogue, Prša et al. 2011; Kirk et al. 2016). Nonetheless, it appears that a mix of EBs and AGN can explain most of the faint blue population with amplitudes ($1 < \Delta K < 1.5$), with CVs likely comprising most of the rest of this population at $\Delta K > 1.5$.

We refer the reader to Section 4.1.4 for a discussion of the H α emission properties of the catalogue. We see there that three faint blue variables with $\Delta K_{\text{all}} > 2$ are also H α emitters, consistent with a CV interpretation. In Section 5.2, we discuss the most intriguing faint blue object in the catalogue, source 363, which is also an H α emitter.

4 THE VARIABLE YSO SAMPLE

4.1 General properties

4.1.1 Spectral indices and amplitudes

In Fig. 9 (upper panel), we plot the distribution of spectral index for the likely YSOs (165/390) that have a 22 or 24 μm detection in WISE or MIPSGAL. Using the divisions of Greene et al. (1994), the overwhelming majority of these sources (95 per cent) are either class I systems, defined by $\alpha > 0.3$, or flat-spectrum systems, defined by $-0.3 < \alpha < 0.3$. This distribution is of course influenced by selection effects given that class II and class III YSOs will typically be too blue to be detected in the WISE W4 or MIPSGAL 24 μm passband. In addition, the gradual decline in the distribution at $\alpha > 0.4$ is influenced by the fact that sources with redder SEDs are more likely to fall below the $K \approx 16$ magnitude limit of the UGPS variable catalogue.

The 156 systems with $\alpha > -0.3$ make up 40 per cent of the full sample of likely YSOs. We can gain a better idea of the proportion of class I or flat-spectrum systems by considering the I1–I2 and W1–W2 colours of faint YSOs lacking a 22 or 24 μm detection. Inspection of our sample of likely YSOs and the 'Cores to
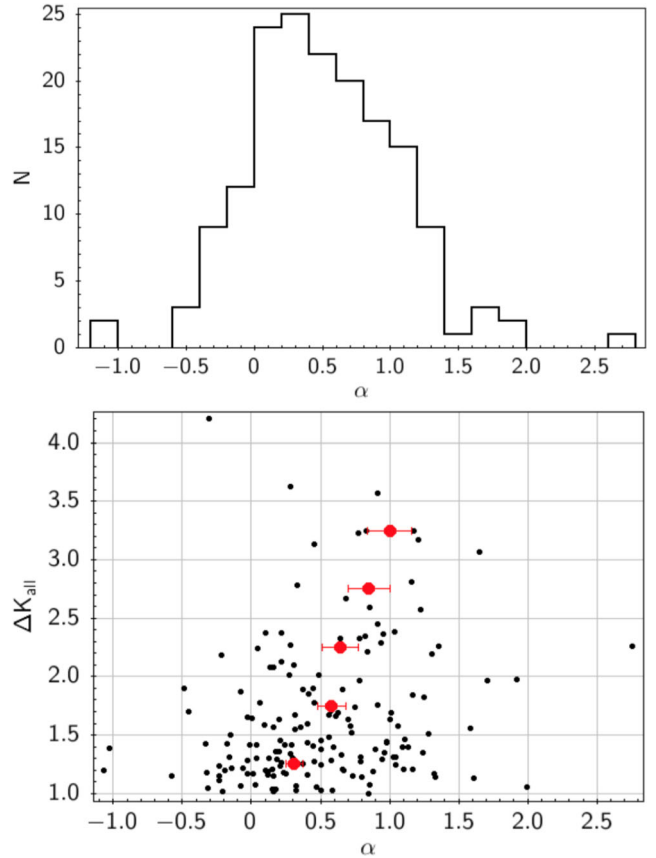

Figure 9. Upper panel: histogram of the distribution of 2–22 μm spectral index, α. Lower panel: amplitude ΔK_{all} versus α. YSOs with larger amplitudes show a subtle tendency to have redder spectral indices, as illustrated by the large red points corresponding to the median of α in amplitude bins of width 0.5 mag, up to $\Delta K_{\text{all}} = 3.25$. Error bars represent the standard error, $\sigma/\sqrt{N}$.

Discs' sample of Evans et al. (2009) indicates that YSOs satisfying the condition 'W1–W2> 1.4 OR I1–I2> 1' almost always have $\alpha > -0.3$. Moreover, at least half of YSOs that satisfy a second condition '0.8<W1–W2<1.4 OR 0.6<I1–I2<1' also have $\alpha > -0.3$. Considering likely YSOs in the catalogue that lack a measurement of spectral index, 52 satisfy the first condition and 80 satisfy the second. If we add the 52 and half of the 80 to the 156 likely YSOs with measured $\alpha > -0.3$, we find that ∼64 per cent are class I or flat-spectrum systems. The true proportion is likely to be higher because some faint YSOs were not detected by *Spitzer* or WISE in any passband. We note that while a few distant YSOs suffer sufficient foreground extinction to influence the calculation of spectral index, this appears to be a very minor effect for the sample of 390 likely YSOs, most of which have a J detection and relatively low extinction in comparison to the VVV sample of CP17a (see Section 4.1.2). We see no significant correlation between distance and spectral index.

The high proportion of class I or flat-spectrum systems supports the result of CP17a that these SED classes are found more frequently amongst high-amplitude YSOs than in the YSO population as a whole. E.g. Dunham et al. (2014) found that class I and flat-spectrum YSOs represent only 28–31 per cent of YSOs in nearby SFRs, being heavily outnumbered by class II systems. Since we have photometry at only two or three epochs we cannot test the result of CP17a that
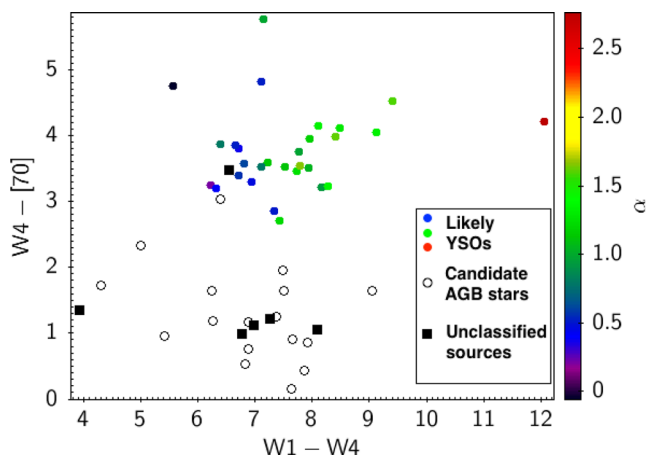
Figure 10. Separation of variable YSOs and dusty Mira variables in the W4–[70] colour. The W4–[70] versus W1–W4 two colour diagram shows a fairly clean separation of YSOs (filled circles) and AGB stars (open circles), supporting our position-based YSO selection method and our mid-IR selection method for dusty AGB stars. Unclassified sources (filled black squares) mostly lie amongst the AGB stars. The YSOs are colour-coded by spectral index, which is closely correlated with the W1–W4 colour.

the trend towards red SEDs is strongest amongst YSOs with eruptive light curves.

In Fig. 9 (lower panel), we plot amplitude against spectral index. There is a subtle but clear tendency for YSOs with higher amplitudes to have redder spectral indices, as illustrated by the large red points that give the median spectral index for bins of width $\Delta K_{all} = 0.5$, in bins from $\Delta K_{all} = 1.25$ to 3.25. Error bars show the standard error for each bin. The Pearson's correlation coefficient, r, for these 165 data points is only 0.221 but this is a significant correlation given the size of the data set: the probability that $|r| > 0.2$ for a set of 100 randomly generated points is only 4.6 per cent, falling to 1.3 per cent for $|r| > 0.25$ (Taylor 1997), so we can be confident in this result. Relatively few YSOs with $\Delta K_{all} > 1.5$ have $\alpha < 0$ and all YSOs with amplitudes $\Delta K_{all} > 2.5$ are class I systems, save for one system with $\Delta K_{all} > 4$ located on the class II/flat-spectrum boundary.

Our cross-match against the *Herschel*/PACS 70 μm data (see Appendix B) recovered 52 members of the catalogue, see Fig. 10. These comprise 29 likely YSOs (27 class I and two flat-spectrum systems), 6 unclassified sources and 17 sources classified in Section 3.4.1 as dusty AGB star candidates via the W3–W4 versus W1–W2 two colour diagram. The YSOs and the AGB stars are quite well separated in the W4–[70] colour, owing to the relative lack of dense cold dust around the AGB stars. This further verifies our WISE-based colour selection of the AGB stars. Moreover, the plot shows that the likely YSOs, identified mainly by our position-based selection, have the colours expected for class I and flat-spectrum systems. Comparison with fig. 2 of CP17b shows that the W4–[70] and W1–W4 colours are very similar to those of spectroscopically confirmed high-amplitude YSOs in the VVV sample as well as the MIPS [24]–[70] and I1–[24] colours of class I or flat-spectrum YSOs in the Perseus cloud complex (Young et al. 2015).

Of the six unclassified sources, five have W4–[70] colours similar to the likely AGB stars. This is unsurprising given that four of these five have WISE colours that place them in the region between our fairly conservative AGB star selection region and the main body of YSOs in Fig. 8. The fifth object, source 183, appears in SIMBAD as an unstudied *IRAS* source (IRAS 18492−0148). With W1−W2

= −0.18, it is in a sparsely populated part of Fig. 8 but inspection of the WISE images and GLIMPSE photometry shows that this colour is erroneous (caused by a rogue W1 datum) and this source is indeed likely to be a dusty Mira variable.

While all the likely YSOs in Fig. 10 have the expected colours, one candidate AGB star (source 158) and one unclassified source (source 278) are located amongst the YSOs. Source 278 was unclassified despite the presence of several adjacent faint green sources in the WISE three colour image, due to concerns that these might be normal background stars reddened by an IRDC (see Section 3.3). The WISE colours in Fig. 8 are similar to those of YSOs so we can be fairly confident that this source is actually a YSO, though we note that the PACS detection has a signal-to-noise ratio of only 2. Source 158 (a high signal-to-noise ratio PACS detection) was classified as a candidate AGB star by Robitaille et al. (2008), using their simple probabilistic colour–magnitude selection of YSOs and AGB stars. The WISE colours also place it firmly in the dusty AGB star region of Fig. 8. The WISE three colour image shows no sign of additional YSOs in the field but there is some fairly bright 12–22 μm nebulosity a few arcminutes east (not unusual given the inner Galaxy mid-plane location) and a bright 22 μm nebula immediately adjacent that might relate either to previous mass loss or to star formation activity. Given the unusual SED, this source is not readily classified.

4.1.2 Luminosities and distances

The bolometric luminosities span a wide range, from $L_{bol} \sim 0.1$ to $\sim 10^3 \, L_\odot$, see Fig. 11, though only rarely exceeding $10^{2.5} \, L_\odot$. (Distances of likely YSOs were taken from the literature via spatial association with individual SFRs, see Appendix B). The plotted luminosities are estimated only for sources with 2–22 μm photometry, using the ratio of measured luminosity in this range, L_{2-22}, to L_{bol} based on data for nearby YSOs from the 'Cores to Discs' project (Evans et al. 2009) and WISE photometry. The plotted luminosities do not include the effect of foreground extinction, which the data in table 9 of that study show would increase the L_{bol} by a factor from 1 to 4 for YSOs with typical extinction and spectral indices in the range $0 < A_V < 12$, $0 < \alpha < 1$. (This assumes that the measured extinction is all in the foreground, rather than the YSO disc and envelope, thereby indicating the maximum possible correction). Individual luminosities are uncertain (and not given in Table 1) especially for sources with $\alpha > 0$ where there is substantial scatter in the L_{bol} versus L_{2-22} ratio. However, we were able to fit this ratio as a function of α and F_{22}/F_{12} (or very similarly F_{24}/F_8) with a standard deviation of 0.15,[2] such that luminosities should typically be correct within a factor of 2 (0.3 dex). The least luminous variables with $L_{bol} \lesssim 0.1 \, L_\odot$ include some nearby sources with low extinction ($A_V = 1$–4 for sources 594, 555 and 101 at $d = 800$–900 pc) and several additional GLIMPSE sources with similar absolute I1–I4 magnitudes that lack 22 or 24 μm detections. Therefore, the presence of YSOs with $\sim 0.1 \, L_\odot$ is reasonably secure, limited only by the sensitivity of the search. This suggests that the episodic accretion phenomenon extends down to the low-mass peak of the initial mass function, though this is of course hard to quantify given the debate over the existence of the stellar birthline (e.g. Baraffe et al. 2009).

---

[2] The equations used were: $L_{2-22}/L_{bol} = 0.39$ ($\alpha < -1.3$) $L_{2-22}/L_{bol} = 1.01 + 0.4\alpha - 0.047F_{22}/F_{12}$ ($-1.3 < \alpha < -0.5$) $L_{2-22}/L_{bol} = 0.71$ ($-0.5 < \alpha < 0$) $L_{2-22}/L_{bol} = 0.83 - 0.275\alpha - 0.217\log(F_{22}/F_{12})$ ($\alpha > 0$).
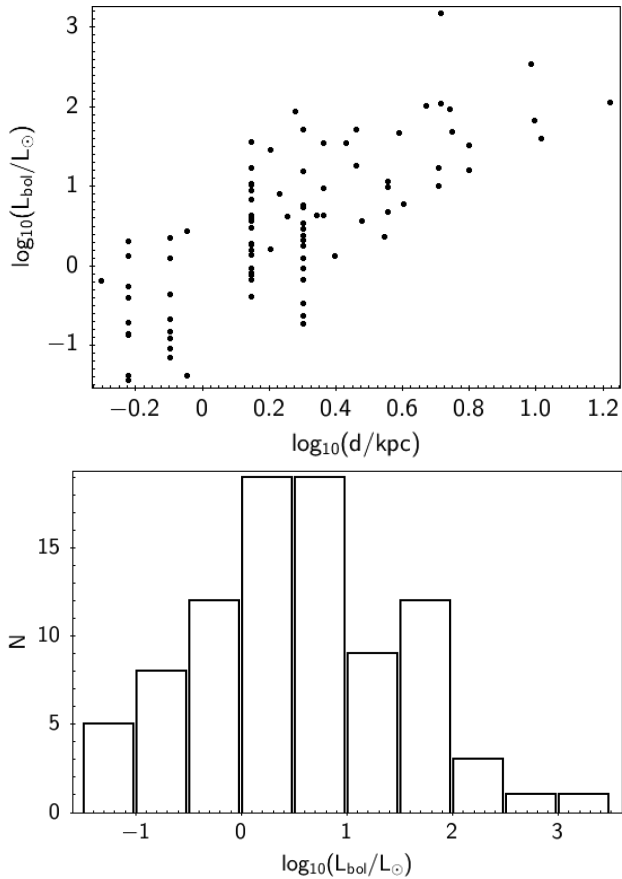
Figure 11. Upper panel: estimated bolometric luminosity versus distance for likely YSOs with 2–22 μm detections. Luminosities are based mainly on the 2010 epoch of 3–22 μm data from the WISE All-Sky catalogue. Lower panel: histogram of estimated bolometric luminosity.

Previous examples of very low-luminosity eruptive variable YSOs include V1180 Cas (Kun et al. 2011), with $L \approx 0.07 \, L_\odot$ in the low state, ASASSN-13db (Holoien et al. 2014) with $L \approx 0.1 \, L_\odot$ pre-outburst and two eruptive candidates with high 3.5 μm amplitudes identified by Antoniucci et al. (2014), referred to as sources 828 and 1247 in that work. A few others (e.g. EX Lup) have $L = 0.1$–1 $L_\odot$ when in the low state, see Audard et al. (2014). Our calculated luminosities are dominated by the WISE data from 2010 so they will correspond to a mix of low state, high state and intermediate values.

The two most luminous sources plotted, with $L_{bol} = 10^{2.5}$–$10^3 \, L_\odot$, are both sources at large distances with very red SEDs ($d > 5 \, \mathrm{kpc}$, $\alpha \gtrsim 0.7$). While a few known optically bright eruptive YSOs in a nearby SFR are saturated in UGPS images (see Section 4.2.2) neither of these two embedded YSOs (sources 325 and 229) are close to the catalogue bright limit in UGPS K and all other sources have $L_{bol} \lesssim 10^{2.0}$. The surveys have sufficient sensitivity to detect luminous YSOs across the Milky Way, as is evident from Fig. 11. Hence the rarity of luminous variables appears to be genuine, even allowing for a factor of 3 or 4 underestimate of luminosity due to extinction. The rarity may be due to the fact that the photospheres of luminous YSOs typically produce more luminosity than the accretion disc even at very early evolutionary stages, e.g. Calvet et al. (1991). One might expect variable extinction to influence the light curve more often than variable accretion amongst luminous YSOs. Only a few luminous eruptive variables ($> 10^3 \, L_\odot$)

Table 2. Expected proportions of YSO light-curve types as a function of UGPS amplitude. Each column is normalized to ∼100 per cent.

Light-curve type	ΔK (mag)			
	>1 (%)	>1.5 (%)	>2 (%)	1.0–1.5 (%)
Short-term variable	11	4	2	15
Eruptive	36	38	36	34
Fader	24	32	40	19
Long-term periodic variable	15	13	14	17
Dippers	12	13	8	12
EBs	1	0	0	2

have been previously identified: the class I YSO V723 Car (Tapia, Roth & Persi 2015) in NGC 3372 and several distant embedded candidates identified by Kumar et al. (2016) from the sample of CP17a as (usually) the most luminous YSOs in their respective SFRs. In addition, a very luminous YSO undergoing episodic accretion, S255IR NIRS3, was recently found by Caratti o Garatti et al. (2016).

We also plotted amplitude against luminosity (not shown) but found no correlation between these two variables. This suggests that in YSOs similar processes occur to cause high-amplitude variability across the measured range of luminosities.

4.1.3 Expected light-curve types

In Paper I, we used the two-year K_s time-series data set of Carpenter et al. (2001) for the Orion nebula Cluster to show that high-amplitude YSOs discovered by our two epoch search should mostly have long-term variability on time-scales of years rather than short-term variability on time-scales of days or weeks. The recent CP17a sample of 441 high-amplitude YSO candidates allows us to revisit that calculation with a longer time series (4 yr), better sampling of long time baselines and far more high-amplitude variables. We randomly sampled 10 000 pairs of points from all the CP17a light curves in each of the YSO light-curve categories defined therein (short-term variable, eruptive, fader, dipper, long-period variable YSO and EB), with a minimum time baseline of 1.8 yr. We find that short-term variables should constitute only 11 per cent of a high-amplitude ($\Delta K > 1$) YSO sample selected using two widely separate epochs. This fraction falls to 4 per cent if a $\Delta K > 1.5$ threshold is used, and 2 per cent above a $\Delta K > 2$ threshold. These results should be applicable to the YSOs in the present UGPS catalogue, allowing for minor caveats such as a small amount of contamination by non-YSOs in the CP17a YSO sample and the fact that UGPS time baselines range from 1.8 to 6.3 yr. We conclude that variability in the overwhelming majority of YSOs in our catalogue is predominantly on time-scales of years. The proportions in the different light-curve categories given by our sampling experiment are listed in Table 2 for various amplitude thresholds and ranges. We see that eruptive light curves and faders should dominate the UGPS sample, especially at higher amplitudes. Eruptive light curves are thought to be caused by episodic accretion in most cases (see CP17b). The same may also be true for the faders and long-period YSOs, though evidence in CP17b was more limited for those light-curve types.

Note that the table does not include the effects of contamination by non-YSOs projected against SFRs, such as pulsating AGB stars, AGN, CVs and EBs (see Section 3.3). While we have attempted to identify most of AGB stars in the sample via colour selection (see Section 3.4.1) a small number will remain. Late M-type AGB
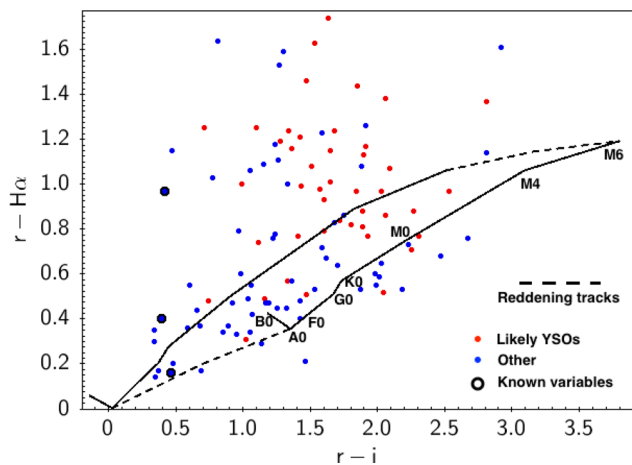
Figure 12. IPHAS $r-\mathrm{H}\alpha$ versus $r - i$ two colour diagram. Solid lines show the MS tracks from B0 to M6, with zero reddening (left track) and $E(B - V) = 2$ (right track). Red points are likely YSOs, most of which show clear evidence for $\mathrm{H}\alpha$ emission, based on location above both tracks. Blue points are other variables, almost half of which are also clearly $\mathrm{H}\alpha$ emitters. The three known variables plotted are enclosed large black circles: the central star of the Necklace nebula, dwarf nova EG Lac and Nova Cyg 2008, in descending order of $r-\mathrm{H}\alpha$. The lower and upper dotted lines are the reddening tracks for A0V and M6V stars, respectively.

stars can have IR spectra that somewhat resemble those of FUors and MNors (e.g. CP17b) so light curves may be required to identify them. Similarly, the proportions of EBs listed in the table are based on the numbers projected against SFRs in the study of CP17a, neglecting the fact that not all of these would be YSOs.

4.1.4 $\mathrm{H}\alpha$ emission

In Fig. 12, we plot the IPHAS $r-\mathrm{H}\alpha$ versus $r - i$ two colour diagram for the 108 stars detected in all three optical passbands of the IPHAS DR2. MS tracks are overlaid for zero extinction (left track) and for $E(B - V) = 2$ (right track) using data from Drew et al. (2005). Stars located above the zero reddening track are identified with high confidence as $\mathrm{H}\alpha$ emitters, given that the photometric uncertainties are nearly always smaller than the distance above the track. Three known variables are marked with large black points: the central star of the Necklace nebula, dwarf nova EG Lac and Nova Cyg 2008, in descending order of $r-\mathrm{H}\alpha$. A further 10 sources are detected in all three passbands of the VPHAS+ survey. These are not plotted in Fig. 12 because the r, i and $\mathrm{H}\alpha$ passbands are sufficiently different to shift the MS tracks appreciably (Drew et al. 2014).

At least 64 per cent of the likely YSOs in the plot (red points) are $\mathrm{H}\alpha$ emitters, with equivalent widths up to 250Å (based on comparison with fig. 6 of Drew et al. 2005). All of the other YSOs may also be $\mathrm{H}\alpha$ emitters (if we allow for extinction up to $E(B - V) = 3$), but this cannot be ascertained from a 2D plot in which locations are determined by three variables (spectral type, extinction and $\mathrm{H}\alpha$ emission). Interestingly, almost half (41 per cent) of the sources not classified as YSOs or known variable stars (blue points) are also clearly identified as $\mathrm{H}\alpha$ emitters. Inspection of the near-IR two colour diagram for these sources (not shown) indicates that $\mathrm{H}\alpha$ emitters with $r - \mathrm{H}\alpha > 1$ typically have locations consistent with reddened YSOs, i.e. they deredden to the red end of the classical T Tauri locus (CTTS) or they appear in the 'protostar' region with large $H - K$ colour excesses. Moreover, the subset of these sources

with W1, W2 and W3 detections (eight objects) are all located in the YSO selection region of the W1–W2 versus W2–W3 plot (Fig. 5). It therefore seems very likely that many of these are YSOs with insufficient adjacent indicators of star formation to pass our selection. We note that the IPHAS and near-IR colours of the more common $\mathrm{H}\alpha$ emitting populations are illustrated in Corradi et al. (2008).

The bluer $\mathrm{H}\alpha$ emitters (with $r - \mathrm{H}\alpha < 1$ and $r - i < 1.5$) are typically located below the CTTS locus in Fig. 5, though many of them have redder $H - K$ colours than would be expected for normal MS stars or giant stars. Some of these blue $\mathrm{H}\alpha$ emitters are faint IR sources with similar optical/IR colours and magnitudes to the dwarf nova EG Lac. Most CVs are $\mathrm{H}\alpha$ emitters (Witham et al. 2008) and, as noted in Section 3.4.4, they are one of the three main populations expected to contribute faint blue variables to the catalogue. In support of this, we see that the two bluest unidentified $\mathrm{H}\alpha$ emitting variable stars (sources 359 and 445, with $r - i < 0.4$) both have unusually high amplitudes ($\Delta K_{\mathrm{all}} = 2.84$ and 2.30, respectively) which supports a CV interpretation. Source 127, a VPHAS+ detection not plotted in Fig. 12, also has blue colours ($r - i = 0.39$ and $J - K = 0.04$), $\mathrm{H}\alpha$ emission and a high-amplitude $\Delta K_{\mathrm{all}} = 3.44$, so it can also be considered a candidate CV.

Other blue $\mathrm{H}\alpha$ emitters may be unusual sources such as source 366, the binary central star of the Necklace PN. A new discovery of interest is source 363, discussed separately in Section 5.2. Sources lacking clear evidence for $\mathrm{H}\alpha$ emission and non-YSOs are often relatively bright and blue IR sources (mean UGPS $K < 14$, $J - K < 2$) whose nature is unclear (see Section 3.4.2). However, some of these are red enough to be on the unreddened CTTS locus.

4.1.5 Colour variability

Some information on the physical origin of the variability can be gleaned from the near-IR colour changes between UGPS and 2MASS. In Fig. 13, we show these changes for the 56 likely YSOs with JHK_{s} fluxes from 2MASS that have 'ph_qual' quality grades A, B or C in all three 2MASS passbands. Most sources are fainter in UGPS than 2MASS due to greater UGPS sensitivity and the bright limit of the catalogue set by UGPS saturation near mean $K = 11$. A linear regression fit shows that, on average, flux changes in the J and H passbands are only slightly greater than the change between K_{s} and K, though there is considerable variation for individual sources. Defining ΔJ and ΔH, respectively, as $J_{\mathrm{UGPS}} - J_{\mathrm{2MASS}}$ and $H_{\mathrm{UGPS}} - H_{\mathrm{2MASS}}$, the equations of best fit are $\Delta J = 1.19(K - K_{\mathrm{s}}) + 0.13$ and $\Delta H = 1.09(K - K_{\mathrm{s}}) + 0.17$.

Considering sources with a large positive or negative change in K (upper panel), we see that only a minority lie close to the reddening track (dashed line). Looking at the lower panel, we see that the six sources at the upper right (sources that faded between 2MASS and UGPS) have larger changes in $H - K$, relative to $J - H$, than would be expected from an increase in reddening alone. These may be cases where an accretion-driven outburst led to a large reduction in extinction at the 2MASS epoch (common in eruptive variables) that then reversed as the outburst faded. In the lower panel, the data are colour-coded by flux change: we see that some sources close to the reddening track at the lower left actually faded whilst becoming bluer on both axes. These correspond to sources at the upper left in the upper panel, far from the reddening track. As noted by Lorenzetti et al. (2007), the wide range in measured colour changes may be due to differing locations and temperatures of the part of the disc that has increased in brightness. Those authors found that EXors often become bluer when brighter if the full amplitude of variability
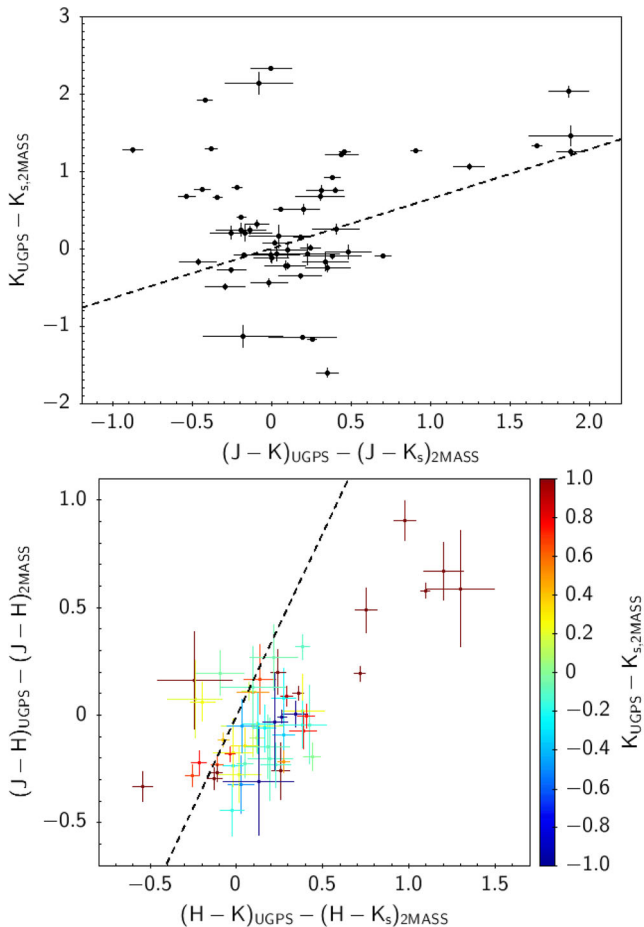
Figure 13. Colour variability. Upper panel: plot of change in flux versus change in colour between UGPS and 2MASS. The reddening track is overlaid as a dashed line. Most sources are fainter in UGPS than 2MASS due to greater survey sensitivity. A few sources with large flux changes lie close to the reddening line but most do not. Lower panel: two colour diagram of colour changes between UGPS and 2MASS, with extinction track overlaid and the change in flux colour-coded. Sources with a large 2MASS:UGPS reddening increase show larger changes in $H - K$ than would be expected from extinction alone. Some sources at the lower left also became fainter while becoming bluer on both axes.

is observed but a wider range of behaviour is observed if only part of the outburst is sampled.

4.2 Spatial groups

In Fig. 1, we show the spatial distribution of the likely YSOs and indicate the locations of overdensities that can be identified with particular well-studied star-forming complexes. Several overdensities are apparent. Below we discuss the well-studied regions containing at least four likely YSOs, except the group in the Serpens OB2 association that was described in Paper I. We also discuss the set of three likely YSOs possibly associated with the massive W43 complex near $l = 31°$. Another set of three likely YSOs (sources 57–59) is located in the S241 H II region. These three all have relatively low amplitudes ($\Delta K_{all} < 1.65$).

An apparent overdensity in the outer galaxy near $l = 217°$ is spatially correlated with two separate little-studied groups of molecular clouds, one at $d \approx 2$–3 kpc in the Perseus arm and another at $d \approx 6$–7 kpc in the Norma-Cygnus arm, see Kamiński et al. (2007). An-

other overdensity of seven sources at $l = 171$–$174°$, $b \approx +2.5°$ corresponds to a large, fairly bright ^{13}CO emission feature visible in the low-resolution maps of Dame, Hartmann & Thaddeus (2001), with a velocity of -17 to $-18\,km\,s^{-1}$. Two sources in this 'L171–174 region' are in the vicinity of the S231/S232/S233/S235 group of H II regions at $l \sim 173$–$174°$ and $d = 1.8$ kpc (Evans & Blair 1981); two more at $l \sim 171$–$172°$ are associated with other molecular clouds in Auriga that appear to be at a similar distance (Liu et al. 2014). While the CO emission breaks down into separate sections in higher resolution maps (Kawamura et al. 1998) it may be that the seven variable sources in the L171–174 region are part of a single large star formation complex. We leave such discussion to detailed studies of large-scale structures, e.g. Kiss, Moór & Tóth (2004) and Liu et al. (2014).

4.2.1 Cygnus X

A large, spatially extended group is located at $75.6 < l < 82.6°$, $-1.5 < b < 3.8°$ corresponding to the massive Cygnus X starforming complex at $d = 1.4$ kpc (Rygl et al. 2012). This region contains 79 likely YSOs and 14 other variables, some of which were listed in Paper I and Contreras Peña (2015). Most of the other variables are relatively faint and unusually red stars (e.g. in the IRAC I1–I2 colour provided by the *Spitzer* Cygnus X project) and some are therefore quite likely to be YSOs with too few adjacent star formation indicators to meet our selection criteria. Fig. 14 shows the locations of the variable stars in this region superimposed on Band A (8.3 μm) images from the Midcourse Space Experiment (MSX, Egan et al. 1998).[3] The major sites of active star formation are labelled (following Schneider et al. 2006, 2007), along with well-studied H II regions and any pre-MS clusters located near individual variables. We see that most of the likely YSOs (red points) are located either near these star formation indicators or in the Cygnus OB2 association at $l = 79$–$81°$ or in bright mid-IR nebulosity (attributable to hot dust or PAH emission in photodissociation regions).

Projected within the bounds of the Cygnus X complex are the more distant region AFGL 2590 at $d = 3.3$ kpc (Rygl et al. 2012) and separately the H II region [WC89] 075.83+0.40 at $d = 5.5$ kpc (Wood & Churchwell 1989). Only one variable YSO appears to be associated with each of these regions: sources 486 and 450, respectively. Chance projections of other more distant YSOs against the extensive Cygnus X complex are of course possible. Many of the 77 likely YSOs that we have associated with the Cygnus X group in column 24 of the catalogue were already identified as YSOs, e.g. 20 stars from the catalogue of Kryukova et al. (2014) and two in the vicinity of the S106 H II region from the catalogue of Gutermuth et al. (2009).

While we have adopted a common distance of 1.4 kpc for all other likely YSOs in Cygnus X, we note that Maia et al. (2016) have recently disputed this (see also Gottschalk et al. 2012), finding that star formation towards this complex is split into layers at $d \sim 0.7$, 1.5 and 3 kpc. Some care regarding this thorny issue is therefore warranted for future studies of these variable stars, though we note that clusters in the sample of Maia et al. (2016) have some spread in age and the older ($\sim$10 Myr) clusters are less likely to host the class I and flat-spectrum systems that dominate the YSO sample. The

---

[3] The MSX data are shown as two images with slightly different contrasts due to limits on the gif-format image sizes, available at the NASA Infrared Survey Archive.
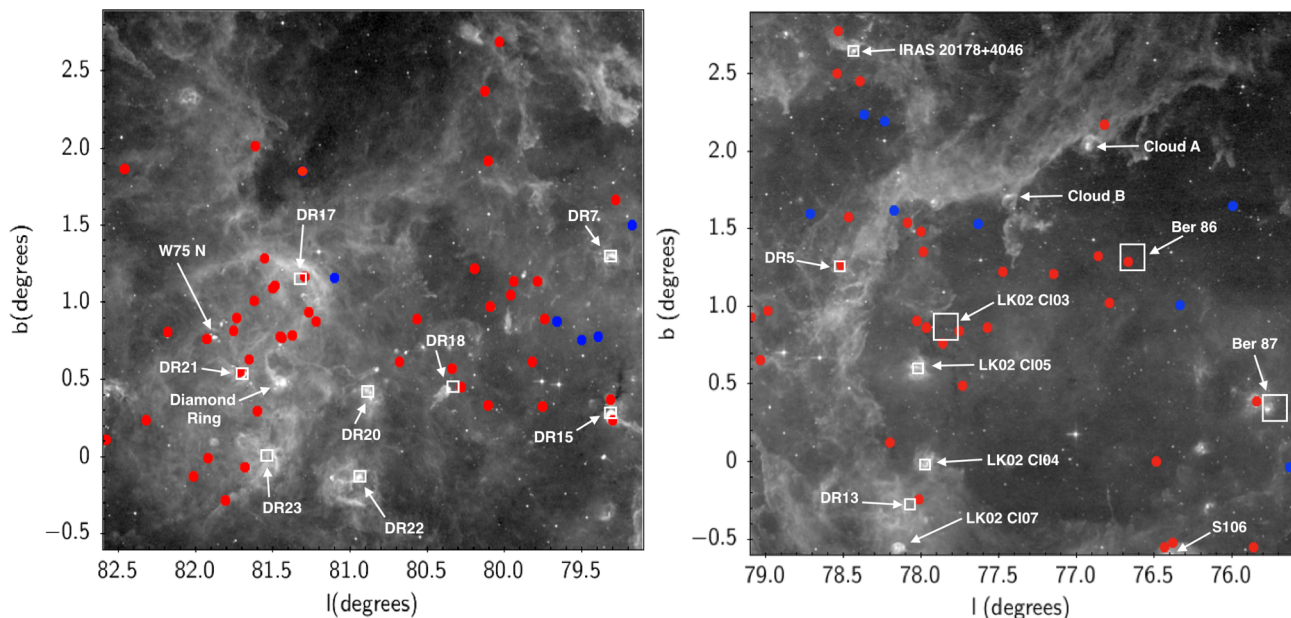
Figure 14. The Cygnus X spatial group. The grey-scale background is the 8.3 µm image data from the MSX satellite. The two panels include almost all of the group. Red circles are likely YSOs and blue circles are other sources. IR-bright SFRs are labelled, along with selected well-known H II regions and pre-MS clusters from Downes & Rinehart (1966) and Le Duigou & Knödlseder (2002) that are located close to variable sources. (Clusters and radio sources are marked with squares, with larger squares for the larger clusters). In the left-hand panel, we see that most of the likely YSOs are located either in the active region of star formation around W75 N, DR21, DR17, DR23 and the Diamond Ring or within the Cyg OB2 association centred near $l = 80°$. In the right-hand panel, there is some concentration of likely YSOs near the LK02 Cl03 cluster and near the upper left portion of the large IR-bright ring that extends from Clouds A and B through DR5, DR13 and down to S106 (see Schneider et al. 2007). However, some likely YSOs are associated with smaller SFRs that are not apparent on this scale.

forthcoming second data release of the *Gaia* mission will of course assist with this and many similar issues concerning other relatively nearby star formation regions.

Ten stars were detected in all three passbands of the IPHAS survey: 9/10 show clear evidence of Hα emission due to location above the MS tracks plotted in Fig. 12. Separately, five stars (sources 40, 80, 93, 109 and 110) are identified as molecular outflow driving sources in Makin & Froebrich (2017) utilizing data from the UWISH2 survey (Froebrich et al. 2011). The amplitudes and mean UGPS K magnitudes of the 77 likely YSOs have a similar distribution to that of the full YSO sample (shown in Figs 3 and 6).

Two sources have amplitudes above 2.5 mag: source 537 (=GPSV35 from Paper I) and source 470. Source 537 has $\Delta K_{all} = 2.81$. It faded from $K_s = 14.04$ in 1998 June (2MASS data) to $K = 15.06$ in 2006 June and then faded further to $K = 16.84$ in 2009 June. It was undetected in the J and H images (from 2009 June), but the WISE and IRAC data both show that it is a very red source (W1–W2 = 2.11, spectral index $\alpha = 1.16$ and I1-I2 = 1.76). Source 537 is one of two variables located in the recently discovered embedded pre-MS cluster [SUH2012] G079.852−01.507 (Solin et al. 2012), located within the LDN 896 dark cloud. This cluster was identified in the UGPS data set and it is very obvious in the WISE three colour images, where an H II region can be seen at the northeastern end of the cluster. The other variable in this cluster, source 538, is similarly faint and red but has a lower amplitude ($\Delta K = 1.16$) and was undetected by 2MASS.

The other very high-amplitude variable, source 470, has $\Delta K = 2.64$. It rose from $K = 18.51$ in 2008 September to $K = 15.88$ in 2011 October. It was undetected by 2MASS. This source is located in the DR5 H II region (Downes & Rinehart 1966) which includes

several YSOs visible within the brightest part of the 12 and 22 µm nebulosity in the WISE three colour images.

A further eight sources have amplitudes $\Delta K_{all} > 2$. However, the highest H-band variability between 2MASS and UGPS is seen in source 521, for which $\Delta H = 4.18$ and $\Delta K_{all} = 1.97$. This source faded from $K_s = 11.90$, $H = 14.27$ ($H − K_s = 2.37$) in 1998 November to $K = 13.87$, $H = 18.45$ ($H − K = 4.58$) in 2006 July before partly recovering to $K = 12.44$ in 2010 October. The change in colour is more than would be expected from a change in extinction alone. The object is located in the dense dust clump BGPS G081.218+00.872 (Rosolowsky et al. 2010).

4.2.2 North America and Pelican nebulae

Adjacent to the Cygnus X group are 17 likely YSOs at $83 < l < 85.5°$, $−1 \lesssim b \lesssim 1°$ associated with the North America nebula (NGC7000) and the Pelican nebula (IC5070), at a distance of only 520–600 pc from the sun (Laugalys & Straižys 2002; Laugalys et al. 2006; Guieu et al. 2009). One other variable is located in this area, source 560(=MSX6C G085.3935+00.1268). We classified this very bright mid-IR source (W2 = 4.69 and W4 = −0.93) as a likely AGB star via the W3–W4 versus W1–W2 diagram (see Section 3.4.1) and it was previously selected as a candidate AGB or post-AGB star by Yung et al. (2014) on the basis of *Akari* colour criteria. Four known highly variable YSOs are located in the region: the classical FUors V1057 Cyg and V1515 Cyg Herbig (1977), the unusual eruptive variable HBC 722 (=V2493 Cyg, Semkov et al. 2010) and VSX J205126.1+440523 (=V2492 Cyg, Itagaki & Yamaoka 2010; Covey et al. 2011), a source that may have both variable extinction and variable accretion (Kóspál
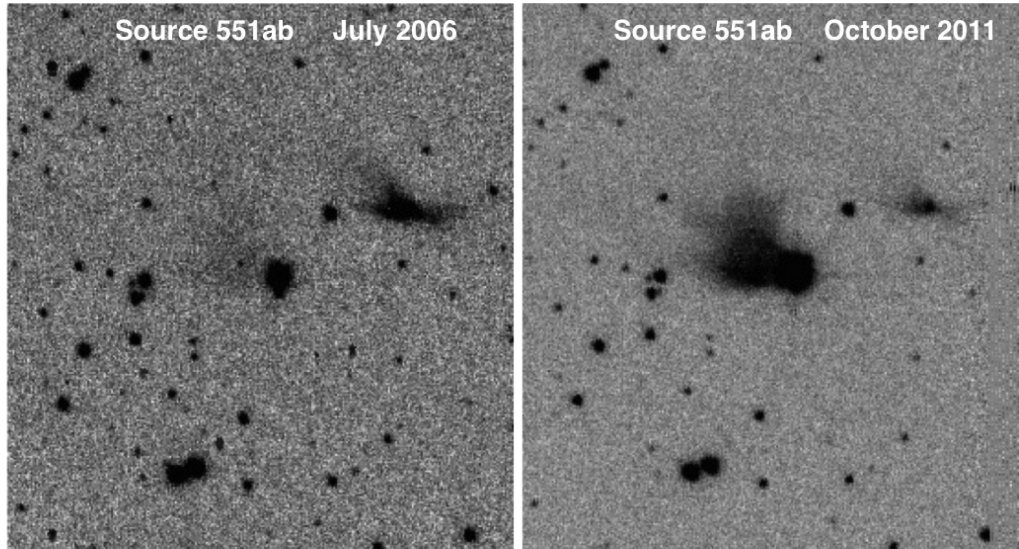
Figure 15. UGPS K images of source 551ab ($=$2MASS J20500940+4426522). This pair of highly variable YSOs within the North America nebula have unusually extensive nebulosity and they may be a bound system. The primary at the centre is the only variable YSO in the catalogue that was identified as an eruptive YSO candidate prior to our UGPS search, see Scholz et al. (2013). The images are 1 arcmin across and they have conventional equatorial orientation.

et al. 2011). These four YSOs are all too luminous to be included in our catalogue owing to saturation.

This region contains two new sources with amplitudes above 2.5 mag, sources 551 and 558. Source 551, with $\Delta K_{all} = 3.62$, is the central star of a cometary nebula that appears much brighter at the second UGPS epoch than the first, see Fig. 15. As noted earlier, it was previously identified by Scholz et al. (2013) as a candidate eruptive variable YSO via two-epoch photometry from *Spitzer*/IRAC and WISE: it had amplitudes 1.70 and 2.00 mag in the $\sim$3.5 and $\sim$4.5 µm passbands, respectively. The central point source rose in brightness by 1.6 mag from $K_s = 14.46$ in 1998 June (2MASS data) to $K = 12.86$ in 2006 July and then rose by a further 2.0 mag to $K \approx 10.83$ in 2011 October. The second UGPS epoch has an uncertainty of 0.1 mag in the point source flux due to the combination of saturation and the (relatively faint) surrounding nebulosity. Cometary nebulae in YSOs are interpreted as reflection nebulae caused by light scattering on paths through a low-density cavity in the circumstellar envelope that has been cleared by an outflow. Scattering may occur at the walls of the cavity (e.g. Whitney & Hartmann 1993) or in the dusty outflow itself (Lucas & Roche 1997). Assuming the variability of the point source is due to episodic accretion, the large rise in brightness of the cometary nebula may be due both to the increased flux from the central star and a reduction in extinction on paths from the star to the cavity during the outburst. The central point source became redder as it became brighter ($H - K_s = 1.55$ in 2MASS in 1998, $H - K = 1.82$ in UGPS in 2006) so its variability cannot be explained as a simple reduction in extinction.

Intriguingly, there is a second spatially extended and highly variable YSO, UGPS J205008.1+442659.9, just 16 arcsec north-west of source 551. In UGPS images, this YSO displays a bipolar nebula around a relatively faint point source. It appeared much brighter than in 2MASS ($K_s = 14.19$ in 1998 June) than in UGPS ($K = 15.26$ in 2006 and $K = 15.71$ in 2011). N.B. We give UGPS point source magnitudes in the default 2 arcsec diameter aperture, which should include a contribution from the surrounding nebula in a broadly similar manner to the 2MASS point source flux, which is based on

data with $\sim$2 arcsec spatial resolution.[4] The large change in flux is not in doubt because UGPS J205008.1+442659.9 is clearly brighter than source 551 in 2MASS images, whereas the reverse is true in the UGPS images. UGPS J205008.1+442659.9 is not in our variable catalogue because of the smaller variation in UGPS and the relative faintness of the point source compared to the surrounding nebula, which led to a profile class $= +1$ (i.e. resolved) at both epochs.

Source 551 and UGPS J205008.1+442659.9 have a projected separation of just 8000–10 000 au for the distance range quoted above so it is likely that they are a weakly bound binary pair that formed at the same time. The companion may therefore be referred to as source 551b. Spatially resolved binaries are likely to be rare in the catalogue, given that most sources are more distant and most binaries have smaller orbital radii. Observation of high-amplitude variability in both members of an embedded pair of supports our view that episodic accretion is quite common in embedded YSOs. Source 551 has spectral index $\alpha = 0.28$ and while the companion is not included in the WISE or *Spitzer*/Cygnus X source catalogues it is clearly an embedded system.

These two variable YSOs with circumstellar nebulae are in a small minority amongst likely YSOs in the catalogue. Connelley & Greene (2010) found that most class I YSOs with FUor-like spectra in nearby SFRs tend to display resolved nebulae in conventional ground-based near-IR images. However, our search method required the candidates to have point source image profiles at the central flux peak, in order to minimize false positives caused by blended stars. The combination of this selection and the large distance to many of the likely YSOs reduces the number with resolved nebulae in the UGPS images.

---

[4] Photometry from both 'filtered' and 'unfiltered' images are available for this source in the WSA. In filtered images, extended nebulosity on scales larger than 5–10 arcsec is removed to aid point source photometry. For this source, we give unfiltered magnitudes in order to better compare with 2MASS but effect of filtering was small in any case (0.04 mag).

The other very high-amplitude YSO in this region, source 558 (=2MASS J20524822+4435182) was identified as a YSO by Guieu et al. ([2009](#)) and Rebull et al. ([2011](#)). It is a point source with $\Delta K_{\rm all}$ = 2.67 and $\alpha = 0.68$ that faded monotonically from $K_{\rm s} = 13.26$ in 2000 May to $K = 14.51$ in 2006 July and $K = 15.92$ in 2011 October. It became much redder as it faded: $J - K_{\rm s} = 2.27$ in 1998 and $J - K = 4.15$ in 2006. These changes are consistent with a change in extinction but the $J - H$ and $H - K$ colours became redder by similar amounts. This is probably not consistent with a change in extinction alone, though we caution that scattered light or large dust grains could cause colour changes arising from variable extinction to depart from the interstellar reddening law.

4.2.3 Gemini OB1 molecular cloud

A spatially extended group of 15 likely YSOs is located in the mid-plane at $188 < l < 195°$, coincident with the Gemini OB1 molecular cloud at $d = 2$ kpc (Carpenter et al. [1995a,b](#)). A further four faint red variable stars in the region (sources 68, 69, 71 and 76) are also plausible YSO candidates, although there is less evidence within 5 arcmin of each of these sources. The Gemini OB1 molecular cloud complex is centred on the S254–S258 H II regions at $l = 192.5$–$192.7°$ (see Chavarría et al. [2008](#)) and four high-amplitude YSOs are located in that vicinity (sources 67, 72, 73 and 75). None of the 15 sources classified as YSOs in our catalogue have amplitudes higher than $\Delta K_{\rm all} = 1.75$ but one of the other four YSO candidates, source 68, has $\Delta K = 2.08$. These 19 sources are all relatively faint (mean $K > 15$) except for sources 61 and 62, which each have mean $K < 13$. Source 61 shows a large Hα excess in the IPHAS $r - H\alpha$ versus $r - i$ two colour diagram.

4.2.4 Rosette complex

A somewhat more compact group of 10 likely YSOs at $206.2 < l < 207.3°$, $-2.6 < b < -1.7°$ is associated with the Rosette complex at $d \approx 1.6$ kpc (e.g. Perez et al. [1987](#)). Only three of these (sources 85, 86 and 88) are located within 10 arcmin of NGC 2244, the ionizing cluster of the Rosette Nebula. The rest are spread out to the south and east amongst the other embedded clusters, ^{13}CO clouds and dark clouds that define the complex, see Román-Zúñiga et al. ([2008](#)), Phelps & Lada ([1997](#)), Poulton et al. ([2008](#)), Blitz & Stark ([1986](#)) and Cambrésy et al. ([2013](#)). The REFL08 cluster hosts two variables (sources 93 and 94) and a third (source 95) is located amongst the extensive group of YSOs with near-IR excess that surrounds the REFL08, PL04 and PL05 clusters (Román-Zúñiga et al. [2008](#); Phelps & Lada [1997](#)). This larger group corresponds approximately to the 'cluster E' identified by Poulton et al. ([2008](#)) using *Spitzer* data. Of the other four variables, one (source 91) is associated with the PL02 cluster (Phelps & Lada [1997](#)), and another (source 87) is in the small [SUH2012] G207.312−02.538 cluster identified by Solin et al. ([2012](#)). The other two are somewhat removed from any of the YSO groups and clusters in the region. Half of the 10 Rosette variables are relatively bright, with mean UGPS $K = 12.5$–14.5.

Source 94 in the REFL08 cluster has the highest amplitude, $\Delta K_{\rm all} = 3.17$. It was previously identified as a likely class I or stage I YSO (WISE J063419.49+041747.9) by Cambrésy et al. ([2013](#)) using WISE colours, and independently by the MYStIX team (Povich et al. [2013](#); Broos et al. [2013](#)) via near to mid-IR excess. It rose by 1.32 mag from $K_{\rm s} = 13.45$ in 1999 November (2MASS data) to $K = 12.13$ in 2007 November and then fell by 3.17 mag to $K = 15.30$ in 2012 March. While there is no 2MASS J

detection, the $H - K_{\rm s}$ and $H - K$ colours agree very closely between the 1999 2MASS epoch and the 2007 UGPS first epoch (values of 1.95 and 1.99, respectively). This would appear to rule out reduced extinction as an explanation for the rise in flux.

Only one likely YSO, source 88 (=CXOU J063211.9+050030), is detected in all three of the IPHAS filters: this source ($\Delta K_{\rm all} = 1.79$) shows a large H$\alpha$ excess in the IPHAS $r - H\alpha$ versus $r - i$ two colour diagram. This is one of two sources in the NGC 2244 cluster that were detected in the X-ray catalogue of Wang et al. ([2008](#)). Source 88 was clearly detected in both the 0.5–8 and 2.5–8 keV ranges, whereas the other (source 89 = CXOU J063205.98+045334.4) had only a 2σ detection.

4.2.5 W51

A group of nine likely YSOs is associated with the W51 star-forming complex at $d \approx 5.6$ kpc (e.g. Parsons [2011](#)). Owing to the large distance this group is compact, the sources all lying within the area $48.72 < l < 49.45°$, $-0.39 < b < -0.18°$. They are spread out in longitude along the central spine of this massive complex where most of the classes I and 0 protostars are located (Kang et al. [2009](#); Kang et al. [2010](#)). None of them are located in the cluster of low-mass YSOs discovered by those authors on the Galactic equator at $l = 49.4$ and $b = 0.0$. The nine sources are relatively faint, as might be expected from the large distance, with 8/9 having mean UGPS $K > 15$; source 293 was somewhat brighter at all three of the UGPS and 2MASS epochs. None of the nine show variations above 2.5 mag but two stars (sources 296 and 297) have $\Delta K_{\rm all} \approx 2.2$. None were detected by the IPHAS survey, which is unsurprising given the substantial extinction towards the complex ($A_{\rm V} \gtrsim 10$, see Kang et al. [2010](#)).

Two additional YSO candidates, sources 286 and 291, were recently identified about 0.5° from the complex by Saral et al. ([2017](#)), see Section 3.3. While these relatively isolated sources did not pass our YSO selection, they are still candidates for association with the region.

4.2.6 NGC 2264/the Cone nebula

A group of six likely YSOs is associated with the NGC 2264 cluster (the region of the Cone nebula) at $d = 740$ pc (Kamezaki et al. [2014](#)). These six are located within the area $202.6 < l < 204.1°$, $1.7 < b < 2.4°$, aligned along the north–south axis that connects the Cone nebula and S Mon. All six are relatively bright (mean UGPS $K < 15.1$) but five have amplitudes $\Delta K_{\rm all} < 1.5$ mag. Source 106 has $\Delta K_{\rm all} = 2.03$ and $\Delta J = 3.90$, the latter being the largest change in J amongst all the likely YSOs in the catalogue. This system fell from $K_{\rm s} = 14.08$ in 1998 to $K = 16.11$ in early 2011 April and recovered to $K = 14.10$ in late 2013 March. The source became much redder in $H - K$ as it faded between 1998 and 2011, far more than would be expected from variable extinction: $H - K_{\rm s} = 0.46$ and $J - H = 0.6$ in 1998, rising to $H - K_{\rm s} = 1.66$ and $J - H = 1.27$ in 2011. The falls in flux in J and H were 3.90 and 3.23 mag, respectively.

The spectral indices are in the range $\alpha = 0.0$–0.4 for four of the six sources; sources 103 and 106 were not detected in W4 but their colours W1–W3 = 4.45 and 4.24, respectively, also suggest class I or flat-spectrum systems, given that W1–W3 and α are well correlated amongst the likely YSOs in the catalogue. The IPHAS data and previous studies (Reipurth et al. [2004](#); Dahm & Simon [2005](#)) show that four sources are Hα emitters: sources 106, 100 (=ESO-HA 400), 103(=ESO HA 414 = NGC 2264 DS 159) and 101(=CSIMon-000959). The first three of these have $r - H\alpha$ above the unreddened

MS locus in Fig. 12. The last, source 101, is one of the reddest CTTS in the optical study of Venuti et al. (2014), with an estimated spectral-type M2 and a bolometric luminosity of $0.34\,L\odot$. Adopting the M2 type allows us to confirm Hα emission despite the lower r −Hα value of 0.77. We estimate an Hα equivalent width of ∼10 Å from fig. 6 of Drew et al. (2005). Given the faint u-band magnitude ($u \approx 23.3$), the accretion estimates reported by Venuti et al. (2014) should be treated with caution for this star. Our computed spectral index, $\alpha = 0.11$, is consistent with a flat-spectrum CTTS.

4.2.7 S86 H II region

A compact group of seven likely YSOs at $59.1 < l < 59.8°$, $-0.2 < b < 0.2°$ is associated with the large S86 H II region (Billot et al. 2010) at $d \approx 2.3\,$kpc (Chapin et al. 2008). This is part of the Vul OB1 association. Three of these stars (sources 360, 362 and 364) are in the vicinity of the well-studied NGC 6823 cluster (e.g. Riaz et al. 2012; Xu & Wang 2012) which has an age of ∼3 Myr. Source 358 is in the pre-MS cluster Collinder 404 (=far-IR cluster [BSP 2011] 19, see Bica et al. 2008; Billot et al. 2011). Three other objects (sources 355, 357 and 361) are located on the outskirts of the H II region. Source 361 is furthest from NGC 6823, in the massive SFR IRAS 19410+2336 (=cluster G3CC 73), see Qiu et al. (2008). This cluster has an independently determined maser parallax distance $d = 2.2\,$kpc (Xu et al. 2009) so it seems certain that it is part of the same complex, in which star formation is thought to have been triggered by the G59.5+0.1 supernova (Billot et al. 2010; Taylor, Wallace & Goss 1992).

Sources 355, 362 and 364 have relatively high-amplitudes, $\Delta K_{\rm all} = 2.17, 2.08$ and 1.98, respectively. Source 355 rose from $K = 16.69$ in 2008 August to $K = 14.52$ in 2011 September and was undetected in 2MASS and WISE and MIPSGAL. The GLIMPSE colour, [3.6]–[4.5] = 0.39, suggests a class II YSO. Source 362 is a fairly bright flat-spectrum system ($\alpha = 0.16$) that rose from $K_s = 13.95$ in 1998 in 2MASS to $K = 11.87$ at the first UGPS epoch in 2008 August and then fell back to $K = 13.69$ by the second UGPS epoch in 2011 September. The $(H - K)$ colour changed only slightly from 1.43 to 1.58 (a 1σ reddening) between 1998 and 2007 despite the ∼2 mag flux increase, which indicates that the variability was not caused by a reduction in extinction. Source 364 is a faint source ($K = 15.69$ in 2007 and $K = 17.67$ in 2011) that was undetected in 2MASS and WISE and MIPSGAL; the GLIMPSE colour, [3.6]–[4.5] = 0.47, suggests a class II YSO.

4.2.8 S236 / NGC 1893

A very compact group of four likely YSOs (sources 29–32) is associated with the S236 H II region and NGC 1893 cluster at $d = 3.6\,$kpc (Prisinzano et al. 2011, see also Caramazza et al. 2008). These four are located within the area $173.57 < l < 173.68°$, $-1.85 < b < -1.57°$. None show variation higher than $\Delta K_s = 1.76$ and these are relatively faint sources in the near-IR (mean UGPS $K > 14.8$). Spectral indices are available for two objects (sources 29 and 31), both of which have steeply rising SEDs, $\alpha = 0.88$ and 1.82, respectively. All four sources were previously identified as YSO candidates by Prisinzano et al. (2011). They were undetected in the IPHAS Hα data. The additional epoch of JHK photometry from Prisinzano et al. (2011) does not significantly increase the amplitude of variation of any of these sources. Similarly, the WISE W1 and W2 fluxes show no large differences from the IRAC I1 and I2 fluxes in Caramazza et al. (2008).

4.2.9 Possible W43 group

The W43 complex at $d = 6.5\,$kpc (Morales et al. 2013) is a very massive SFR but only three likely YSOs (sources 165–167) may be associated with it, located at $30.74 < l < 31.00°$, $-0.05 < b < 0.07°$. Sightlines in the mid-plane region near $l = 31°$ pass along the Scutum-Centaurus spiral arm and the region contains several high-amplitude sources classified as likely YSOs, so this set of three sources does not stand out as an overdensity. The most noteworthy is source 167 (=SSTGLMC G030.9948-00.0384), which has a very high amplitude ($\Delta K = 3.42$) and a very red SED ($\alpha = 2.02$). It was identified as a red YSO candidate in the Robitaille et al. (2008) list of red *Spitzer* sources and it rose from $K = 18.02$ in 2005 June to $K = 14.60$ in 2011 August. It was undetected in 2MASS and the UGPS J and H images, but it brightened by 1.73 and 1.89 mag at $\lambda \sim 3.5$ and 4.5μm, respectively, between the GLIMPSE epoch in 2003 and WISE data in 2010. Source 167 is associated with the H II region [KB94] 9 at approximate distance $d = 8.0\,$kpc (Kuchar & Bania 1994) but the authors noted the region may in fact be part of the W43 complex. A similar possible association with W43 applies to source 165 in the H II region [KB94] 8. The last of the three, source 166, is in the W43 cluster. The fourth YSO candidate, source 171, was identified in the general vicinity of W43 by Saral et al. (2017), though it is a relatively isolated source not included in our selection of likely YSOs, see Section 3.3.

4.3 New pre-MS clusters and groups

Many of the likely YSOs in the catalogue were identified by spatial association with five or more red sources in the WISE three colour images. While most such cases involve known clusters or diffuse groups on the outskirts of large SFRs, simple visual inspection of the UGPS and WISE images indicates that some are substantial pre-MS clusters not identified as such in the SIMBAD data base or the papers listed therein. In Table 3, we list the 18 cases where variable sources are associated with pre-MS clusters, SFRs or compact stellar groups that appear to be new discoveries. The epoch J2000.0 coordinates are estimated from visual inspection of the WISE and UGPS images. Many of them are located in little-studied parts of the outer Galaxy. For more details of associated mm and submm sources and references for the distances, see the individual catalogue entries for each variable source.

5 OTHER SOURCES OF INTEREST

5.1 The highest amplitude sources

Of the 43 sources in the high-amplitude tail with $\Delta K_{\rm all} > 2.5$, only 20 are classified as likely YSOs. However, that classification is given to five of the seven sources with the very highest amplitudes, $\Delta K_{\rm all} > 3.5$. We are unable to determine the nature of most of the very high-amplitude sources not classified as likely YSOs, though some may certainly be relatively isolated YSOs. Below we briefly discuss a few of the highest amplitude systems.

(i) Source 282 ($\Delta K_{\rm all} = 4.60$) has the highest amplitude in the catalogue. It is classified as a likely YSO due to location in the H II region GRS G048.60+00.20 at $d = 10.6\,$kpc (Kuchar & Bania 1994), seen clearly as an SFR in the WISE three colour images. The source brightened from $K = 18.02$ in 2007 August to $K = 13.42$ in 2011 August. It was undetected in all other optical to mid-IR bandpasses (adjacent bright sources inhibit detection in the relatively low-resolution WISE images).

Table 3. New pre-MS clusters associated with individual variable stars.

Cluster	Source number	RA	Dec.	d/kpc	Comment
1	3	52.517	55.772		See Fig. 4
2	4	52.701	54.817		A compact little cluster, members blended in WISE, see Fig. 4
3	13	60.935	51.451	2.5	A small embedded group near Camargo 441 and S206 H II region (=NGC 1491)
4	36	81.735	38.751		
5	45	84.094	36.661		
6	62	92.091	21.349	2	In the Gem OB1 molecular cloud
7	63	92.181	31.415		A filamentary SFR
8	66	92.849	16.549	2	Compact cluster in Gem OB1, largely unresolved in WISE
9	70	93.035	20.247	2	In the Gem OB1 molecular cloud
10	92	98.297	8.564		
11	118	104.765	− 4.889	2	Connected to pre-MS cluster [FSR2007] 1129 = [KPS2012] MWSC 1042
12	122	104.985	− 3.934		
13	190	283.639	7.948		
14	250	286.441	5.022		An embedded cluster candidate associated with IRDC G39.046−0.877
15	370	297.008	26.098		A cluster with a tightly packed core, unresolved in WISE.
16	374	297.547	23.918	0.8	
17	469	306.415	36.985	1.4	In the Cygnus X complex, associated with BGPS G075.861−00.551 mm core.
18	599	325.504	52.699		See Fig. 4

(ii) As noted earlier, source 391 (Nova Cyg 2008) has the second highest amplitude, $\Delta K_{all} = 4.40$.

(iii) Source 266 ($\Delta K_{all} = 4.20$) is located in molecular cloud GRSMC 43.30−0.33 at $d = 3$ kpc (Simon et al. 2001). It is unique amongst the YSOs in the high-amplitude tail in having a negative spectral index ($\alpha = -0.31$), corresponding to a class II YSO. It rose very slightly from $K_s = 15.06$ (2MASS data) in 1999 to $K = 14.86$ in 2008 April, but then rose to $K = 10.86$ in 2011 July. The UGPS near-IR colours from 2008 place it in the region of reddened CTTS. It was undetected in IPHAS.

(iv) Source 570 ($\Delta K_{all} = 3.80$) is an isolated source not classified as a YSO. However, the *Spitzer*/IRAC colours (I1–I2 = 1.44) indicate a red object with circumstellar matter. This is supported by UGPS near-IR colours consistent with a lightly reddened CTTS or perhaps a more strongly reddened CV. Source 570 faded from $K = 14.70$ in 2006 July to 18.50 in 2011 September. It was undetected in IPHAS and the WISE images.

(v) Source 133 (=GPSV1, $\Delta K_{all} = 3.75$) is a likely YSO located in the Serpens OB2 association. It was discussed in Paper I as a possible FUor, based on the large rise in flux and slow rate of decline. CO absorption was not detected in the low-quality spectrum presented in that work.

(vi) Sources 551 and 167 ($\Delta K_{all} = 3.62$ and 3.42, respectively) have been mentioned earlier as members of the North American/Pelican group and the possible W43 group, respectively.

(vii) Source 190 ($\Delta K_{all} = 3.57$ and $\alpha = 0.97$) is a likely YSO located in a previously uncatalogued group or small cluster of YSOs apparent in the WISE three colour images (see Table 3). Unusually for a class I system, it is detected in all three of the IPHAS optical passbands. However, the colours $r - i = 2.27$ and $r - H\alpha = 0.88$ do not clearly establish an Hα excess. It faded from $K = 13.87$ in 2010 June to $K = 17.44$ in 2012 August and it was undetected in 2MASS.

(viii) Source 127 ($\Delta K_{all} = 3.43$) was mentioned earlier as one of three faint blue Hα-emitting sources that we regard as candidate CVs.

(ix) Among the remaining likely YSOs with amplitudes above 3 mag, only source 615 ($\Delta K_{all} = 3.25$ and $\alpha = 1.18$) is notable as having a well-determined distance. It is a member of the embedded

pre-MS cluster no. 43 identified by Kumar et al. (2006), near the S138 H II region and S138 IR cluster at $d = 5.1$ kpc. Source 615 faded from $K = 15.14$ in 2006 July to $K = 18.39$ in 2011 October. It was undetected in 2MASS.

(x) Source 156 (=V1360 Aql or IRAS 18432−0149) is notable as the highest amplitude OH/IR star in the catalogue, with $\Delta K_{all} = 3.80$. Other previously known variable stars with amplitudes above 3 mag are source 389 ($\Delta K_{all} = 3.20$, mentioned earlier as a likely D-type symbiotic star, and source 301 ($\Delta K_{all} = 3.30$) which we classified as a likely carbon star (see Section 3.4.1).

5.2 Source 363

The strangest of the isolated Hα emitters is source 363, with near-IR colours $J - H = -0.60$, $H - K = 0.67$ and $J - K = 0.07$ measured in 2010 July, see Fig. 16. This source has a redder $r - i$ colour than the three CV candidates ($r - i = 1.26$ and $r - H\alpha = 1.11$ in 2005 July) located closer to the YSOs in the IPHAS two colour diagram. It faded by 1.97 mag from $K = 15.72$ to 17.69 between 2006 July and 2010 July. At $l = 55.4°$ and $b = -2.5°$ it lies outside the *Spitzer*/GLIMPSE footprint and the location is blended with adjacent stars at the 6 arcsec resolution of WISE, preventing a mid-IR detection. It was not quite bright enough to be included in the 2MASS Point Source Catalogue or the 2MASS Point Source Reject Table, but a source is visible at the location in the 2MASS J, H and K_s images, apparently at an intermediate state somewhat brighter in all three passbands than in 2010. Precise measurement is problematic due to blending with the adjacent source 2 arcsec north and slightly west, measured in UGPS with $J = 17.02$. However, the peak of the image profile in the 2MASS images is coincident with the UGPS coordinates in all three passbands indicating that $J < 17$ in 2MASS, considerably brighter than the $J = 17.76$ UGPS datum in 2010. It is therefore significant that the source does not appear unusually blue in a 2MASS three colour images, but similar to the other stars in this lightly reddened field with typical colours $J - H = 0.4$–0.8.

The optical flux in r, as measured by the UVEX survey (Groot et al. 2009) and the IPHAS survey, has also shown variation of
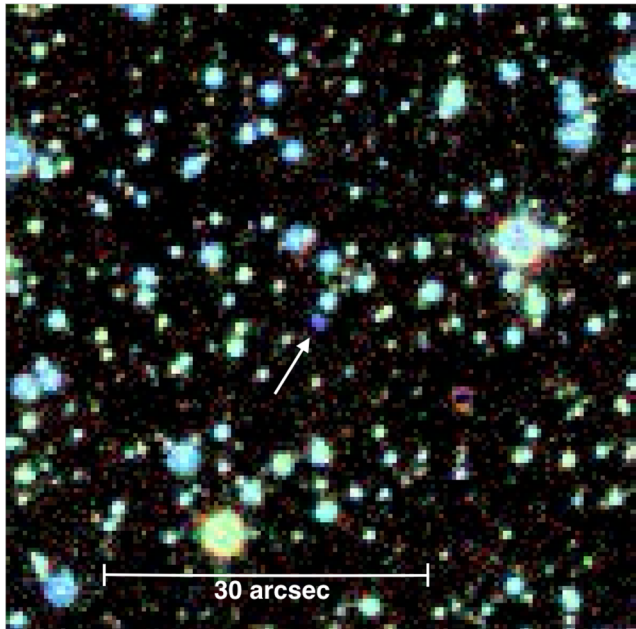
Figure 16. UGPS near-IR three colour image of source 363 (2010 July data, with red, green and blue representing K, H and J, respectively). The source is indicated with an arrow and the image has conventional equatorial orientation. The deep blue colour of the object reflects the extreme measurement $J - H = -0.6$.

Table 4. Optical photometry of source 363 (Vega system).

Data	i	Hα	r	g	u
IPHAS 2005 July	19.27	19.42	20.54	N/A	N/A
IPHAS 2007 May	–	–	21.14	N/A	N/A
UVEX 2010 July	N/A	N/A	19.22	20.75	20.0:
UVEX 2011 August	N/A	N/A	19.93	20.50	19.63

Notes. The IPHAS data were taken in contemporaneous r, i, Hα sets, and UVEX data in u, g, r contemporaneous sets.

almost 2 mag, see Table 4. The photon-noise uncertainties on the optical measurements are under 0.05 mag, though we note that the UVEX 2010 data have a significant calibration uncertainty due to off-axis location of the source in the focal plane. It is clear from blinking the images that the r flux faded substantially between 2010 July and 2011 August, while the u and g fluxes either remained constant or increased. The negative UGPS $J - H$ colour is unique in the catalogue, considerably bluer than typical CVs (Hoard et al. 2002; Corradi et al. 2008) or white dwarfs (Girven et al. 2011; Leggett et al. 2011). The very negative $u - g$ colour is also bluer than is typically found in white dwarfs, comparable to an early B-type star (Drew et al. 2014). Inspection of the UGPS stacked images and individual exposures shows no problem with the measurement and the large changes in r magnitude are obvious in the IPHAS and UVEX images. The $J - K$ colour is also very blue for the field, though the $H - K$ colour is amongst the redder sources present. One possibility is that the apparently extreme $J - H$ colour is an illusion caused by fading of the source in the 7.5 min interval between the J and H observations. Common varieties of EB are ruled out by the Hα emission but interacting binary systems containing compact objects can show large changes in flux on this time-scale. E.g. Bogdanov et al. (2015) describe high-amplitude optical variations on time-scale of minutes in PSR J1023+0038, a millisecond pulsar that appears to alternate between accretion disc-dominated LMXB-like

behaviour and discless pulsar-like behaviour. The available optical-IR data do not allow us to determine the nature of this system; time-series monitoring and pointed X-ray and radio observations would better constrain the possibilities.

5.3 The nearest sources

Several of the likely YSOs in the catalogue are located within 1.5 kpc, close enough for high-resolution imaging studies to resolve structures such as envelopes, discs and jets. This may help to determine the cause of variability, e.g. Liu et al. (2016) and Dong et al. (2016). We have already described the North America/Pelican group at 520–600 pc, the NGC 2264/Cone nebula group at ~800 pc and the Cygnus X group at 1.4 kpc. Below we list the other likely YSOs at $d \leq 1$ kpc and one source projected in a mature open cluster.

(i) Source 284 ($\Delta K_{all} = 1.02$) is close to the well-studied YSO V1352 Aql (=AS 353 A) and the bright HH32 outflow, located in the Lynds 673 dark cloud. Herbig & Jones (1983) state that this cloud is in front of other molecular clouds in Aquila and gives the distance as 300 pc using a somewhat uncertain method based on velocity dispersion of foreground stars. While this distance is considered uncertain, source 284 may well be the nearest member of the catalogue. Although the amplitude is relatively low, the IPHAS colours from 2004 August provide clear evidence for Hα excess ($r - i = 1.51$ and $r - H\alpha = 1.08$), implying active accretion. The near-IR colours became slightly bluer as it faded from $K_s = 11.72$ in 1999 July (2MASS data) to $K = 12.49$ in 2007 August, but they remained consistent with a lightly reddened CTTS. It then rose to $K = 11.47$ in 2011 July. It was undetected by WISE.

(ii) The W40 cloud in the Aquila rift is host to two or three catalogue members. Sources 148 and 149 (GPSV48 and GPSV42, respectively, in Contreras Peña 2015 and Paper I) are located within the region studied by Mallick et al. (2013). In addition, source 150 (=GPSV43 from Paper I) has mid-IR WISE colours consistent with a flat-spectrum YSO and may well be part of the same region, though it is located almost half a degree south of the centre of the young cluster. It is not classified as a likely YSO in the catalogue due to its relative isolation. This region is at $d \approx 500$ pc (Radhakrishnan et al. 1972). All three sources have amplitudes $\Delta K_{all} < 1.5$ and all were undetected by IPHAS and VPHAS+ due to their red SEDs.

(iii) Source 413 ($\Delta K_{all} = 1.40$) is located in the IRAS 20050+2720 pre-MS cluster at $d \approx 700$ pc (Günther et al. 2012) in the slightly part of this region which those authors referred to as cluster core E. The only detections are the UGPS near-IR data and the source is relatively faint (mean $K = 15.80$).

(iv) Source 605 ($\Delta K_{all} = 1.15$) is a faint blue source ($J - H = 0.25$, $H - K = 0.1$ and mean UGPS $K = 15.34$) projected in the outskirts of the ~250 Myr-old cluster NGC 7243 at $d \approx 700$ pc (Jilinski et al. 2003). It was not detected by WISE. Inspection of the catalogue of Jilinski et al. (2003) indicates that most sources outside the central part of the cluster are not members. Moreover, source 605 appears to lie below the cluster MS on a near-IR CMD. The relatively low amplitude permits an EB interpretation and the blue colours ($J - H = 0.25$ and $H - K = 0.1$) are consistent with this and the fact that 2MASS JHK_s fluxes are fairly consistent with the UGPS JHK_c data (within 2σ) tends to support this. An AGN or CV interpretation is also possible, see Section 3.4.4. Unfortunately, the source lies just outside the IPHAS area ($b = -5.24$). Panstarrs/PS1 mean optical colours are consistent with a blue source but they cannot be used to estimate a spectral type without information on the observing dates.

(v) Source 374 ($\Delta K_{\mathrm{all}} = 2.33$ and $\alpha = 0.78$) is located in the *Planck* core PLCKECC G060.75−01.23 ($d = 800$ pc). This core is associated with IRAS 19480+2347, seen in the UGPS and WISE images as a new embedded cluster (no. 16 in Table 3). Source 374 faded from $K_s = 12.06$ in 2000 April (2MASS data) to $K = 14.39$ in 2006 July and then recovered to $K = 12.37$ in 2011 September. The near-IR colours were similar in the 2000 and 2006 observations (becoming slightly bluer in $J − H$ and slightly redder in $H − K$), indicating that the drop in brightness was not caused by extinction. The source was not detected by IPHAS.

(vi) Source 555 ($\Delta K_{\mathrm{all}} = 1.11$ and $\alpha = −0.23$) is located in the [DBY94] 089.2+03.6 molecular cloud ($d = 800$ pc, Dobashi et al. 1994). This lightly reddened flat-spectrum system had similar colours and brightness ($K \approx 14.4$) in 2MASS in June 2000 and UGPS in September 2011 but was fainter in 2013 August. The IPHAS photometry from 2003 November ($r − i = 1.10$ and $r − \mathrm{H}\alpha = 1.25$) showed a large H$\alpha$ excess, indicating active accretion.

(vii) Source 581 ($\Delta K_{\mathrm{all}} = 1.17$ and $\alpha = 0.02$) is located in the [DBY94] 092.9+01.7 molecular cloud ($d = 800$ pc, Dame & Thaddeus 1985). This bright system had similar colours and fluxes ($K \approx 12.5$) in 2MASS in 1998 November and UGPS in 2010 October, but was fainter in 2012 October. The IPHAS photometry from 2005 July ($r − i = 2.04$ and $r − \mathrm{H}\alpha = 0.52$) are consistent with a highly reddened A-type star with no Hα excess at that time.

(viii) Source 586 ($\Delta K_{\mathrm{all}} = 1.19$ and $\alpha = 0.12$) is located in molecular cloud [DBY94] 090.3−02.3 ($d = 800$ pc, Dobashi et al. 1994, specifically in bright nebula [B77] 27, on the edge of the Lynds 989 dark cloud. This source is highly reddened but bright in K, rising from $K = 13.06$ in 2011 August to $K = 11.87$ in 2013 July.

(ix) The AFGL 490 region at $d = 900$ pc in the outer galaxy hosts two variable YSOs. Source 1 ($\Delta K_{\mathrm{all}} = 2.28$ and $\alpha = 0.94$) is YSO no. 25 in the catalogue of Gutermuth et al. (2009) and source 2 ($\Delta K_{\mathrm{all}} = 1.21$) is YSO no. 337 in the same catalogue. The region is further analysed in Masiunas et al. (2012). Source 1 rose from $K_s = 15.26$ in 1998 December (2MASS data) to $K = 12.99$ in 2005 October and then faded to $K = 14.25$ in 2008 October. This very red source was undetected in J. Source 2 has near-IR colours indicating a CTTS. It dipped between 1998 December and 2005 October before recovering to its original brightness in 2008 October.

(x) Source 594 ($\Delta K_{\mathrm{all}} = 1.22$ and $\alpha = −0.14$) is located in IC 1396A (the Elephant Trunk nebula), a bright-rimmed cloud on the periphery of the giant H II region IC 1396 ionized by the Trumpler 37 cluster ($d \approx 0.9$ kpc, Contreras et al. 2002). It rose from $K = 15.66$ in September 2011 to $K = 14.44$ in 2013 September.

(xi) Source 168 ($\Delta K_{\mathrm{all}} = 1.41$) is a relatively faint, very red source (mean UGPS $K = 15.28$) located in a cluster of far-IR sources, no. 12 in the list of Billot et al. (2011), at $d \approx 900$ pc.

(xii) Source 602 ($\Delta K_{\mathrm{all}} = 1.48$) is located in the IC 5146 pre-MS cluster (the Cocoon nebula) at $d = 1$ kpc (Harvey et al. 2008). Its near-IR colours are consistent with a CTTS. It is a relatively faint source (mean UGPS $K = 15.57$).

6 SUMMARY AND CONCLUSIONS

We have searched the UGPS two-epoch data set for highly variable stars across some 1470 deg^2 of the Galactic plane and compiled a catalogue of 618 sources with amplitudes >1 mag in K, nearly all of which are new discoveries. About 60 per cent of these sources are YSOs, based on spatial association with SFRs at distance ranging from ∼300 pc to 10 kpc or more, identified using either the SIMBAD data base or inspection of the WISE three colour images. YSO

luminosities (determined mainly from WISE data taken in 2010) range from 0.1 to 10^3 L$_\odot$, though only rarely exceeding $10^{2.5}$ L$_\odot$.

There is also a population of dusty AGB stars with high mass-loss rates, typically very red sources at the bright end of the magnitude distribution, some of which are identified here as new candidates. Most are likely to be O-rich systems. Our WISE-based colour selection of dusty Mira variables differs slightly from the AGB star selection of Koenig & Leisawitz (2014) and it appears to be better for selecting the very reddest AGB stars. However, their system is better for bluer, more typical AGB stars, which are generally absent from UGPS due to saturation.

Amongst the fainter sources with relatively blue near-IR colours there may be comparable proportions of CVs, EBs and AGN, as well as rarer variables such as the binary PN central stars. Within this group, we identify three new candidate CVs by their Hα emission, high amplitudes (2–3.5 mag) and blue colours. There is also an Hα emitting source of unknown nature with $J − H = −0.6$ and $\Delta K \approx 2$, an outlier with respect to the rest of the catalogue. A small population of bright blue variable sources of unknown nature is present: these present easy targets for follow-up work.

More than half of the likely YSOs in the sample are class I or flat-spectrum systems, a higher proportion than in the YSO population in general (e.g. Dunham et al. 2014). Simulations of two-epoch sampling of the VVV light curves for YSOs from CP17a indicate that variations will usually be due to long-term flux changes on time-scales of years. Many of these can reasonably be expected to be examples of episodic accretion, often located in relatively nearby SFRs with less foreground extinction than the VVV sample. This is supported by evidence for active accretion from the Hα emission detected in many catalogue members by the IPHAS survey. The catalogue should therefore provide a rich sample of eruptive variable YSOs for investigation by the community. The substantial groups of variable YSOs in well-studied regions such as Cygnus X, the North America/Pelican nebula region, the Rosette complex, the NGC 2264/Cone nebula region and the Gemini OB1 cloud are statistically valuable samples. This panoramic two-epoch study complements recent more focused high cadence studies, e.g. the IR study of Cygnus OB2 by Roquette et al. (2017) and the optical study of NGC 2264 by Venuti et al. (2017).

The amplitude distributions for both the YSOs and the remainder of the sample decline steeply from 1 to 2.5 mag before flattening off, with a low level tail extending up to 5 mag. However, the much better sampled VVV sample of CP17a does not show this break in behaviour so we caution against overinterpretation, given the small number statistics at the highest amplitudes and the wide variety of YSO light curves seen in VVV. The higher amplitude YSOs have a redder distribution of SEDs, as in the VVV sample. While most pre-MS catalogue members have lower amplitudes than classical FUors and EXors, it is only by studying the full range of amplitudes and time-scales attributable to accretion-driven variability that we are likely to come to understand the underlying physical causes. E.g. photometric monitoring of the variables in this catalogue would allow us to test predictions of unsteady accretion models such as those of D'Angelo & Spruit (2010, 2012), in which cycles of eruption and quiescence can emerge naturally in discs that are truncated close to the co-rotation radius by the stellar magnetosphere. While those models were proposed as an explanation for EXors, the range of amplitudes and time-scales would include the new 'MNor' class suggested by CP17b to describe variations in more embedded systems that vary on slightly longer time-scales, often with lower amplitudes than the classical EXors and a diverse mixture of EXor-like and FUor-like spectra. A difficulty with this

model (see Hartmann, Herczeg & Calvet 2016) is that the measured accretion rates in EXors do not drop to zero between outbursts, but it is still worthy of consideration.

The large proportion of YSOs confirms our earlier finding in Paper I and CP17a that they dominate the high-amplitude near-IR variable sky on Galactic disc sightlines, extending the previous result to a much wider range of longitudes. The observed surface density of variable YSOs is similar to that seen in Paper I and the magnitude distribution rises towards our sensitivity limit even in nearby SFRs. This confirms our initial result in Paper I that the mean space density of high-amplitude YSOs is higher than that of Mira variables, the commonest type of high-amplitude variable seen in the optical waveband, see e.g. the General Catalogue of Variable Stars (Samus et al. 2010).

We note that our selection of point sources will tend to exclude YSOs with bright circumstellar nebulosity, commonly seen in systems with FUor-like spectra (Connelley & Greene 2010). This may lead to a bias against systems with near edge-on discs, particularly in nearby SFRs, that should be taken account of in follow-up work.

We encourage more detailed investigation of the sources in this catalogue by the astronomical community.

ACKNOWLEDGEMENTS

REFERENCES

Acero F. et al., 2015, ApJS, 218, 23
Ackermann M. et al., 2015, ApJ, 810, 14
Ageorges N., Eckart A., Monin J.-L., Menard F., 1997, A&A, 326, 632
Alexander M. J., Kobulnicky H. A., 2012, ApJ, 755, L30
Alexander M. J., Kobulnicky H. A., Kerton C. R., Arvidsson K., 2013, ApJ, 770, 1
Anderson L. D., Bania T. M., 2009, ApJ, 690, 706
Anderson L. D., Bania T. M., Jackson J. M., Clemens D. P., Heyer M., Simon R., Shah R. Y., Rathborne J. M., 2009, ApJS, 181, 255
Anderson L. D., Bania T. M., Balser D. S., Rood R. T., 2012, ApJ, 754, 62
Antoniucci S., Giannini T., Li Causi G., Lorenzetti D., 2014, ApJ, 782, 51
Armstrong D. J., Gómez Maqueo Chew Y., Faedi F., Pollacco D., 2014, MNRAS, 437, 3473
Arvidsson K., Kerton C. R., Foster T., 2009, ApJ, 700, 1000
Audard M. et al., 2014, Protostars and Planets VI. University of Arizona Press, Tucson, AZ, p. 387
Avalos M., Lizano S., Franco-Hernández R., Rodríguez L. F., Moran J. M., 2009, ApJ, 690, 1084
Balanutsa P. et al., 2014, Astron. Telegram, 5787

Balog Z., Kenyon S. J., 2002, AJ, 124, 2083
Bania T. M., Anderson L. D., Balser D. S., 2012, ApJ, 759, 96
Baraffe I., Chabrier G., Gallardo J., 2009, ApJ, 702, L27
Baraffe I., Vorobyov E., Chabrier G., 2012, ApJ, 756, 118
Barentsen G. et al., 2014, MNRAS, 444, 3230
Beerer I. M. et al., 2010, ApJ, 720, 679
Beichman C. A., 1988, Astrophys. Lett. Commun., 27, 67
Belczyński K., Mikołajewska J., Munari U., Ivison R. J., Friedjung M., 2000, A&AS, 146, 407
Benjamin R. A. et al., 2003, PASP, 115, 953
Bernes C., 1977, A&AS, 29, 65
Bica E., Dutra C. M., Barbuy B., 2003a, A&A, 397, 177
Bica E., Dutra C. M., Soares J., Barbuy B., 2003b, A&A, 404, 223
Bica E., Bonatto C., Dutra C. M., 2008, A&A, 489, 1129
Billot N., Noriega-Crespo A., Carey S., Guieu S., Shenoy S., Paladini R., Latter W., 2010, ApJ, 712, 797
Billot N. et al., 2011, ApJ, 735, 28
Blandford R. D., Rees M. J., 1978, in Wolfe A. M., ed., BL Lac Objects. University of Pittsburgh, Pittsburgh, PA, p. 328
Blitz L., Stark A. A., 1986, ApJ, 300, L89
Bogdanov S. et al., 2015, ApJ, 806, 148
Bonnell I., Bastien P., 1992, ApJ, 401, L31
Bronfman L., Nyman L.-A., May J., 1996, A&AS, 115, 81
Broos P. S. et al., 2013, ApJS, 209, 32
Bruch A., Fischer F.-J., Wilmsen U., 1987, A&AS, 70, 481
Buckner A. S. M., Froebrich D., 2013, MNRAS, 436, 1465
Budding E., Erdem A., Çiçek C., Bulut I., Soydugan F., Soydugan E., Bakiş V., Demircan O., 2004, A&A, 417, 263
Calvet N., Patino A., Magris G. C., D'Alessio P., 1991, ApJ, 380, 617
Calvet N., Muzerolle J., Briceño C., Hernández J., Hartmann L., Saucedo J. L., Gordon K. D., 2004, AJ, 128, 1294
Camargo D., Bonatto C., Bica E., 2015, MNRAS, 450, 4150
Cambrésy L., Beichman C. A., Jarrett T. H., Cutri R. M., 2002, AJ, 123, 2559
Cambrésy L., Marton G., Feher O., Tóth L. V., Schneider N., 2013, A&A, 557, A29
Campbell B., Persson S. E., Matthews K., 1989, AJ, 98, 643
Caramazza M., Micela G., Prisinzano L., Rebull L., Sciortino S., Stauffer J. R., 2008, A&A, 488, 211
Caratti o Garatti A. et al., 2012, A&A, 538, A64
Caratti o Garatti A. et al., 2016, Nat. Phys., 13, 276
Carey S. J. et al., 2009, PASP, 121, 76
Carpenter J. M., Snell R. L., Schloerb F. P., 1995a, ApJ, 445, 246
Carpenter J. M., Snell R. L., Schloerb F. P., 1995b, ApJ, 450, 201
Carpenter J. M., Hillenbrand L. A., Skrutskie M. F., 2001, AJ, 121, 3160
Casali M. et al., 2007, A&A, 467, 777
Casoli F., Combes F., Dupraz C., Gerin M., Boulanger F., 1986, A&A, 169, 281
Chapin E. L. et al., 2008, ApJ, 681, 428
Chavarría L. A., Allen L. E., Hora J. L., Brunt C. M., Fazio G. G., 2008, ApJ, 682, 445
Chengalur J. N., Lewis B. M., Eder J., Terzian Y., 1993, ApJS, 89, 189
Churchwell E. et al., 2006, ApJ, 649, 759
Churchwell E. et al., 2009, PASP, 121, 213
Cieza L. A. et al., 2016, Nature, 535, 258
Codella C., Palumbo G. G. C., Pareschi G., Scappini F., Caselli P., Attolini M. R., 1995, MNRAS, 276, 57
Cody A. M. et al., 2014, AJ, 147, 82
Cody A. M., Hillenbrand L. A., David T. J., Carpenter J. M., Everett M. E., Howell S. B., 2017, ApJ, 836, 41
Cohen M., 1980, AJ, 85, 29
Connelley M. S., Greene T. P., 2010, AJ, 140, 1214
Contreras Peña C. E., 2015, PhD thesis, University of Hertfordshire
Contreras Peña C. et al., 2014, MNRAS, 439, 1829
Contreras Peña C. et al., 2017a, MNRAS, 465, 3011
Contreras Peña C. et al., 2017b, MNRAS, 465, 3039
Contreras M. E., Sicilia-Aguilar A., Muzerolle J., Calvet N., Berlind P., Hartmann L., 2002, AJ, 124, 1585

Corradi R. L. M. et al., 2008, A&A, 480, 409
Corradi R. L. M. et al., 2011, MNRAS, 410, 1349
Covey K. R. et al., 2011, AJ, 141, 40
Cutri R. M. et al., 2012, Technical Report, Explanatory Supplement to the WISE All-Sky Data Release Products. Available at: http://wise2.ipac.caltech.edu/docs/release/allsky/expsup/
Cyganowski C. J. et al., 2008, AJ, 136, 2391
D'Angelo C. R., Spruit H. C., 2010, MNRAS, 406, 1208
D'Angelo C. R., Spruit H. C., 2012, MNRAS, 420, 416
Dahm S. E., Simon T., 2005, AJ, 129, 829
Dame T. M., Thaddeus P., 1985, ApJ, 297, 751
Dame T. M., Hartmann D., Thaddeus P., 2001, ApJ, 547, 792
Davis C. J. et al., 2009, A&A, 496, 153
Delgado A. J., Alfaro E. J., Cabrera-Cano J., 1997, AJ, 113, 713
Di Francesco J., Johnstone D., Kirk H., MacKenzie T., Ledwosinska E., 2008, ApJS, 175, 277
Dickel H. R., Wendker H., Bieritz J. H., 1969, A&A, 1, 270
Dickinson D. F., Turner B. E., 1991, ApJS, 75, 1323
Dirienzo W. J., Indebetouw R., Brogan C., Cyganowski C. J., Churchwell E., Friesen R. K., 2012, AJ, 144, 173
Dobashi K., 2011, PASJ, 63, S1
Dobashi K., Bernard J.-P., Yonekura Y., Fukui Y., 1994, ApJS, 95, 419
Dong R., Vorobyov E., Pavlyuchenkov Y., Chiang E., Liu H. B., 2016, ApJ, 823, 141
Downes D., Rinehart R., 1966, ApJ, 144, 937
Drew J. E. et al., 2005, MNRAS, 362, 753
Drew J. E. et al., 2014, MNRAS, 440, 2036
Dunham M. K. et al., 2010, ApJ, 717, 1157
Dunham M. M. et al., 2014, Protostars and Planets VI. University of Arizona Press, Tucson, AZ, p. 195
Dutra C. M., Bica E., 2001, A&A, 376, 434
Eden D. J., Moore T. J. T., Plume R., Morgan L. K., 2012, MNRAS, 422, 3178
Eden D. J., Moore T. J. T., Morgan L. K., Thompson M. A., Urquhart J. S., 2013, MNRAS, 431, 1587
Eder J., Lewis B. M., Terzian Y., 1988, ApJS, 66, 183
Egan M. P., Shipman R. F., Price S. D., Carey S. J., Clark F. O., Cohen M., 1998, ApJ, 494, L199
Elia D. et al., 2013, ApJ, 772, 45
Ellsworth-Bowers T. P. et al., 2013, ApJ, 770, 39
Engels D., Kreysa E., Schultz G. V., Sherwood W. A., 1983, A&A, 124, 123
Enoch M. L., Evans N. J., II, Sargent A. I., Glenn J., 2009, ApJ, 692, 973
Evans N. J. II, Blair G. N., 1981, ApJ, 246, 394
Evans N. J., II, et al., 2009, ApJS, 181, 321
Faustini F., Molinari S., Testi L., Brand J., 2009, A&A, 503, 801
Fazio G. G. et al., 2004, ApJS, 154, 10
Findeisen K., Hillenbrand L., Ofek E., Levitan D., Sesar B., Laher R., Surace J., 2013, ApJ, 768, 93
Fontani F., Cesaroni R., Furuya R. S., 2010, A&A, 517, A56
Forbes D., 2000, AJ, 120, 2594
Froebrich D., Scholz A., Raftery C. L., 2007, MNRAS, 374, 399
Froebrich D. et al., 2011, MNRAS, 413, 480
Georgelin Y. P., Georgelin Y. M., 1970, A&A, 6, 349
Getman K. V., Feigelson E. D., Sicilia-Aguilar A., Broos P. S., Kuhn M. A., Garmire G. P., 2012, MNRAS, 426, 2917
Ghisellini G., Padovani P., Celotti A., Maraschi L., 1993, ApJ, 407, 65
Girven J., Gänsicke B. T., Steeghs D., Koester D., 2011, MNRAS, 417, 1210
Gottschalk M., Kothes R., Matthews H. E., Landecker T. L., Dent W. R. F., 2012, A&A, 541, A79
Greene T. P., Wilking B. A., Andre P., Young E. T., Lada C. J., 1994, ApJ, 434, 614
Groenewegen M. A. T., de Jong T., Geballe T. R., 1994, A&A, 287, 163
Groot P. J. et al., 2009, MNRAS, 399, 323
Guieu S. et al., 2009, ApJ, 697, 787
Günther H. M. et al., 2012, AJ, 144, 101
Gutermuth R. A., Heyer M., 2015, AJ, 149, 64
Gutermuth R. A., Megeath S. T., Myers P. C., Allen L. E., Pipher J. L., Fazio G. G., 2009, ApJS, 184, 18

Gyulbudaghian A. L., 2011, Astrophysics, 54, 384
Hartmann L., Herczeg G., Calvet N., 2016, ARA&A, 54, 135
Harvey P. M. et al., 2008, ApJ, 680, 495
Hashimoto O., 1994, A&AS, 107, 445
Hennemann M., Birkmann S. M., Krause O., Lemke D., 2008, A&A, 485, 753
Herbig G. H., 1977, ApJ, 217, 693
Herbig G. H., Jones B. F., 1983, AJ, 88, 1040
Herbst W., Shevchenko V. S., 1999, AJ, 118, 1043
Herbst W., Herbst D. K., Grossman E. J., Weinstein D., 1994, AJ, 108, 1906
Hoard D. W., Wachter S., Clark L. L., Bowers T. P., 2002, ApJ, 565, 511
Holoien T. W.-S. et al., 2014, ApJ, 785, L35
Horner D. J., Lada E. A., Lada C. J., 1997, AJ, 113, 1788
Hosokawa T., Offner S. S. R., Krumholz M. R., 2011, ApJ, 738, 140
Høg E. et al., 2000, A&A, 355, L27
Ishihara D., Kaneda H., Onaka T., Ita Y., Matsuura M., Matsunaga N., 2011, A&A, 534, A79
Itagaki K., Yamaoka H., 2010, Central Bureau Electronic Telegrams, 2426
Jilinski E. G., Frolov V. N., Ananjevskaja J. K., Straume J., Drake N. A., 2003, A&A, 401, 531
Jiménez-Esteban F. M., García-Lario P., Engels D., Perea Calderón J. V., 2006, A&A, 446, 773
Kamezaki T. et al., 2014, ApJS, 211, 18
Kamiński T., Miller M., Tylenda R., 2007, A&A, 475, 569
Kang M., Bieging J. H., Povich M. S., Lee Y., 2009, ApJ, 706, 83
Kang M., Bieging J. H., Kulesa C. A., Lee Y., Choi M., Peters W. L., 2010, ApJS, 190, 58
Kato T., Uemura M., 2001, Inf. Bull. Var. Stars, 5158, 1
Kawamura A., Onishi T., Yonekura Y., Dobashi K., Mizuno A., Ogawa H., Fukui Y., 1998, ApJS, 117, 387
Kenyon S. J., Hartmann L. W., Strom K. M., Strom S. E., 1990, AJ, 99, 869
Kerton C. R., 2002, AJ, 124, 3449
Kerton C. R., Brunt C. M., 2003, A&A, 399, 1083
Kharchenko N. V., Piskunov A. E., Schilbach E., Röser S., Scholz R.-D., 2013, A&A, 558, A53
Kirk B. et al., 2016, AJ, 151, 68
Kiss C., Moór A., Tóth L. V., 2004, A&A, 418, 131
Knapp G. R., Pourbaix D., Platais I., Jorissen A., 2003, A&A, 403, 993
Koenig X. P., Leisawitz D. T., 2014, ApJ, 791, 131
Kolpak M. A., Jackson J. M., Bania T. M., Clemens D. P., Dickey J. M., 2003, ApJ, 582, 756
Kóspál Á. et al., 2011, A&A, 527, A133
Kouzuma S., Yamaoka H., 2012, ApJ, 747, 14
Kronberger M. et al., 2006, A&A, 447, 921
Kryukova E. et al., 2014, AJ, 148, 11
Kuchar T. A., Bania T. M., 1994, ApJ, 436, 117
Kuchar T. A., Clark F. O., 1997, ApJ, 488, 224
Kumar M. S. N., Keto E., Clerkin E., 2006, A&A, 449, 1033
Kumar M. S. N., Contreras Peña C., Lucas P. W., Thompson M. A., 2016, ApJ, 833, 24
Kun M. et al., 2011, ApJ, 733, L8
Kurtz S., Churchwell E., Wood D. O. S., 1994, ApJS, 91, 659
Kwok S., Volk K., Bidelman W. P., 1997, ApJS, 112, 557
Lada C. J., Lada E. A., 2003, ARA&A, 41, 57
Laugalys V., Straižys V., 2002, Baltic Astron., 11, 205
Laugalys V., Straižys V., Vrba F. J., Boyle R. P., Philip A. G. D., Kazlauskas A., 2006, Baltic Astron., 15, 483
Lawrence A. et al., 2007, MNRAS, 379, 1599
Le Duigou J.-M., Knödlseder J., 2002, A&A, 392, 869
Lee Y., Snell R. L., Dickman R. L., 1991, ApJ, 379, 639
Lee Y., Snell R. L., Dickman R. L., 1996, ApJ, 472, 275
Leggett S. K., Lodieu N., Tremblay P.-E., Bergeron P., Nitta A., 2011, ApJ, 735, 62
Leistra A., Cotera A. S., Liebert J., 2006, AJ, 131, 2571
Lennon D. J., Dufton P. L., Fitzsimmons A., Gehren T., Nissen P. E., 1990, A&A, 240, 349

Lewis J. S., Grinspoon D. H., 1990, Science, 249, 1273

Lim B., Sung H., Bessell M. S., Kim J. S., Hur H., Park B.-G., 2015, AJ, 149, 127

Lin D., Webb N. A., Barret D., 2012, ApJ, 756, 27

Liu T., Wu Y., Zhang H., Qin S.-L., 2012, ApJ, 751, 68

Liu W. M., Padgett D. L., Terebey S., Angione J., Rebull L. M., McCollum B., Fajardo-Acosta S., Leisawitz D., 2014, AJ, 147, 133

Liu H. B. et al., 2016, Sci. Adv., 2, e1500875

Lockman F. J., Pisano D. J., Howard G. J., 1996, ApJ, 472, 173

Lorenzetti D., Giannini T., Larionov V. M., Kopatskaya E., Arkharov A. A., De Luca M., Di Paola A., 2007, ApJ, 665, 1182

Lucas P. W., Roche P. F., 1997, MNRAS, 286, 895

Lucas P. W. et al., 2008, MNRAS, 391, 136

Lumsden S. L., Hoare M. G., Urquhart J. S., Oudmaijer R. D., Davies B., Mottram J. C., Cooper H. D. B., Moore T. J. T., 2013, ApJS, 208, 11

Lundquist M. J., Kobulnicky H. A., Alexander M. J., Kerton C. R., Arvidsson K., 2014, ApJ, 784, 111

Lundquist M. J., Kobulnicky H. A., Kerton C. R., Arvidsson K., 2015, ApJ, 806, 40

Magnier E. A., Volp A. W., Laan K., van den Ancker M. E., Waters L. B. F. M., 1999, A&A, 352, 228

Maia F. F. S., Moraux E., Joncour I., 2016, MNRAS, 458, 3027

Maíz Apellániz J. et al., 2015, A&A, 579, A108

Makin S. V., Froebrich D., 2017, ApJS, in press (arXiv:1708.00394)

Mallick K. K., Kumar M. S. N., Ojha D. K., Bachiller R., Samal M. R., Pirogov L., 2013, ApJ, 779, 113

Marston A. P. et al., 2004, ApJS, 154, 333

Marton G., Tóth L. V., Paladini R., Kun M., Zahorecz S., McGehee P., Kiss C., 2016, MNRAS, 458, 3479

Marton G. et al., 2017, preprint (arXiv:1705.05693)

Masiunas L. C., Gutermuth R. A., Pipher J. L., Megeath S. T., Myers P. C., Allen L. E., Kirk H. M., Fazio G. G., 2012, ApJ, 752, 127

Massey P., Johnson K. E., Degioia-Eastwood K., 1995, ApJ, 454, 151

Matsuura M. et al., 2005, A&A, 434, 691

Mauerhan J. C., Van Dyk S. D., Morris P. W., 2011, AJ, 142, 40

May J., Alvarez H., Bronfman L., 1997, A&A, 327, 325

Mayne N. J., Naylor T., 2008, MNRAS, 386, 261

Mercer E. P. et al., 2005, ApJ, 635, 560

Meyer A. W., Smith R. G., Charnley S. B., Pendleton Y. J., 1998, AJ, 115, 2509

Minniti D. et al., 2010, New A, 15, 433

Moffat A. F. J., Jackson P. D., Fitzgerald M. P., 1979, A&AS, 38, 197

Molinari S. et al., 2010, PASP, 122, 314

Molinari S. et al., 2016, A&A, 591, A149

Morales E. F. E., Wyrowski F., Schuller F., Menten K. M., 2013, A&A, 560, A76

Morgan D. H., Cannon R. D., Hatzidimitriou D., Croke B. F. W., 2003, MNRAS, 341, 534

Muzerolle J., Furlan E., Flaherty K., Balog Z., Gutermuth R., 2013, Nature, 493, 378

Nagayama T., Omodaka T., Handa T., Honma M., Kobayashi H., Kawaguchi N., Ueno Y., 2011, PASJ, 63, 719

Nakano S., Sato H., Nishimura H., Nakamura T., Wakuda S., Yamaoka H., Pearce A., 2003, IAU Circ., 8190, 1

Nielbock M., Klass U., 2013, Technical Report, Zero magnitude conversion for the PACS Photometer, https://www.cosmos.esa.int/documents/12133/996891/Zero+magnitude+conversion+for+the+PACS+Photometer/, last accessed on 21-August-2017

Nikoghosyan E. H., Azatyan N. M., Khachatryan K. G., 2017, A&A, 603, A26

Otero S., Hümmerich S., Bernhard K., Sozynski I., 2014, J. Am. Assoc. Var. Star Obs., 42, 13

Parsons H. A. L., 2011, PhD thesis, University of Hertfordshire

Patriarchi P., Morbidelli L., Perinotto M., Barbaro G., 2001, A&A, 372, 644

Peretto N., Fuller G. A., 2009, A&A, 505, 405

Perez M. R., The P. S., Westerlund B. E., 1987, PASP, 99, 1050

Phelps R. L., Lada E. A., 1997, ApJ, 477, 176

Phillips J. P., 2007, MNRAS, 376, 1120

Poglitsch A. et al., 2008, in Oschmann J. M. Jr., de Graauw M. W. M., MacEwen H. A., eds, Proc. SPIE Conf. Ser. Vol. 7010, Space Telescopes and Instrumentation 2008: Optical, Infrared, and Millimeter. SPIE, Bellingham, p. 701005

Poulton C. J., Robitaille T. P., Greaves J. S., Bonnell I. A., Williams J. P., Heyer M. H., 2008, MNRAS, 384, 1249

Povich M. S. et al., 2013, ApJS, 209, 31

Prisinzano L., Sanz-Forcada J., Micela G., Caramazza M., Guarcello M. G., Sciortino S., Testi L., 2011, A&A, 527, A77

Prša A. et al., 2011, AJ, 141, 83

Puga E., Hony S., Neiner C., Lenorzer A., Hubert A.-M., Waters L. B. F. M., Cusano F., Ripepi V., 2009, A&A, 503, 107

Qiu K. et al., 2008, ApJ, 685, 1005

Radhakrishnan V., Goss W. M., Murray J. D., Brooks J. W., 1972, ApJS, 24, 49

Ragan S. E., Bergin E. A., Gutermuth R. A., 2009, ApJ, 698, 324

Raiteri C. M. et al., 2014, MNRAS, 442, 629

Raj A. et al., 2015, AJ, 149, 136

Ramírez Alegría S., Marín-Franch A., Herrero A., 2014, A&A, 567, A66

Rathborne J. M., Jackson J. M., Chambers E. T., Stojimirovic I., Simon R., Shipman R., Frieswijk W., 2010, ApJ, 715, 310

Rebull L. M. et al., 2011, ApJS, 193, 25

Reich P., Reich W., Furst E., 1997, A&AS, 126

Reid M. J., Menten K. M., Brunthaler A., Zheng X. W., Moscadelli L., Xu Y., 2009, ApJ, 693, 397

Reipurth B., Pettersson B., Armond T., Bally J., Vaz L. P. R., 2004, AJ, 127, 1117

Riaz B., Martín E. L., Tata R., Monin J.-L., Phan-Bao N., Bouy H., 2012, MNRAS, 419, 1887

Rieke G. H., Lebofsky M. J., 1985, ApJ, 288, 618

Rieke G. H. et al., 2004, ApJS, 154, 25

Rivilla V. M., Jiménez-Serra I., Martín-Pintado J., Sanz-Forcada J., 2014, MNRAS, 437, 1561

Robitaille T. P. et al., 2008, AJ, 136, 2413

Rodríguez-Flores E. R., Corradi R. L. M., Mampaso A., García-Alvarez D., Munari U., Greimel R., Rubio-Díez M. M., Santander-García M., 2014, A&A, 567, A49

Román-Zúñiga C. G., Elston R., Ferreira B., Lada E. A., 2008, ApJ, 672, 861

Romanova M. M., Kulkarni A. K., Lovelace R. V. E., 2008, ApJ, 673, L171

Roquette J., Bouvier J., Alencar S. H. P., Vaz L. P. R., Guarcello M. G., 2017, A&A, 603, A106

Rosolowsky E. et al., 2010, ApJS, 188, 123

Rygl K. L. J., Brunthaler A., Reid M. J., Menten K. M., van Langevelde H. J., Xu Y., 2010, A&A, 511, A2

Rygl K. L. J. et al., 2012, A&A, 539, A79

Rygl K. L. J. et al., 2014, MNRAS, 440, 427

Samus N. N., Kazarovets E. V., Kireeva N. N., Pastukhova E. N., Durlevich O. V., 2010, Odessa Astron. Publ., 23, 102

Saral G. et al., 2017, ApJ, 839, 108

Schlingman W. M. et al., 2011, ApJS, 195, 14

Schneider N., Bontemps S., Simon R., Jakob H., Motte F., Miller M., Kramer C., Stutzki J., 2006, A&A, 458, 855

Schneider N., Simon R., Bontemps S., Comerón F., Motte F., 2007, A&A, 474, 873

Scholz A., Froebrich D., Wood K., 2013, MNRAS, 430, 2910

Seaquist E. R., Ivison R. J., 1994, MNRAS, 269, 512

Semkov E. H., Peneva S. P., Munari U., Milani A., Valisa P., 2010, A&A, 523, L3

Shimoikura T. et al., 2013, ApJ, 768, 72

Simon R., Jackson J. M., Clemens D. P., Bania T. M., Heyer M. H., 2001, ApJ, 551, 747

Simon R., Rathborne J. M., Shah R. Y., Jackson J. M., Chambers E. T., 2006, ApJ, 653, 1325

Simpson R. J. et al., 2012, MNRAS, 424, 2442

Skrutskie M. F. et al., 2006, AJ, 131, 1163

Smith L. et al., 2014, MNRAS, 443, 2327

Solin O., Ukkonen E., Haikala L., 2012, A&A, 542, A3

Solomon P. M., Rivolo A. R., Barrett J., Yahil A., 1987, ApJ, 319, 730

Stauffer J. et al., 2014, AJ, 147, 83

Stead J. J., Hoare M. G., 2009, MNRAS, 400, 731

Stephenson C. B., 1989, Publications of the Warner & Swasey Observatory. Case Western Reserve University, Cleveland, OH

Straižys V. et al., 2014, AJ, 148, 89

Sylvester R. J., Kemper F., Barlow M. J., de Jong T., Waters L. B. F. M., Tielens A. G. G. M., Omont A., 1999, A&A, 352, 587

Tadross A. L., 2009, Ap&SS, 323, 383

Takalo L. O., Kidger M. R., de Diego J. A., Sillanpaa A., Nilsson K., 1992, AJ, 104, 40

Tapia M., Roth M., Persi P., 2015, MNRAS, 446, 4088

Taylor J. R., 1997, An Introduction to Error Analysis, the Study of Uncertainties in Physical Measurements, 2 edn. University Science Books, Mill Valley, CA

Taylor A. R., Wallace B. J., Goss W. M., 1992, AJ, 103, 931

Tej A., Ghosh S. K., Kulkarni V. K., Ojha D. K., Verma R. P., Vig S., 2007, A&A, 468, 1001

Testi L., Palla F., Natta A., 1998, A&AS, 133, 81

Teyssier D., Hennebelle P., Pérault M., 2002, A&A, 382, 624

Tisserand P. et al., 2009, A&A, 501, 985

Tu X., Wang Z.-X., 2013, Res. Astron. Astrophys., 13, 323

Urquhart J. S. et al., 2011, MNRAS, 418, 1689

van der Veen W. E. C. J., Habing H. J., 1990, A&A, 231, 404

van Loon J. T. et al., 1998, A&A, 329, 169

van Loon J. T., Cohen M., Oliveira J. M., Matsuura M., McDonald I., Sloan G. C., Wood P. R., Zijlstra A. A., 2008, A&A, 487, 1055

Veneziani M. et al., 2013, A&A, 549, A130

Venuti L. et al., 2014, A&A, 570, A82

Venuti L. et al., 2017, A&A, 599, A23

Viironen K. et al., 2009, A&A, 504, 291

Vorobyov E. I., Basu S., 2015, ApJ, 805, 115

Walmsley C. M., Churchwell E., Kazes I., Le Squeren A. M., 1975, A&A, 41, 121

Wang J., Townsley L. K., Feigelson E. D., Broos P. S., Getman K. V., Román-Zúñiga C. G., Lada E., 2008, ApJ, 675, 464

Wang K., Wu Y. F., Ran L., Yu W. T., Miller M., 2009, A&A, 507, 369

Watson C., Araya E., Sewilo M., Churchwell E., Hofner P., Kurtz S., 2003, ApJ, 587, 714

Webb J. R., Smith A. G., Leacock R. J., Fitzgibbons G. L., Gombola P. P., Shepherd D. W., 1988, AJ, 95, 374

Weights D. J., Lucas P. W., Roche P. F., Pinfield D. J., Riddick F., 2009, MNRAS, 392, 817

Werner M. W. et al., 2004, ApJS, 154, 1

Whitney B. A., Hartmann L., 1993, ApJ, 402, 605

Wienen M., Wyrowski F., Schuller F., Menten K. M., Walmsley C. M., Bronfman L., Motte F., 2012, A&A, 544, A146

Williams S. J., Fuller G. A., Sridharan T. K., 2004, A&A, 417, 115

Wink J. E., Altenhoff W. J., Mezger P. G., 1982, A&A, 108, 227

Witham A. R., Knigge C., Drew J. E., Greimel R., Steeghs D., Gänsicke B. T., Groot P. J., Mampaso A., 2008, MNRAS, 384, 1277

Wolk S. J. et al., 2015, AJ, 150, 145

Wood D. O. S., Churchwell E., 1989, ApJS, 69, 831

Wouterloot J. G. A., Brand J., Fiegle K., 1993, A&AS, 98, 589

Wright E. L. et al., 2010, AJ, 140, 1868

Wu Y., Liu T., Meng F., Li D., Qin S.-L., Ju B.-G., 2012, ApJ, 756, 76

Xu Y., Reid M. J., Menten K. M., Brunthaler A., Zheng X. W., Moscadelli L., 2009, ApJ, 693, 413

Xu J.-L., Wang J.-J., 2012, A&A, 543, A24

Yang X., Chen P., He J., 2004, A&A, 414, 1049

Young K. E., Young C. H., Lai S.-P., Dunham M. M., Evans N. J. II, 2015, AJ, 150, 40

Yun J. L., Clemens D. P., 1995, AJ, 109, 742

Yung B. H. K., Nakashima J.-i., Henkel C., 2014, ApJ, 794, 81

Zhang B., Zheng X. W., Reid M. J., Menten K. M., Xu Y., Moscadelli L., Brunthaler A., 2009, ApJ, 693, 419

Zhu Z., Hartmann L., Gammie C., 2009, ApJ, 694, 1045

SUPPORTING INFORMATION

Supplementary data are available at *MNRAS* online.

Table 1. Catalogue of 618 high-amplitude IR variable stars from UGPS.

Table1.tar.gz

Please note: Oxford University Press is not responsible for the content or functionality of any supporting materials supplied by the authors. Any queries (other than missing material) should be directed to the corresponding author for the article.

APPENDIX A: DETAILS OF THE VARIABLE STAR SEARCH

A1 Stage 1: searches of SQL data tables

The 45 variables in Paper I and the 26 variables in Contreras Peña (2015) were found by searching the fifth, seventh and eighth UKIDSS data releases. In each release, we selected candidates for visual inspection having $\Delta K \geq 1$ mag in the two epochs of K photometry given in the *gpsSource* table as $k\_1apermag3$ and $k\_2apermag3$, which provide photometry in the default 2 arcsec diameter aperture. We selected only stars having $K < 16$ mag in at least one of the two measurements and for which no serious post-processing photometric warnings are found ($k\_1ppErrBits < 256$ and $k\_2ppErrBits < 256$). One effect of the latter cut was to exclude stars that were flagged as close to saturation at either epoch. Further quality constraints were to require a stellar image profile ($mergedClass = -1$), low ellipticity ($k\_1Ell < 0.3$, $k_2Ell < 0.3$) and coordinates that agreed within 0.5 arcsec at the two epochs. These last three cuts were designed to minimize the number of false positives caused by blended stars. Finally, we rejected any candidates located in bad fields, identified by having more than 10 candidates in one 13×13 arcmin array.

A2 Stage 2: initial search of fits catalogues

The early searches were very inefficient due to bad pixels and severe source confusion in the more crowded parts of the Galactic plane. As the survey approached completion, we realized that searches for both variable stars and high proper motion stars would be easier in less crowded parts of the Galactic plane. A data set covering 900 deg^2 of two-epoch sky at longitudes $60 < l < 230°$ was compiled at Hertfordshire for the purpose of finding high proper motion stars, see Smith et al. (2014). That data set included all data taken up 2013 March 31. The number of false positive high proper motion stars was shown to be far lower at $l > 60°$ (due to fewer blends) than at smaller longitudes so we decided to search that the data set for high-amplitude variables.

This search was based on the publicly available FITS catalogues for each UGPS stacked 'multiframe' image in the K filter alone (multiframes consist of four images for the four array detectors in WFCAM. Source magnitudes were extracted from the FITS catalogues with the FITSIO_CAT_LIST.F program that forms part of the public software release of the CASU (http://casu.ast.cam.ac.uk/surveys-projects/software-release). This

search differed slightly from the earlier searches of the SQL data base.

(i) First, sources with potentially bad pixels in the photometric aperture were excluded from the search, since the FITSIO_CAT_LIST.F program sets the image profile-based *class* parameter to −7 in these cases. This flag is not set in the data releases at the WSA, which is why bad pixels were a serious issue in our earlier searches.

(ii) Second, the stellar profile cut used *class* = −1 at each epoch rather than *mergedclass* = −1, i.e. it was based on the profile classification in the two *K* images rather than the merged classification from all available passbands and epochs.

(iii) Third, the FITS catalogues do not include the *ppErrBits* flags so our initial selection included stars that would have been flagged as close to saturation (or even in some cases clearly saturated, since visual inspection shows that not all saturated stars have the profile *class* = −9 that is applied when saturation is detected by the CASU data reduction pipeline.)

(iv) Fourth, not all the FITS catalogues had been through the various quality control procedures implemented for public SQL data releases. These quality issues would be expected to further increase the number of false positive candidates arising from various causes including poor weather or gross electronic defects. We did however gain greater completeness because high-amplitude variables can be readily detected even in poorer quality data.

Following visual inspection, this search of a ∼900 deg^2 area at $l > 60°$ yielded 297 genuine variables from only 501 candidates, including 32 discovered in our earlier searches. This 59 per cent success rate was due to the rarity of blends in less crowded parts of the Galactic plane and the far smaller number of sources with bad pixels. The bona fide variables include some sources that are flagged as close to saturation in the DR10 *gpsSource* table with the $k\_1ppErrBits$ or $k\_2ppErrBits$ parameters. However, comparison with 2MASS K_s data across a large area shows that effects of saturation on UGPS photometry are typically small (<0.05 mag) for stars with 2MASS magnitudes $11 < K_{s,2MASS} < 12$ that are not blended in 2MASS. The photometry can be useful as bright as $K = 10$, depending on seeing, sky background and source location on the WFCAM arrays. In order to ensure that at least one of the two epochs was always well measured, we excluded all candidates that were obviously saturated at both epochs. This done by simple visual inspection but no source in our catalogue of variables has $K < 11$ at both epochs. A close-to-saturation warning flag is set in the catalogue for all measurements where the issue may be significant. This flag was set either if the relevant measurement had bit 16 of the *ppErrBits* flag set in the WSA (see wsa.roe.ac.uk/ppErrBits.html) or, if the data were not in DR10, the flag was set for measurements brighter than $K = 11.5$, $H = 13$ and $J = 13$. We note that bona fide variables were always very easy to identify by visual inspection of the FITS images even if one epoch was saturated.

A3 Stage 3: final searches of FITS catalogues

Final searches were undertaken when the complete UGPS data set became available, again using the publicly available FITS catalogues, since data taken after 2012 January 31 are not available in the most recent SQL DR (DR10) at the WSA. An additional 375 deg^2 of two epoch sky at $60 < l < 230°$ were available, based on a second epoch obtained between 2013 April 01 and the end of UKIDSS operations on 2013 December 31. We further expanded the search of the $60 < l < 230°$ area by exploring the third epoch of data that were taken for a small proportion of UGPS fields due to doubts

about the data quality at one of the two earlier epochs. The data base created for the proper motion search had used the first and last images in the sequence to maximize time baseline; we now used the second and third images in the sequence, provided the second image was separated from the other two by at least 1.5 yr. We chose not to use first and third images for additional searches, owing to the low ratio of genuine to false candidates found with the second and third images. In addition, we modified the FITSIO_CAT_LIST.F program to stop it from overwriting the stellar profile classification when potentially bad pixels were included in the photometric aperture. By recording the information separately, we were able to search for highly variable sources classified as stellar ($k_{1,2}class = −1$) even if potentially bad pixels were present. We found that candidate variables with the bad pixel flag were mostly located at the edges of the field and were not real variables, but the minority of candidates further from the edges were often genuine. A threshold distance of 83 pixels from the array edges in X and Y was applied.

These searches yielded only 86 real variables from 350 new candidates, most of them arising from the new area and only a small proportion arising from the third epoch or sources flagged as having a bad pixel. We note that a single bad pixel appeared to have a very small effect on the photometry (smaller than the recorded uncertainty) for the relatively bright variable stars in our catalogue, based on comparison of source magnitudes in different photometric apertures. In some cases no identifiable bad pixel was visible in the images, presumably because the effect was small or intermittent. Consequently, we flag the nine affected sources in our catalogue (see Appendix B), but we have not attempted to correct the photometry.

Lastly, we expanded the search to the two-epoch sky at $30 < l < 60°$, finding 202 real variables from 595 candidates. This very reasonable ratio of real variables to candidates shows that high stellar density has much less effect on two-epoch variability searches than on our past two-epoch high proper motion searches. The ratio becomes much worse at $l \leq 30°$, see Section 2, so that region was not searched due to lack of available time (though some of this area was included in the initial SQL searches). For similar reasons, we did not attempt to mine any third epoch of data in the $30 < l < 60°$ region, though the few candidates with the bad pixel flag were included.

APPENDIX B: CATALOGUE DESCRIPTION

Columns 1 and 2 give a running number and the UGPS designation; column 3 gives any other name by which a source is already known. Equatorial and Galactic coordinates are given in columns 4–7. Columns 8–13 give the contemporaneous UGPS *J*, *H* and *K* magnitudes, the latter denoted 'K_c', and their the associated errors. The other UGPS *K* magnitude is denoted 'K_o', given in columns 14, with the error in column 15. We note that the *J*, *H* and K_c fluxes given here were taken from the *gpsSource* or *gpsDetection* tables in DR10 at the WSA (carefully avoiding the occasional non-contemporaneous entries in *gpsSource*) rather than the FITS catalogues, in order to benefit from small (≤0.03 mag) improvements to the calibration of the four WFCAM arrays that are not available in the FITS catalogues. The K_o photometry were left unchanged because many of these data are not available in the DR10 *gpsSource* table. We impose a floor of 0.02 mag on the errors, representing the typical calibration uncertainty for well-measured sources. Column 16 contains a flag ('*a*' or '*b*') indicating whether the 'K_c'

Table B1. *K* fluxes for Table 1 entries where *JHK* photometry were taken at a third epoch.

Number	K_a	K_b	K_c	MJDobs a	MJDobs b	MJDobs c
243	11.98	13.36	12.96	53638.24097	55776.41255	53503.58199
244	15.78	17.22	16.24	53638.24097	55776.41255	53503.58199
572	16.11	14.61	15.42	53915.50097	56208.25244	55463.36109

corresponds to the first UGPS epoch (*a*) or the second (*b*).[5] In three cases the flag is 'c', indicating that the contemporaneous *JHK*c photometry were taken at a third epoch when the K_c magnitude was between the other two *K* magnitudes. In these cases K_o is left blank and *K* data from all three epochs are given in Table B1.

Columns 17 and 18 give the modified Julian date of epochs *a* and *b*. Column 19 indicates whether the source had a 'possible-saturation' warning in each of *J*, *H*, K_c and K_o in sequence (see Appendix A). E.g. '0010' would indicate that the K_c measurement might be influenced by saturation but *J*, *H* and K_o were not. Column 20 flags any cases where bad pixels may be present that might possibly reduce the precision of photometry in K_c or K_o by listing the affected measurement (see Appendix A). Column 21 gives the amplitude of variation, ΔK, based on the two UGPS fluxes in Table 1 (or the maximum and minimum fluxes for the three sources in Table 2). ΔK is marginally below unity in six sources despite our initial selection requirement, owing to the small calibration differences between data in the FITS catalogues and the *gpsSource* table noted above. Column 22 gives the amplitude $\Delta K_{all} = K_{max} - K_{min}$ after taking account of a third epoch in K_s from the 2MASS Point Source Catalogue (Skrutskie et al. 2006), where available. We note that measurements in the UKIRT MKO *K* filter and 2MASS K_s filter typically agree within a few hundredths of a magnitude for most non-variable stars. Transformation between systems is generally not possible for individual stars of unknown spectral type, on Galactic plane sightlines with unknown extinction.

The later columns in Table 1 contain information based mainly on other public data sets and searches of the literature via the SIMBAD data base, see Section 3. Column 23 indicates the likely type of astronomical object, if known. Column 24 gives distances to likely YSOs derived from the associated SFR, based on references in the literature that are indicated in column 25. In column 26, we identify the SFR or cluster associated with each YSO, provided there is significant literature mentioned in SIMBAD. If no cluster or SFR is listed, we name any mm source, submm source, or IRDC that is coincident with the source. Information from the WISE colour images is included if a substantial uncatalogued cluster is present. References to the named region and/or the source itself are given in column 27. These searches also reveal whether the source was previously known as a variable star or other source of interest, named in column 3. In column 28, we indicate whether the source is associated with any of the nine well-studied spatial groups of four or more pre-MS variables listed in Section 4.2, provided it is classified as a likely YSO in column 23.

In column 29, we give the 2–22 µm spectral index, $\alpha = d(\log(\lambda F_\lambda))/d(\log(\lambda))$. In almost all cases, it is based on the average of the two UGPS *K* fluxes and the four contemporaneous

W1, W2, W3 and W4 fluxes from the WISE All-Sky data release which was based on data obtained in 2010. We found that using either the brighter or fainter of the two UGPS *K* fluxes instead of the average typically changed α by 0.2, which indicates the uncertainty caused by this non-contemporaneous passband. The spectral index is given only for the 157 sources classified as YSOs that were measured in W4 and further eight sources for which 24 µm photometry is available from MIPSGAL (Rieke et al. 2004; Carey et al. 2009; Gutermuth & Heyer 2015), but not in WISE. In these eight cases, we combined MIPSGAL photometry with *Spitzer*/IRAC photometry (Fazio et al. 2004), rather than WISE. Column 30 gives the discrete SED index classification for the YSOs as class I, flat spectrum or II, based on the spectral index.

Columns 31–33 give contemporaneous optical photometry in the *r*, *i* and narrow-band Hα filters taken either from the IPHAS DR2 (Drew et al. 2005; Barentsen et al. 2014), for sources at Dec. $\delta > +1.3°$, or from the VPHAS+ data set (Drew et al. 2014) for more southerly sources. Column 34 gives the modified Julian date of the IPHAS or VPHAS+ observations, as appropriate. 2MASS photometry in the *J*, *H* and K_s passbands is given in columns 35–37 and the WISE W1–W4 photometry is given in columns 38–41. MIPSGAL 24 µm data are given in column 42, and IRAC photometry are given in columns 43–46 for bands I1–I4. The *Spitzer*/IRAC data are from the GLIMPSE, GLIMPSE3D, GLIMPSE360, Deep GLIMPSE, Cygnus X and SMOG public surveys (Benjamin et al. 2003; Churchwell et al. 2009) which were not contemporaneous with MIPSGAL or UGPS.

Inspection of the WISE images indicated that some sources with a W3 or W4 flux in the All-Sky catalogue were actually not detected or poorly measured in that passband, due to the effect of bright nebulosity on the background estimation and the use in WISE catalogues of list-driven photometry applied to all passbands for detections in any passband. Koenig & Leisawitz (2014) investigated this issue in detail for SFRs in the outer Galaxy for the AllWISE data set, which has similar characteristics to the All-Sky data set for this issue. They found that in every passband, the genuine and false WISE detections have different but overlapping distributions in plots of the reduced χ^2 statistic for a point source detection versus the signal-to-noise ratio. We used quality cuts on the W3 and W4 photometries similar to those proposed in that work to identify sources for visual inspection in all four WISE passbands: we checked ~90 sources located above the diagonal lines in their Fig. 1 (the *w4rchi2* versus *w4snr* and *w3rchi2* versus *w3snr* plots) that also had *w4rchi2* > 2 or *w3rchi2* > 2, as appropriate. WISE fluxes in one or more passbands were removed for slightly under half of these. Our adopted reduced χ^2 thresholds are slightly more relaxed then those adopted for a reliable selection in Koenig & Leisawitz (2014), since we saw a slightly broader distribution of bona fide sources in the reduced χ^2 versus signal-to-noise ratio plane (perhaps due to increased source confusion in the inner Galaxy) and we aimed more for completeness than reliability. Only one source had photometry removed in the W1 or W2 passbands, due to blending rather than poorly measured background. We did not go so far as to visually check all WISE detections in all passbands, nor all optical, *Spitzer* and UGPS

---

[5] Our alphabetical notation of epochs *a* and *b* is used to distinguish our catalogue from data in the *gpsSource* table in the UKIDSS public data releases at the WSA, which typically uses K_1 and K_2 in the way that we use K_c and K_o, respectively. Our selection of measurements occasionally differs from those used for the primary detection of each source in DR10.

photometry in all passbands (only the K measurements, the few available MIPSGAL 24 μm measurements and *J*, *H* in addition for sources with unusual near-IR colours). A small amount of erroneous photometry may therefore remain in the catalogue. We retained the small number of obviously blended WISE detections if the WISE active deblending appeared to be successful, checking the higher resolution *Spitzer*/IRAC images where possible for confirmation.

Matches to 2MASS and IRAC data used a 1 arcsec cross-match radius whereas matches to the lower resolution WISE and MIPS-GAL data sets used a 2 arcsec cross-match radius. All matches with separations over 0.4 arcsec were then matched back against the UGPS DR10 data base in order to identify, inspect and remove any mismatches to another UGPS source. One such mis-match occurred for source 273, for which the 2MASS counterpart with coordinates 0.77 arcsec north of the UGPS variable appears to be a blend of source 273 and an adjacent UGPS source 1.06 arcsec to the north. All other mis-matches were to sources >1 arcsec from the UGPS coordinates. Three very bright WISE sources (sources 241, 273 and 301) required a larger cross-match radius of 3 arcsec due to slightly incorrect coordinates in the WISE All-Sky source catalogue (an issue that was fixed in the more recent AllWISE source catalogue, created from non-contemporaneous data).

In column 47, we give the 70 μm flux in mJy from the PACS instrument (Poglitsch et al. 2008) on the *Herschel* satellite. These data were obtained by cross-matches to (i) the Hi-GAL first DR (Molinari et al. 2010, 2016) covering $-70 < l < 68°$, $|b| < 1°$ and (ii) the *Herschel*/PACS Point Source Catalogue (Marton et al. 2017) which includes all PACS data from the satellite (though there is limited coverage outside the mid-plane region). Most matches were from the Hi-GAL data set and we used the Hi-GAL data release as the first choice, though the two catalogues agree well for sources in common. Hi-GAL data were taken in 2010–2011 (typically about 1 yr after the WISE All-Sky data). Initially, we found 64 matches, using a 6 arcsec matching radius (similar to the beam size). We found that matches with no corresponding WISE W4 detection almost always had separations over 3 arcsec from the UGPS source, while those with W4 detections had separations under about 3 arcsec. We therefore retained only the 52 matches with a W4 detection, leading to an effective cross-match radius of 3.1 arcsec. Most of these have a signal-to-noise ratio over 5 but we have included the small number of low significance detections. The conversion to a Vega magnitude system in Fig. 10 of the main text was done with the zero-point given by Nielbock & Klass (2013).

This paper has been typeset from a TEX/LATEX file prepared by the author.